ADVERTIMENT. La consulta d'aquesta tesi queda condicionada a l'acceptació de les següents condicions d'ús: La difusió d'aquesta tesi per mitjà del servei TDX (www.tesisenxarxa.net) ha estat autoritzada pels titulars dels drets de propietat intel·lectual únicament per a usos privats emmarcats en activitats d'investigació i docència. No s'autoritza la seva reproducció amb finalitats de lucre ni la seva difusió i posada a disposició des d'un lloc aliè al servei TDX. No s'autoritza la presentació del seu contingut en una finestra o marc aliè a TDX (framing). Aquesta reserva de drets afecta tant al resum de presentació de la tesi com als seus continguts. En la utilització o cita de parts de la tesi és obligat indicar el nom de la persona autora.

ADVERTENCIA. La consulta de esta tesis queda condicionada a la aceptación de las siguientes condiciones de uso: La difusión de esta tesis por medio del servicio TDR (www.tesisenred.net) ha sido autorizada por los titulares de los derechos de propiedad intelectual únicamente para usos privados enmarcados en actividades de investigación y docencia. No se autoriza su reproducción con finalidades de lucro ni su difusión y puesta a disposición desde un sitio ajeno al servicio TDR. No se autoriza la presentación de su contenido en una ventana o marco ajeno a TDR (framing). Esta reserva de derechos afecta tanto al resumen de presentación de la tesis como a sus contenidos. En la utilización o cita de partes de la tesis es obligado indicar el nombre de la persona autora.

WARNING. On having consulted this thesis you're accepting the following use conditions: Spreading this thesis by the TDX (www.tesisenxarxa.net) service has been authorized by the titular of the intellectual property rights only for private uses placed in investigation and teaching activities. Reproduction with lucrative aims is not authorized neither its spreading and availability from a site foreign to the TDX service. Introducing its content in a window or frame foreign to the TDX service is not authorized (framing). This rights affect to the presentation summary of the thesis as well as to its contents. In the using or citation of parts of the thesis it's obliged to indicate the name of the author

THERMO-MECHANICAL ANALYSIS OF WELDING PROCESSES

NARGES DIALAMI

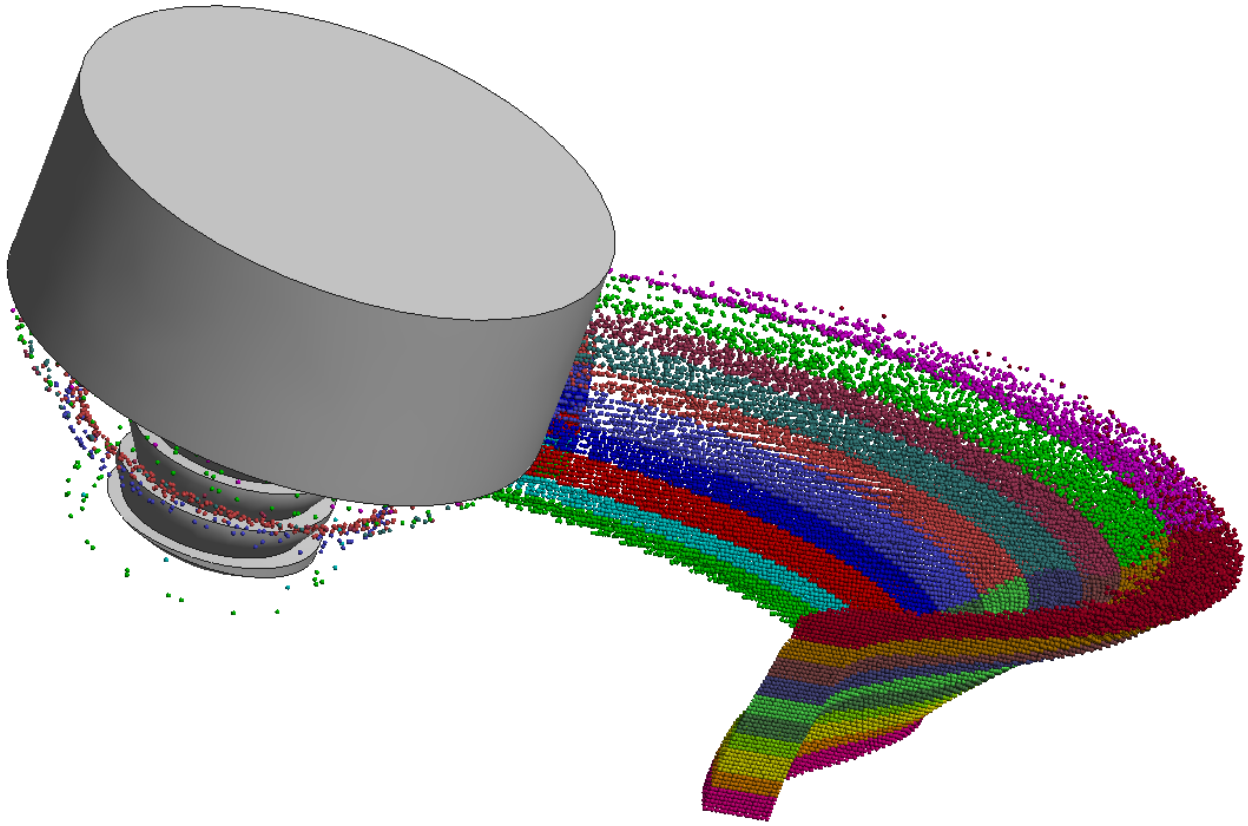

DOCTORAL THESIS
BARCELONA, MARCH 2014

Universitat Politécnica de Cataluña
Departament de resistència de materials
Programa de Doctorado en Análisis Estructural

DOCTORAL THESIS

THERMO-MECHANICAL ANALYSIS OF WELDING PROCESSES

NARGES DIALAMISHABANKAREH

Advisors: Michele Chiumenti
Miguel Cervera

Barcelona, March 2014

UNIVERSITAT POLITÈCNICA DE CATALUNYA
BARCELONATECH
Escola de Doctorat

Acta de calificación de tesis doctoral	Curso académico:

Nombre y apellidos

Programa de doctorado

Unidad estructural responsable del programa

Resolución del Tribunal

Reunido el Tribunal designado a tal efecto, el doctorando / la doctoranda expone el tema de la su tesis doctoral titulada _____

_____.

Acabada la lectura y después de dar respuesta a las cuestiones formuladas por los miembros titulares del tribunal, éste otorga la calificación:

☐ NO APTO ☐ APROBADO ☐ NOTABLE ☐ SOBRESALIENTE

(Nombre, apellidos y firma) Presidente/a	(Nombre, apellidos y firma) Secretario/a	
(Nombre, apellidos y firma) Vocal	(Nombre, apellidos y firma) Vocal	(Nombre, apellidos y firma) Vocal

_____, _____ de _____ de _____

El resultado del escrutinio de los votos emitidos por los miembros titulares del tribunal, efectuado por la Escuela de Doctorado, a instancia de la Comisión de Doctorado de la UPC, otorga la MENCIÓN CUM LAUDE:

☐ SÍ ☐ NO

(Nombre, apellidos y firma) Presidenta de la Comisión de Doctorado	(Nombre, apellidos y firma) Secretaria de la Comisión de Doctorado

Barcelona a _____ de _____ de _____

Acknowledgment

I would like to express my deepest appreciation to all those who provided me the possibility to complete this thesis.

I would like to thank my supervisors, Profs. Michele Chiumenti and Miguel Cervera, with all my heart for their support during the learning process of this thesis. Those were the ones who helped me with their brilliant scientific advices, assistance and guidance to overcome the complexity of the work.

A special gratitude I give to Prof. Eugenio Oñate, the one who introduced me with the group and was the starting point for the PhD and my stay in Barcelona.

I would like to thank Prof. Jean-Phillipe Ponthot for giving me the opportunity to be a part of his group and sharing his deep knowledge with me during my stay from beginning of March until beginning of June 2012 in University of Liege, Belgium. This collaboration led to fruitful results in form of several publications.

I am also truly indebted and thankful to Prof. Carlos Agelet de Saracibar for his guidance and support.

I take this opportunity to acknowledge the financial support received from Spanish ministry of science and innovation through FPI grant.

I would like to thank all my officemates who provided me a friendly work ambient.

I would like to thank my mother and father, who have supported me throughout entire process, both by keeping me harmonious and helping me putting pieces together. I will be grateful forever for their endless love. I would like to express my gratitude to my siblings whom they were beside me all over the process and, last but not the least, Pavel, for his kindness, help and support he has shown during the past years it has taken me to finalize this thesis. He was the one who was next to me when I needed, encouraging and cheering me up.

Abstract

This thesis deals with the numerical simulation of welding processes. The analysis is focused either at global level, considering the full component to be jointed, or locally, studying more in detail the heat affected zone (HAZ). Even if most of the considerations are quite general, two specific welding technologies are studied in depth: multi-pass arc-welding and its extension to Shaped Metal Deposition (SMD) processes (global level analysis) and Friction Stir Welding (FSW) technology (local framework). Both welding techniques are used in many industrial applications and particularly in the aeronautic and aerospace industries, where the quality of the joining is of essential importance.

The analysis at global (structural component) level is performed defining the problem in the Lagrangian setting while, at local level, both Eulerian and Arbitrary Lagrangian Eulerian (ALE) frameworks are used. More specifically, to model the FSW process, an apropos kinematic framework which makes use of an efficient combination of Lagrangian (pin), Eulerian (metal sheet) and ALE (stirring zone) descriptions for the different computational sub-domains is introduced for the numerical modeling. As a result, the analysis can deal with complex (non-cylindrical) pin-shapes and the extremely large deformation of the material at the HAZ without requiring any remeshing or remapping tools.

A fully coupled thermo-mechanical framework is proposed for the computational modeling of the welding processes proposed both at local and global level. A staggered algorithm based on an isothermal fractional step method is introduced.

To account for the isochoric behavior of the material when the temperature range is close to the melting point or due to the predominant deviatoric deformations induced by the visco-plastic response, a mixed finite element technology is introduced. The Variational Multi Scale (VMS) method is used to circumvent the LBB stability condition allowing the use of linear/linear P1/P1 interpolations for displacement (or velocity, ALE/Eulerian formulation) and pressure fields, respectively. More in detail, the accuracy of the GLS and OSGS stabilization techniques are compared. The same stabilization strategy is adopted to tackle the instabilities of the temperature field, inherent characteristic of convective dominated problems (thermal analysis in ALE/Eulerian kinematic framework).

At global level, the material behavior is characterized by a thermo-elasto-viscoplastic constitutive model. A smooth transition model is presented to

represent the material behavior in the full temperature range from solid (elasto-plastic) to liquid-like (purely viscous) behavior passing through the semi-solid (mushy) phase. Both strain-hardening and thermal softening phenomena are considered.

The analysis at local level is characterized by a rigid thermo-visco-plastic constitutive model. Different thermally coupled (non-Newtonian) fluid-like models as Norton-Hoff or Sheppard-Wright, among others are tested.

The balance of energy equation is solved in its enthalpy format for a treatment of the phase-change phenomena. Both latent heat and thermal shrinkage effect are considered. An accurate definition of the heat source (laser, arc, electron beam, etc...), as well as the heat generation induced by the visco-plastic dissipation or the frictional contact (Coulomb and Norton model) are described. Both heat convection (Newton's law) and heat radiation models are introduced to dissipate heat through the boundaries of the component.

An ad-hoc technique to account for the use of a filler material in the shape metal deposition (SMD) process is developed. The element activation methodology proposed allows for an accurate layer-by-layer deposition of the material without introducing spurious stress/strain fields.

To better understand the material flow pattern in the stirring zone, a (Lagrangian based) particle tracing is carried out while post-processing FSW results. The final numerical tool developed to study the FSW process is able to give detailed information concerning the characteristics of the weld and their relationship with the welding process parameters (e.g. advancing and rotation velocities).

The simulation tool presented in this work is validated with analytical results and calibrated with experimental data.

This thesis is a collection of research articles supplemented with some introductory chapters summarizing the state-of-the-art, the motivations and objectives of the work as well as the main contributions and some suggested lines for future work. It comprises 7 already-published (or accepted for publication) peer-review journal articles which are integral part of this work.

Resumen

Esta tesis se centra en el estudio numérico del proceso de soldadura. El análisis realizado tiene en consideración tanto los fenómenos globales, como los efectos locales que ocurren en la zona térmicamente afectada (HAZ) cerca de la unión. Teniendo en cuenta las diferentes técnicas industriales de soldadura, en este trabajo nos hemos centrado en dos técnicas específicas: el proceso de deposición por capas o "Shaped Metal Deposition (SMD) process" a nivel global y el proceso de soldadura por fricción y batido o "Friction Stir Welding (FSW)" a nivel local. Estas técnicas se utilizan en muchas aplicaciones industriales y en particular en la industria aeronáutica y aeroespacial, donde la calidad de la unión es esencial.

Para el análisis a nivel global (estudio de un componente estructural) se utiliza un marco Lagrangiano, mientras que a nivel local, se utiliza una combinación de varios enfoques. Más concretamente, para modelar el proceso de FSW se crearon diferentes subdominios computacionales estudiándose cada uno de ellos con un enfoque cinemático diferente: Lagrangiano para el "pin", Euleriano para la chapa, mientras en la zona de la chapa cerca del pin donde se concentran las deformaciones (stirring zone), el marco utilizado a sido el Arbitrariamente Lagrangiano-Euleriano (ALE). Este análisis nos permite estudiar herramientas caracterizadas por geometrías complejas (no solamente cilíndricas). Además es posible analizar las grandes deformaciones del material en la zona de proceso (HAZ) sin la necesidad de remallar y utilizar algoritmos de re-mapeo variables.

En este trabajo se propone un análisis termo-mecánico acoplado con un método de de paso fraccionado iso-térmico para la simulación numérica de los procesos de soldadura, tanto a nivel local como global.

Se propone además una formulación de elementos finitos mixta (desplazamientos/presión) para tener en cuenta el comportamiento isócorico del material en consecuencia del comportamiento visco-plástico del mismo (deformaciones mayoritariamente deviatoricas). Se introduce el Método Variacional Multiescala (VMS) para evitar las restricciones la condición de estabilidad LBB, permitiendo el uso de interpolaciones lineales P1/P1 para los campos de desplazamiento (o velocidad, en el caso de formulación ALE/Euleriana) y presión, respectivamente. Más en detalle, se comparan las técnicas de estabilización GLS (Galerkin Least Squares) y OSGS (Orthogonal Sub-grid Scales). Se utiliza la misma estrategia de estabilización para hacer frente a las inestabilidades del campo de temperaturas, características de los problemas de convección dominante (análisis térmico en el marco euleriano o ALE).

Abstract v

A nivel global (estructural), el comportamiento del material se caracteriza por un modelo constitutivo elasto-termo-viscoplástico. Se propone una transición suave en función del rango de temperatura para representar el cambio de estado de material, desde sólido (elasto-plástico) a líquido (respuesta puramente viscosa) pasando por la fase semi-sólida durante el cambio de fase. El modelo plástico incluye los fenómenos de endurecimiento por deformación así como de ablandamiento térmico.

A nivel local, el análisis se caracteriza por un modelo constitutivo rígido-termo-visco-plástico. Se estudian, diferentes modelos (típicamente fluidos no Newtonianos) como Norton-Hoff o Sheppard-Wright, entre otros.

La ecuación de balance de energía se resuelve en el formato de entalpía incluyendo el fenómeno de cambio de fase en términos de calor latente y contracción térmica. Los modelos de convección y radiación de calor se usan para disipar del calor a través del contorno del dominio. En este trabajo se detallan diferentes modelos de fuentes energéticas (láser, arco, haz de electrones, etc ..) para simular a nivel global el aporte de calor en la zona de proceso. Análogamente, se tiene en cuenta la generación del calor inducido por la disipación visco-plástica y por el contacto con fricción (modelo de Coulomb y de Norton) para la simulación numérica del proceso de FSW.

Para el proceso SMD se desarrolla una técnica ad-hoc para la deposición del material de aporte. La estrategia de activación de elementos propuesta en este trabajo permite simular de forma precisa la deposición de las diferentes capas de material en el proceso de SMD sin dar lugar a la aparición de campos de tensión/deformación espurios.

Finalmente, para analizar el movimiento del material en la zona de proceso de FSW se han implementado unos trazadores materiales. De esta manera es posible visualizar en la fase de post-‘procesamiento el movimiento del material alrededor de la herramienta de FSW. A través de este método es posible sacar información acerca de la calidad de la unión soldada, así como optimizar los parámetros del proceso de FSW, como velocidades de rotación y avance.

Esta tesis se compone de una recopilación de 7 artículos publicados en revistas internacionales indexadas, así como de una introducción , que resume el estado de arte actual, las motivaciones y objetivos del estudio realizado, las principales aportaciones y mejoras desarrolladas, así como las líneas de trabajo futuro

Contents

Abstract **ix**

1 Introduction **1**
1.1 Motivation and challenges 6
1.1.1 Physical model 6
1.1.2 Numerical model 8
1.2 State of the art 16
1.2.1 Industrial background of FSW 16
1.2.2 Experimental analysis of FSW 20
1.2.3 Analytical and Numerical modeling of FSW 24
1.2.4 Industrial background of SMD 36
1.2.5 Experimental and numerical modeling of SMD 38
1.3 Outline 41

2 Thermal problem **45**
2.1 Thermal problem at the global level 49
2.2 Thermal problem at the local level 49
2.3 Boundary conditions 52
2.4 Thermal constitutive model 53
2.4.1 Thermal contact model 53
2.5 Friction model 54
2.5.1 Coulomb's friction law 54
2.5.2 Norton's friction law 56
2.6 Weak form of the thermal problem 57
2.7 Discrete weak form of the thermal problem 57
2.8 Paper contributions 58

3 Mechanical problem **59**
3.1 Constitutive model 61
3.1.1 Mechanical constitutive model at global level 61
3.1.2 Mechanical constitutive model at local level 67
3.2 Weak form of the mechanical problem 72
3.2.1 Boundary conditions 73
3.3 Discrete weak form of the mechanical problem 74
3.4 Paper contributions 74

4 Stabilization methods **77**
4.1 Pressure stabilization 77
4.2 Convective stabilization 82
4.3 Paper contribution 85

5 Element activation strategy for the SMD process **87**
5.1 Paper contribution 91

6 Apropos Kinematic framework for FSW process **93**
6.1 Paper contribution 99

7 Particle tracing technique **101**
7.1 BES method 104
7.2 BFECC method 104
7.3 RK4 method 106
7.4 Paper contribution 108

8 Conclusion and future work **109**
8.1 Contributions 109
8.2 Lines for future work 112

Chapter 1

Introduction

Welding is a fabrication technique to join materials, commonly metals or thermoplastics. Usually it is performed by melting the workpieces and inserting a filler material, to form the weld pool of the molten material. Then the weld cools down and creates a strong joint. Welding has become the method of choice for its strength, efficiency and versatility. Welding is produced by either heating of the materials to a suitable temperature with or without the application of pressure, or by the application of pressure alone, with or without the use of filler metal. This is in contrast with soldering and brazing, which involve melting a lower-melting-point material known as filler material between the workpieces to form a bond between them, without melting the workpieces.

Welding technology is widely used in a lot of industries such as aerospace, automotive, shipbuilding or nuclear. The different industries have different requirements in structural design. On one hand, the aerospace, automotive and ship-building industries often try to manufacture lighter, thinner steel structures to reduce weight and material as their main goal. On the other hand, in nuclear and heavy industries, safety considerations make the structural components thicker and thus the distortion problems are relatively small. In these cases, the residual stresses are on the focus.

Figure 1.1: Forge welding

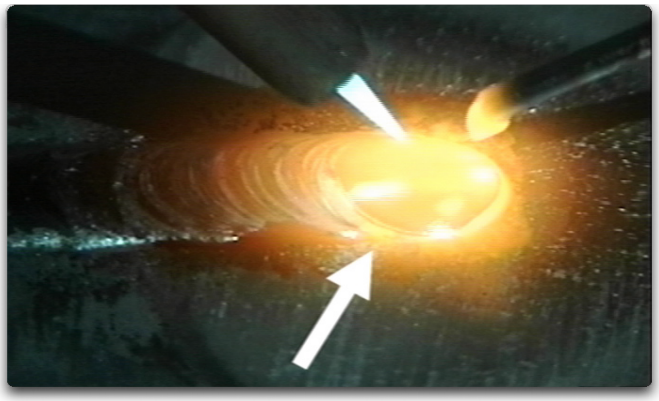

Figure 1.2: Oxyfuel welding

There are several different ways to weld, and improvements and innovations are being continuously invented up-to-date. The main factors for their distinction is the source of the energy used for welding, and the means of protection or cleaning of the welded material. Some involve sophisticated machinery and advanced technology, including a gas flame, an electric arc, a laser, an electron beam, friction stirs, and ultrasonic waves. The oldest type of welding was forge welding which consists of heating up the pieces to be fixed together and then hammering them until they amalgamate (Figure 1.1). Blacksmithing has been used for centuries to join iron and steel. Arc welding and oxyfuel welding were among the first processes to develop later, and electric resistance welding followed soon after (Figure 1.2). With the advent of electricity, the process became easier and faster, and it played an important part of the industry (Figure 1.3).

Welding technology advanced quickly as the demand for reliable and inexpensive joining methods grew. Several modern welding techniques were developed, including manual methods like shielded metal arc welding, now one of the most popular welding methods, as well as semi-automatic and automatic processes such as gas metal arc welding, submerged arc welding, flux-cored arc welding and electroslag welding. Arc welding is done through the use of an electrical current, and can be performed by using inexpensive equipment. Gas welding is widely used for repairing work, especially for joining pipes and tubes. It is common in the jewelry industry, as well as for connecting plastics and other materials that cannot stand high temperatures. Resistance welding involves the use of additional sheets of metal to encase the pieces to be welded together. It is the most environmentally-friendly of all methods, but it requires costly equipment that cannot be used in all situations. Energy beam welding, such as laser beam or electron beam welding, are the most modern techniques used (Figure 1.4). These methods are fast and accurate, but the high equipment cost makes them prohibitive for many industries.

Developments continued with new techniques such as electromagnetic impact welding and friction stir welding (Figure 1.5 and 1.6). Today, progress continues while the traditional techniques are already stablished. Robot welding is commonplace in industrial settings, and researchers continue to develop new welding methods and gain greater understanding of welding. The necessity to improve the welding quality and reduce the costs for the new techniques is always demanding. Researchers are interested in finding new and defect free techniques and in improving the already existing and the

Figure 1.3: Electric resistance welding

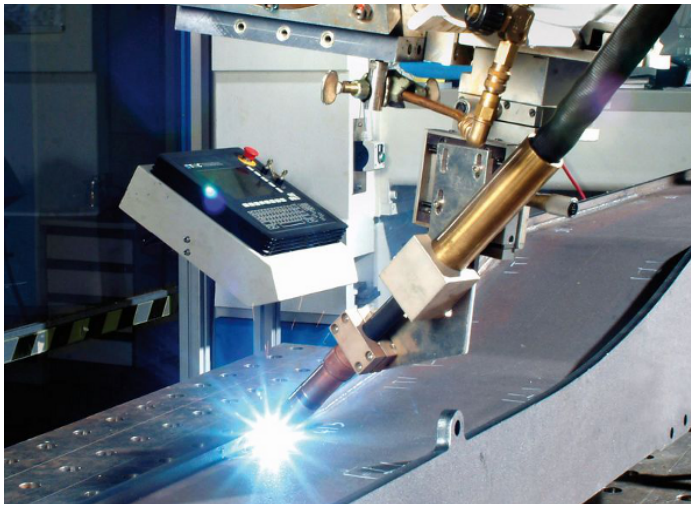

Figure 1.4: Laser beam welding

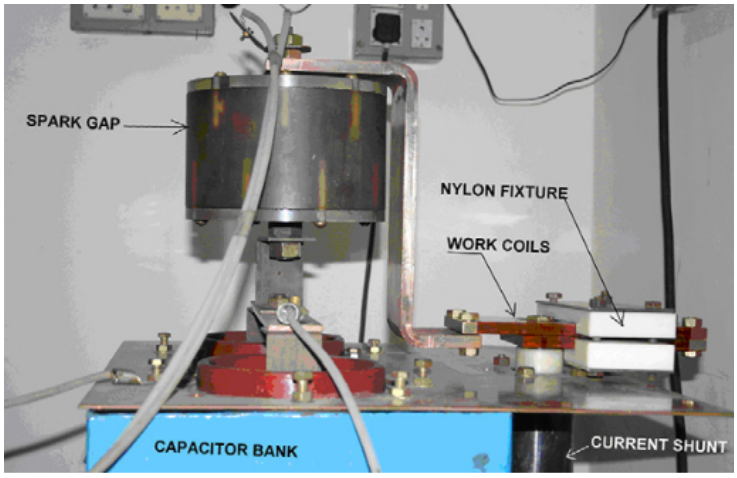

Figure 1.5: Electromagnetic impact welding

Figure 1.6: Friction stir welding

next recent types of welding.

1.1 Motivation and challenges

Information about the shape, dimensions and residual stresses in a component after welding and mechanical properties of the welded joint are of great interest in order to improve the quality and to prevent failures during manufacturing or in service. The process of welding can be analyzed either experimentally or numerically.

Welding is difficult to analyze experimentally; however, process parameters and different fixture set-ups can be evaluated without doing a large number of experiments. An experiment can be designed to answer one or more carefully formulated questions. The goals must be clarified perfectly to choose the appropriate parameters and factors. Otherwise the goal is not achieved and the experiment must be repeated. Different welded specimens are produced by varying the process parameter. The properties and microstructure changes in weld are investigated. For instance, the tensile strength of the produced joint is tested at room temperature. Microstructure of the weld is analyzed by means of optical microscopy or microhardness measurements.

The alternative to the experimental welding analysis is numerical modeling and simulation. Computer-based models provide the opportunity to improve theories of design and increase their acceptance. Simulations are useful in designing the manufacturing process as well as the manufactured component itself. To do an appropriate modeling, the physics of the problem must be well-understood.

1.1.1 Physical model

Welding simulation is a problem of complex nature; the process is highly nonlinear and coupled. Different physical phenomena occur during the welding process, involving the thermal, mechanical, electrical and metallurgical interactions. High temperatures cause phase change and metallurgical transformations; thus the material properties depend on temperature and metallurgical phase proportions. Moreover, the temperature field is a function of many welding parameters such as welding speed, welding sequence and environmental conditions. Formation of distortions and residual stresses in

weldments depend on many interrelated factors such as thermal field, material properties, structural boundary conditions, type of welding operation and welding conditions. The process is also time longing, because the cooling is usually slow and the loads and boundary conditions may change with the time and temperature.

The challenging issues in physical modeling of the welding process are divided into three parts:

Complex thermal behavior: Heat transfer mechanisms including convection, radiation and conduction have a significant role on the process behavior. Convection and radiation fluxes dissipate heat significantly through the work-pieces to the surrounding environment while conduction heat flux occurs between the work-pieces and the support. Additionally, for many welding types, phase changes may occur. During phase change, a considerable amount of latent heat is released or absorbed, with a strong non-linear thermal behavior. During welding, as the molten pool moves through the material, the growth rate and temperature gradient vary considerably across the weld pool. The growth rate increases while the temperature gradient decreases. Consequently, the microstructure that develops varies noticeably from the edge to the centerline of the weld.

Non-linear behavior and localized nature: In the welding, the mechanical behavior is non-linear due to the high strain rates and visco-plastic material. The strong non-linear region is limited to a small area and the remaining part of the model is mostly linear. However, the exact boundaries of the non-linear zone are not known a-priori. It is generally believed that strain and strain rate during the welding are high. Knowledge of strain and strain rate is important for understanding the subsequent evolution of grain structure, and it serves as a basis for verification of various models as well.

Coupled nature: The thermal and mechanical problems are strongly coupled (the thermal loads generate changes in the mechanical field). The mechanical effects coupled to the thermal ones include internal heat generation due to plastic deformations or viscous effects, heat transfer between contacting bodies, heat generation due to friction, etc. The thermal effects are also coupled to the mechanical ones; for instance, thermal expansion, temperature-dependent mechanical properties, temperature gradients in work-pieces, etc.

An adequate physical model of the welding process must account for all these phenomena including thermal, mechanical and coupling aspects.

1.1.2 Numerical model

Among several numerical modeling techniques, the Finite Element (FE) framework is found to be suitable for the simulation of welding and proven to be a versatile tool for predicting a component's response to the various thermal and mechanical loads. The FE method also offers the possibility to examine different aspects of the manufacturing process without having a physical prototype of the product. To this end, a specialized thermo-mechanical coupled model needs to be implemented in a finite element program, and the predictive capabilities of the theory and its numerical implementation must be validated.

The numerical simulation of the welding process has many complex and challenging aspects that are difficult to deal with: the welding process is described by the equilibrium and energy equations governing the mechanical and thermal problems and they are coupled. Additionally, both of them are non-linear. This has important implications upon the complexity of the numerical model. Consequently, a robust and efficient numerical strategy is crucial for solving such highly non-linear coupled finite element equations. In such process, several assumptions are commonly assumed.

It is important to distinguish between two different kinds of welding analyses carried out at *local* or *global* level, respectively.

In local level analysis, the focus of the simulation is the heat affected zone. Focusing on FSW process, the simulation is intended to compute the heat power generated either by visco-plastic dissipation or by friction at the contact interface. At this level, the process phenomena that can be studied are the relationship between welding parameters, the contact mechanisms in terms of applied normal pressure and friction coefficient, the setting geometry, the material flow within the heat affected zone, its size and the corresponding consequences on the microstructure evolution, etc.

A simulation carried out at global level studies the entire component to be welded. In this case, a moving heat power source is applied to a control volume representing the actual heat affected zone at each time-step of the analysis. The effects induced by the welding process on the structural behavior are the target of this kind of study. These effects are distortions, residual stresses or weaknesses along the welding line, among others.

The aim of this work is to develop a robust numerical tool able to simulate the welding process considering its complex features at local level as well as global level. As it is impossible to simulate all the welding processes with a

single tool, the work is focused on the simulation of two demanding and innovative welding processes at local and global level, respectively: Friction Stir Welding (FSW) and Shaped Metal Deposition (SMD). However, work is in progress to consider other welding processes and to generalize the developed tool for welding simulation.

Mechanical problem

A quasi-static mechanical analysis can be assumed as the inertia effects in welding processes are negligible due to the high viscosity characterization. At local level, the volumetric changes are found to be negligible, and incompressibility can be assumed. To deal with the incompressible behavior, a very convenient and common choice is to describe the formulation splitting the stress tensor into its deviatoric and volumetric parts. Dealing with the incompressible limit requires the use of mixed velocity-pressure interpolations. The problem suffers from instability if the standard Galerkin FE formulation is used, unless compatible spaces for the pressure and the velocity field are selected (Ladyzhenskaya-Babuška–Brezzi (LBB) stability condition). Due to this, pressure instabilities appear if equal velocity-pressure interpolations are used. Thus, the challenging issue of pressure stabilization rises up.

The welding process is characterized by very high strain rates as well as a wide temperature range going from the environmental temperature to the melting point. Hence, the constitutive laws adopted should depend on both variables. The constitutive theory applied must be specialized to capture the features of the thermo-mechanically coupled strain rate and temperature dependent large deformation. According to the split of the stress tensor, different rate-dependent constitutive models can be used for modeling of the welding process. At typical welding temperatures, the large strain deformation is mainly visco-plastic. Depending on the welding type of interest and its behavior, rigid-visco-plastic or elasto-visco-plastic constitutive models can be used. The choice of each one of these constitutive models depends on the scope of the work. Not only the prediction of the temperature evolution, but the accurate residual stress evaluation field generated during the process and the estimation of the hot-cracking risk are the objective of the welding simulation. The selected constitutive model must appropriately define the material behavior and has to be calibrated by the temperature evolution. For instance, a constitutive model that can represent the liquid, mushy and solid phases is necessary for multi-pass welding processes. The challenge arises

from the extremely non-linear behavior of these constitutive models and, therefore, from the numerical point of view, a special treatment is obligatory. Moreover, the localized large strain rates usually involved in welding processes make the problem even more complex.

Thermal problem

The thermal problem is defined by the balance of energy equation. This equation controls the temperature and the solidification evolution and it is enthalpy based. Different assumptions can be made for welding simulation at local or global level. For instance, in FSW simulation, the plastic dissipation term appearing in the energy equation has a critical role on the process behavior and it is the main source of heat generation. However, when studying the SMD process, the dissipation term can be neglected in front of the heat flux coming from the heat source (laser, arc, electron beam, etc)

The definition of the heat source is one of the key points when studying the welding process. There are various heat source types ranging from point sources to distributed ones with different degrees of sophistication. However, in global level simulations, the mesh density used to discretize the geometry is not usually fine enough to define the welding pool shape or a non-uniform heat source. This is only done if the simulation of the welding pool is the objective itself (local level analysis). If the global structure is considered, the size of the heat source is of the same dimension than the element size generally used for a thermo-mechanical analysis. Therefore, when the global model is taken into account, the resulting mesh density is usually too coarse to represent the actual shape of the heat source.

Depending on the framework used to describe the formulation of the coupled thermo-mechanical problem, a convective term might appear in the thermal governing equations. Therefore convection instabilities of the temperature appear for convection dominated problems. It is well known that in diffusion dominated problems, the solution is stable. However, in convection dominated problems, the stabilizing effect of the diffusion term becomes insufficient and oscillations appear in the temperature field. The threshold between stable and unstable solutions is usually expressed in terms of the Peclet number.

Kinematic framework

Establishing an appropriate kinematic framework for the simulation of welding is one of the main objectives of this work.

If the welding process is studied at global level, a Lagrangian framework is an appropriate choice for the description of the problem. Lagrangian settings, in which each individual node of the computational mesh represents an associated material particle during motion, are mainly used in structural mechanics. Classical applications of the Lagrangian description in large deformation problems are the simulation of vehicle crash tests and the modeling of metal forming operations. In these processes, the Lagrangian description is used in combination with both solid and structural (beam, plate, shell) elements. Numerical solutions are often characterized by large displacements and deformations and history-dependent constitutive relations are employed to describe elasto-plastic and visco-plastic material behavior. The Lagrangian reference frame allows easy tracking of free surfaces and interfaces between different materials.

In a local simulation, the main focus of the simulation is the Heat Affected Zone (HAZ) where the use of a Lagrangian framework is not always advantageous. Focusing on FSW, in the HAZ, the large distortions would require continuous re-meshing. The alternative is to use Eulerian or Arbitrary Lagrangian Eulerian (ALE) methods. Eulerian settings are widely used in fluid mechanics. Here, the computational domain and reference mesh are fixed and the fluid moves with respect to the grid. The Eulerian formulation facilitates the treatment of large distortions in the fluid motion. Its handicap is the difficulty to follow free surfaces and interfaces between different materials or different media (e.g., fluid-fluid and fluid-solid interfaces).

An Arbitrary Lagrangian Eulerian (ALE) formulation which generalizes the classical Lagrangian and Eulerian descriptions is particularly useful in flow problems involving large distortions in the presence of mobile and deforming boundaries. Typical examples are problems describing the interaction between a fluid and a flexible structure and the simulation of metal forming processes. The key idea in the ALE formulation is the introduction of a computational mesh which can move with a velocity different from (but related to) the velocity of the material particles. With this additional freedom with respect to the Eulerian and Lagrangian descriptions, the ALE method succeeds to a certain extend in minimizing the problems encountered in the classical kinematical descriptions, while combining their respective ad-

vantages at best.

In the simulation of FSW, it is adroit to introduce an apropos kinematic framework for the description of different parts of the computational domain. Despite the efficiency of the idea, the mesh moving strategy and the treatment of the domains interaction are challenging.

Coupled problem

The numerical solution of the coupled thermo-mechanical problem involves the transformation of an infinite dimensional transient system into a sequence of discrete non-linear algebraic problems. This is achieved by means of the FE spatial descritization procedure, a time-marching scheme for the advancement of the primary nodal variables, and with a time iteration algorithm to update the internal variables of the constitutive equations.

Regarding the time-stepping schemes, two types of strategies can be applied to the solution of the coupled thermo-mechanical problems:

The first possibility is a monolithic (simultaneous) time-stepping algorithm which solves both the mechanical and the thermal equilibrium equations together. It advances all the primary nodal variables of the problem simultaneously. The main advantage of this method are that it enables stability and convergence of the whole coupled problem. However, in simultaneous solution procedures, the time-step as well as time-stepping algorithm has to be equal for all subproblems, which may be inefficient if different time scales are involved in the thermal and the mechanical problem. Another important disadvantage is the considerably high computational effort required to solve the monolithic algebraic system and the necessity to develop software and solution methods specifically for each coupled problem.

A second possibility is a staggered algorithm (block-iterative or fractional-step), where the two subproblems are solved sequentially. Usually, a staggered solution (arising from an operator split and a product formula algorithm (PFA)) yields superior computational efficiency.

Staggered solutions are based on an operator split, applied to the coupled system of non-linear ordinary differential equations, and a product formula algorithm, which leads to splitting of the original monolithic problem into two smaller and better conditioned subproblems (within the framework of classical fractional step methods). This leads to the partition of the original problem into smaller and typically symmetric (physical) subproblems. After this, the use of different standard time-stepping algorithms developed

for the uncoupled subproblems is straightforward, and it is possible to take advantage of the different time scales involved. The major drawback of these methods is the possible loss of accuracy and stability. However, it is possible to obtain unconditionally stable schemes using this approach, providing that the operator split preserves the underlying dissipative structure of the original problem.

Activation technology

When simulating multipass welding processes or, similarly, metal deposition processes, the creation of the new layers of filler material on a substrate is a challenging issue. At each pass a new layer of the filler material is deposited and added to the previous substrate allowing the fabrication of the desired geometry. Therefore, the computational domain varies in time due to the introduction of the new material.

An activation methodology must be formulated to simulate the deposition of the different layers of filler material. There are two different approaches to simulate the multi-pass welding: *quiet elements* and *born-dead elements* techniques.

When using quiet elements, all the elements including the welding layers, which will be deposited during the process simulation, are included into the initial computational model. The elements are active during the whole analysis but the stiffness and the thermal conductivity is very low so that the inactive (*quiet*) elements do not affect the rest of the model. According to the metal deposition process, the activated elements are re-established with their real thermo-physical properties. The drawbacks of the method are following. Firstly, the simulation process is performed assembling all the elements and therefore, solving the full system of equations. This leads to a high computational cost. Secondly, decreasing the stiffness of the quiet elements gives an ill-conditioned system matrices with numerical problems as a result such as a reduction of the convergence ratio of iterative solvers. Finally, fictitious strains and temperature gradients in the quiet elements are accumulated and produce initial spurious stresses and heat fluxes when the elements are activated.

Using *born-dead elements*, the elements that are inactive are not part of the system of equations until they are activated. The elements in this activation strategy are classified into: active, inactive and activated elements. The active elements (elements of the base material) are assembled into the

global matrix while the inactive elements are not considered as a part of the model. At each time-step a number of activated elements are switched on according to the deposition of the filler material according to the user-defined welding-path. Only active and activated elements are assembled into the solution model. The drawback of the born-dead technique is that the system matrices have to be redimensioned and reallocated each time an element is activated.

In this work, the born-dead elements technique is used.

Particle tracing

One of the main issues in the study of FSW at local level, is the heat generation. The generated heat must be enough to allow for the material to flow and to obtain a deep heat affected zone. Insufficient heat forms voids as the material is not softened enough to flow properly. The visualization of the material flow is very useful to understand its behavior during the weld. A method approving the quality of the created weld by visualization of the joint pattern is advantageous. It can be used to investigate the appropriate process parameters to create a qualified joint. However, following the position of the material during the welding process is not an easy task, neither experimentally or numerically.

The experimental material visualization is difficult and needs metallographic tools. This is why establishing a numerical method for the visualization of the material trajectory in order to gain insight to the heat affected zone and the material penetration within the work-piece thickness is one of the main objective of the work. Particle tracing is a method used to simulate the motion of material points, following their positions at each time-step of the analysis. This method can be naturally applied to the study of the material flow in the welding process. In the Lagrangian framework, as the mesh nodes represent the material points, the trajectories are the solution of the governing system of equations. When using Eulerian and ALE framework the solution does not give directly information about the material position. However, the velocity field obtained can be integrated to get an insight of the extent of material mixing during the weld.

Integration of the velocity field is proposed at postprocess level to follow the material motion (displacement field). This obliges the modeler to use an appropriate time integration method for the solution of the ODE equation in order to track the particles. Moreover, a search algorithm must be executed

to find the position of the material points in the Eulerian or ALE meshes.

1.2 State of the art

In this section the state of the art includes two innovative welding process: FSW and SMD. Firstly, the industrial background of the FSW is briefly described in section 1.2.1 and then in sections 1.2.2 and 1.2.3 the experimental, numerical and analytical analyses of FSW existing in the literature are mentioned. Section 1.2.4 provides the industrial background of SMD and section 1.2.5 summarizes experimental and numerical analyses of SMD performed up to date.

1.2.1 Industrial background of FSW

Friction stir welding (FSW) is a solid state joining technology in which no gross melting of the welded material takes place. It is a relatively new technique (developed by The Welding Institute (TWI), in Cambridge, UK, in 1991) widely used over the past decades for joining aluminium alloys. Recently, FSW has been applied to the joining of a wide variety of other metals and alloys such as magnesium, titanium, steel and others. FSW is considered to be the most significant development in metal joining in decades and, in addition, is a "green" technology due to its energy efficiency, environmental friendliness, and versatility. This process offers a number of advantages over conventional joining processes (such as e.g. fusion welding). The main advantages, often mentioned, include: (a) absence of the need for expensive consumables such as a cover gas or flux; (b) ease of automation of the machinery involved; (c) low distortion of the work-piece; and (d) good mechanical properties of the resultant joint [144] [184]. Additionally, since it allows avoiding all the problems associated to the cooling from the liquid phase, issues such as porosity, solute redistribution, solidification cracking and liquation cracking are not encountered during FSW[1]. In general, FSW has been found to produce a low concentration of defects and is very tolerant to variations in parameters and materials. Furthermore, since welding occurs by the deformation of material at temperatures below the melting temperature, many problems commonly associated with joining of dissimilar alloys can be avoided, thus high-quality welds are produced. Due to this fact, it has been widely used in different industrial applications where met-

[1]However it must be noted that, as in the traditional fusion welds, there also exist a softened heat affected zone (HAZ) and a tensile residual stress parallel to the weld.

allurgical characteristics should be retained, such as in aeronautic, naval and automotive industry.

During FSW, the work-piece is placed on a backup plate and it is clamped rigidly to eliminate any degrees of freedom. A nonconsumable tool, rotating at a constant speed, is inserted into the welding line between two pieces of sheet or plate material (which are butted together) and generates heat. This heat is produced, on one hand, by the friction between the tool shoulder and the work-pieces, and, on the other hand, by the mechanical mixing (stirring) process in the solid state. This results in the plastification of the material close to the tool at very high strain rates and leads to the formation of the joint. In detail, the plasticized material is stirred by the tool and the heated material is forced to flow around the pin tool to its backside thus filling the hole in the tool wake as the tool moves forward. As the material cools down, a solid continuous joint between the two plates emerges.

Usually the tool is tilted at an angle of $1 - 3^o$ away from the direction of travel, although some tool designs allow it to be positioned orthogonally to the work-piece. The welding tool consists of a shoulder and a pin. The length of the pin tool is slightly less than the depth of weld and the tool shoulder is kept in close contact with the work-piece surface (see Figure 1.7). The tool serves three primary functions, that is, heating of the work-piece, movement of material to produce the joint (stirring), and containment of the hot metal beneath the tool shoulder. The function of the pin tool is to heat up the weld metal by means of friction and plastic dissipation, and, through its shape and rotation, force the metal to move around its form and create a weld. The function of the shoulder is to heat up the metal through friction and to prevent it from being forced out of the weld. The tool shoulder restricts metal flow to a level equivalent to the shoulder position, that is, approximately to the initial work-piece top surface.

Depending on the geometrical configuration of the tool, material movement around the pin can become complex, with severe gradients in temperature and strain rate. This environment creates a challenge for modelers due to the resulting coupled thermo-mechanical nature, the large deformation and strain rates near the pin. Since FSW is not a symmetric process, two sides of the tool are differentiated. One can see in Figure 1.8 that the work-pieces being joined by the weld are either on the *retreating* or *advancing* side of the rotating tool. The retreating side is the one where the tool rotating direction is opposite to the tool moving direction and parallel to the metal flow direction. In contrast, the advancing side is the one where the

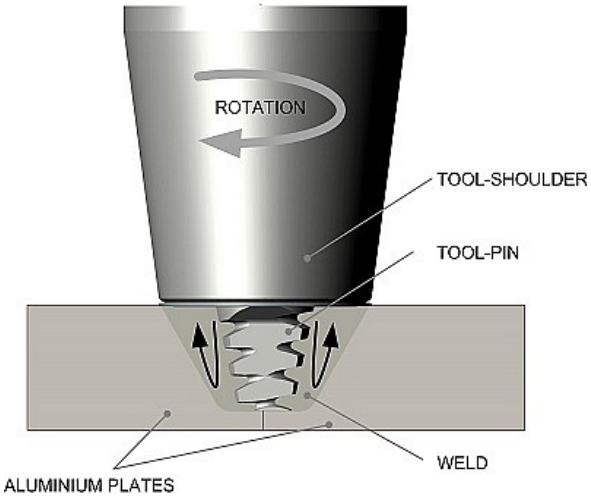

Figure 1.7: Schematic representation of friction stir welding process

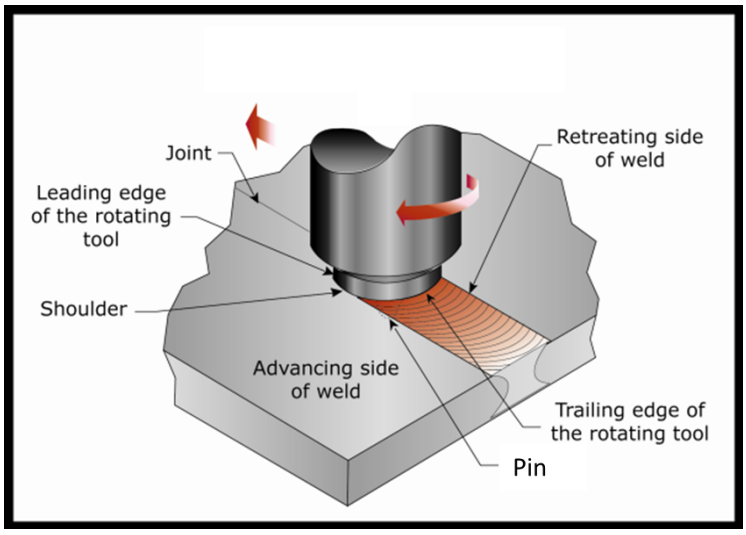

Figure 1.8: Definition of Friction Stir Welding zones [72]

tool rotation direction is the same as the tool moving direction and opposite to the metal flow direction. This unsymmetric nature results in a different material flow on the different sides of the tool and has a large effect on many applications, especially lap joints [33]. The periodic "onion flow" pattern that is left behind as the tool advances is schematically illustrated in Figure 1.8.

During the early development of FSW, the process appeared simple, compared to many conventional welding practices. However, as development continued, the complexity of FSW was realized. It is now known that properties following FSW are a function of both controlled and uncontrolled variables (response variables) as well as external boundary conditions. For example, investigators have now illustrated that post-weld properties depend on:

- Tool travel speed: influences total heat.
- Tool rotation rate: influences total heat.
- Tool design: shoulder diameter, scroll or concave shoulder, features on the pin and pin length influence the extent of the material.
- Tool tilt: It influences the contact pressure. There exist lower contact pressure (or incomplete contact) on the leading edge of the shoulder due to tool tilt (typically between 0° and 3°).
- Material thickness: influences cooling rate and through-thickness temperature gradients.

These parameters must be carefully calibrated according to the welding process and the selected material, respectively. The strong coupling between the temperature field and the mechanical behavior is the key-point in FSW and its highly non-linear relationship makes the process setup complex. The operative range for most of the welding process parameters is rather narrow requiring a tedious characterization and sensitivity analysis. This is why, despite the apparent simplicity of this novel welding procedure, computational modeling is considered a very helpful tool to understand the leading mechanisms that govern the material behavior, attracting more and more the research interest.

Finite element modeling is an option which can help to determine process parameters that would otherwise require further experimental testing for validation and analysis. The weld quality depends largely on how the material

is heated, cooled and deformed. Hence a prior knowledge of the temperature evolution within the work-piece would help in designing the process parameters for a welding application. Research in the field of FSW joints has been limited possibly due to proprietary publishing restriction within industry. For this reason Finite Element Analysis (FEA) could be also very beneficial. Two process parameters of interest for FSW welds are tool travel rates and rotational tool velocities. With respect to this, a lot of emphasis has been laid on FEA analysis, as it may broaden the scope of application of FSW. Another important process parameter in FSW is the heat flux. This can be also easily included in the FEA. The heat flux should be high enough to keep the maximum temperature in the work-piece around 80% to 90% of the melting temperature of the work-piece material, so that welding defects are avoided [39].

Moreover, analytical and numerical methods have a role to play, although numerical methods dominate due to the accuracy and ease-to-use of modern workstations and software. Numerical modeling is based on discretized representations of specific welds, using finite element, finite difference, or finite volume techniques. These methods can capture much of the complexity in material constitutive behavior, boundary conditions, and geometry, but in practice, a limited range of conditions tends to be studied in depth. Therefore, it is good modeling practice to explore simplifications to the problem that give useful insight across a wider domain, for example, making valid two-dimensional (2-D) approximations to inherently three dimensional (3-D) behavior. It is also essential to deliver a model that is properly validated and whose sensitivity is known to uncertainty in the input material and process data—ideals that are rarely carried through in practice.

1.2.2 Experimental analysis of FSW

In the attempt to better understand FSW, many investigators have used experimental techniques to visualize the material flow and to estimate characteristics of FSW. Tang et al. [173] performed different measurements of temperature field of the work-piece while Donne et al. [73] measured residual stresses in FSW for 2024-T3 and 6013-T6 aluminium.

Most of the studies done so far are based on the experimental study of material flow tracing. Two different tracer techniques were established by different researchers for visualization of the material flow; the first was a tracer technique by marker material where a dissimilar material is inserted

into the weld line. The second technique was to weld two dissimilar materials with the FSW process and then see the material mixing. The marker materials were different Al-composites [123], [148], [157], steel balls [62], copper foil [94], [70], plasticine and brass rods [108]. The used dissimilar base materials were different magnesium alloys [106], aluminum to copper alloys [143], [1].

Reynolds et al. [148] used Al-composites, a 1.8 mm thick 5454-O in a base plate of 2195-T8. They stated that the material in the centerline was transported backwards approximately one pin diameter while material on the advancing side of the pin rounded the pin and ended up almost in its original insertion point.

Colligan [62] developed a concept to understand the material flow by inserting steel balls as tracers embedded in the weld path. They used steel shot makers embedded in the weld zone of AA-6061-T6 and AA-7075-T6 aluminum alloys. The weld process was then stopped at specific intervals. The weld line was there after radiographed to see the steel balls' movement. The result showed two types of material flow through X-ray analysis; simple extrusion and chaotic mixing, depending on location in weld zone.

Dickerson et al. [70] used copper stripes as tracer material. They performed experiments with 0.1 mm thick copper sheets placed transversally and longitudinally to the weld line to examine the material flow. The method included a stop action technique were the flow was "frozen" in the weld path. They obtained the flow pattern by using metallography, 2D X-rays analysis and X-rays tomography, showing that copper sheets embedded into aluminium AA-2024-T3 could be successfully used as marker material. Some impressive 3D images of the exit hole demonstrated the material flow during welding. They showed how the size of the deformation region increased toward the tool shoulder. The analysis package was able to produce planar sections (CT Scans) through the weld. Similarly, Guerra et al. [94] used copper foils placed along the joint line of friction stir weld in AA-6061 Al alloy. Once the steady state of welding was established, they stopped the tool. Using metallographic analysis, they demonstrated that several flow zones could be distinguished around the pin: a rotational zone where the plate material rotated with the velocity of the pin, a transition zone where no marker material was found and which was subjected to a very different thermo-mechanical history. They showed that there was a difference between the advancing and retreating sides of the tool. Moreover, the two sides had different thermo-mechanical histories and properties. This investigation also showed that the shoulder was the prime source for the material flow near the

top of the weld, and the pin geometry only had a minor effect. But on the lower part the geometry of the pin was the dominant factor for material movement. Schmidt et al. [155] used copper stripes to estimate the flow velocity in FSW welds. Two different procedures were developed to estimate the average velocity. The experimental work supported the presence of sticking condition at the tool/matrix interface. A demonstration of the tremendous potential and successful applications of the FSW process for aluminium airframe structures could be found in Talwar et al. [172]. Seidel and Reynolds [157] carried out similar experiments. However, they embedded AA-5454 aluminum alloy in AA-2195 aluminum alloy. The inserts were placed before welding in strategic positions in the depth of the weld at various positions relative to the weld line. The final position was determined by successive sections which were digitally recorded, and was found to be highly dependent on the welding conditions. They observed a difference of the material flow between the advancing side and the retreating side. The deformation region was quite narrow; there was a bulge in the material in the wake of the pin; and a small amount of material was dragged forward on the advancing side. They also provided 3D maps of the marker flow which indicated a modest vertical flow. Comparisons were made between welds of different pitches (forward movement per revolution), which showed that the hotter the weld (i.e. the lower the weld pitch), the greater the mixing, particularly in the vertical direction. The authors concluded that the increased mixing at the lower weld pitch was caused by greater mobility due to the lower flow stress at the higher temperature. An alternative explanation was the lower weld pitch increased the augering action of the tool. In any case, the experiment showed that different welding parameters resulted in significantly different flow characteristics.

London et al. [123], [124] used AI-30%SiC markers because the material could be easily viewed when etched while not greatly altering the material flow. Both continuous and discrete markers were used. They showed how all the material in-line with the pin flowed around the retreating side. London et al. [123] concluded that the material can make several revolutions of the tool before rejoining the bulk flow. They demonstrated the layered material flow left from a marker that was originally placed along the weld centreline. When the marker was shifted toward the advancing side, the distribution of material increased. In the second paper, London et al. [124] used AI-20%W, which could be distinguished from the aluminium when analyzed by X-ray. This enabled a 3D analysis of the weld without sectioning. Finally, the work

demonstrated significant uplift of material away from the pin, while near the tool on the advancing side the material was pushed downwards.

In detail, they placed 0.38 mm steel balls at various locations in the material prior to welding. After welding the final position was determined by X-ray. Observations revealed that:

- The markers that started on the retreating side of the weld were not distributed as widely as those on the advancing side;
- The material that was in-line with the pin, was swept around the retreating side;
- Most of the markers were pushed upwards, irrespective of their start position.

Tungsten wire was used to visualize the flow in Schneider and Nunes [156] with the final position being determined by X-ray. The tungsten wire broke into fragments near the rotation zone and then flowed around the tool. The final position of the wire was perpendicular to the welding direction. It was unclear how much the flow was influenced by the fracturing of the tungsten wire. Finally, Nowak et al. [141] examined the flow during the FSW of polycarbonate and found similar flow fields to those observed in aluminium. Because of polycarbonate's different properties, it was necessary to use an unthreaded pin. This could be a useful technique for visualizing the flow because of the opportunities afforded by its transparent properties.

Johnson [106] welded dissimilar materials, not in order to understand the FSW process and flow, but to get good quality magnesium welds. He concluded that success was due to which material was placed on the advancing side and the retreating side respectively. This shows that the FSW process was an asymmetrical process and the sides had different heat and material flow due to the rotation of the tool. Abdollah et al. [1] welded aluminium to copper and produced welds with reasonable weld quality. In the mix zone intermetallic compounds were observed. Ouyang et al. [143] also tried to FSW aluminium to copper but found it difficult to produce good welds due to the brittle intermetallic compounds. They suggested that some kind of interlayer should be used to produce sound welds.

With the friction stir weld of dissimilar materials to analyze the material flow, Li et al. [119] demonstrated very complex vortex flows associated to the

FSW of AA-2024 aluminum to AA-6061 aluminum, showing that the flow pattern depends on the welding parameters.

In the work of McClure et al. [128] the material on the advancing side and part of the retreating side of the pin was found to rotate several times around the tool before being deposited. In an experiment with an unthreaded tool the rotation zone around the tool was absent. In another investigation that used copper marker material, Guerra et al. [93] showed how the material along the joint line flowed around the retreating side of the tool. The authors found that the material near the shoulder did not have full contact with the pin.

Liechty et al. [120] tried another way of modeling the material flow. Whereas most experimental investigations were carried out metallic materials, Liechty et al. used plasticine as base material. Plasticine was an amorphous clay material which were previously used to model extrusion of metals. The stress-strain behavior was similar to metals and the experiments could be performed at much lower cost. In these trials no dissimilar material was present. Instead the marker plasticine was colored. The experiment showed that high rotation speeds resulted in the material rotating around the tool many revolutions travelling forward with it. Also a vertical (surface-weld root) motion during welding was observed.

1.2.3 Analytical and Numerical modeling of FSW

In FSW the tool generates heat via a combination of friction at the tool surface and viscous dissipation within the deformed material. This heat is conducted into the tool and welded material, and is then convected from the top surface or conducted into the backing plate. The majority of both analytical and numerical models are used to describe this heat flow and to see its effect on the entire piece during and after FSW. The following section lists some works performed to model FSW. They are divided in: analytical and numerical modeling of FSW, thermal and thermo-mehanical modeling, global analysis and local modeling of the heat input and use of different kinematic frameworks.

Analytical modeling

Thermal models are used to describe the heat flow in the FSW process. Midling and Grong [129] presented a transient analytical model that used a

modified version of Rykalin's infinite rod solution and predicted the weld temperature and microstructure. The microstructural evolution was predicted for 6082-T6 and AI-SiC, and indicated that a narrow HAZ was obtained when a high specific power was used in conjunction with a short duration heating cycle.

Grong [91] described how Rosenthal's [149] analytical solution to the heat equation could be used to predict the thermal profile. Three different analytical solutions existed for thin, medium and thick plate. The appropriate solution was determined by the power and speed of the heat source, and the physical dimensions and thermal properties of the material being welded using a dimensionless heat flow map. When using the medium plate solution, it was necessary to superimpose virtual heat sources to include the effect of plate thickness and width. Finally, analytical solutions assumed constant thermal properties.

Early work by Russell and Shercliff [150], [151] used a point heat source which was considered adequate because the temperature in the HAZ was of interest. The analytical solution was extended by McClure et al. [127], and Gould and Feng [90] by distributing the heat source over the shoulder. The distributed heat source was integrated to find the temperature at a particular position in the material. The heat source intensity increased with the distance from the centre of the tool in McClure et al. [127] and was imposed on a ring around the shoulder in Gould and Feng [90]. Imposing the heat source as a ring resulted in a large temperature peak around the shoulder. When the heat input was correctly adjusted, reasonable correlation was obtained with experimental results.

Finally, an inverse problem approach was used by Fonda and Lambrakos [78]. Rather than using thermocouple measurements, they examined the weld microstructure and assumed that the edge of the heat affected zone corresponded to a peak weld temperature of 250°C. Using this knowledge, they worked backwards to find the heat input and weld thermal profile at all points in the weld. Stewart et al. [171] also used an analytic thermal model, however the main emphasis of this work was material flow.

Song and Kovacevic [170] developed a mathematical model to describe the detailed three-dimensional transient heat transfer process. Their work was both theoretical and experimental. An explicit central differential scheme was used in solving the control equations. The heat input from the tool shoulder was modeled as frictional heat and the heat from the tool pin as uniform volumetric heat generated by the plastic deformation near the pin.

Moving coordinates and a non-uniform grid mesh were introduced to reduce the difficulty of modeling the heat generation due to the movement of the tool pin.

Recently Seret et. al [160] validated a computational model applied to the simulation of FSW, by comparing its numerical solutions to analytical solutions for some thermo-mechanical problems. Momentum balance, flow incompressibility and energy balance are used as governing laws.

Numerical modeling

As previously discussed, numerical modeling and simulation is an important tool for understanding the mechanisms of the FSW process. It enables obtaining both the qualitative and quantitative insight of the welding characteristics without performing costly experiments. Flexibility of the numerical methods (in particular FEM) in treating complex geometries and boundary conditions defines an important advantage of these methods against their analytical counterparts.

The FSW simulation typically involves studies of the transient temperature and its dependence on the rotation and advancing speed, residual stresses in the work-piece, etc. This simulation is not an easy task since it involves the interaction of thermal, mechanical and metallurgical phenomena. Up to now several researchers have carried out computational modeling of FSW.

Thermal modeling To date, most of the research interest devoted to the topic was focused on the heat transfer and thermal analysis in FSW while the mechanical aspects were neglected. Among others, Gould and Feng [90] proposed a simple heat transfer model to predict the temperature distribution in the work-piece. Chao and Qi [37], [38] developed a moving heat source model in a finite element analysis and simulated the transient evolution of the temperature field, residual stresses and residual distortions induced by the FSW process. Their model was based on the assumption that the heat generation came from sliding friction between the tool and material. This was done by using Coulomb's law to estimate the friction force. Moreover, the pressure at the tool surface was set constant and thereby enabled a radially dependent surface heat flux distribution generated by the tool shoulder. In this model the heat generated by the pin was neglected.

Nguyen and Weckman [137] demonstrated a transient thermal FEM model for friction welding which was used to predict the microstructure of 1045 steel. Measured power data was used to calculate the heat input and a constant temperature boundary condition at the welding interface was invoked. In another FEM thermal model by Mitelea and Radu [132] friction welding of dissimilar materials was modeled. The paper compared different heat flux distributions to determine which gave the best agreement with experimental results. To conclude both analytical and numerical techniques were used to describe the heat flow in friction welding, with a more accurate solution being obtained with the latter. Because friction welding is a short duration process, a transient model was more appropriate than one that used a steady state solution.

Colegrove et al. [59], [61] and Frigaard et al. [82] developed 3D heat flow models for the prediction of the temperature field. They used the CFD commercial software FLUENT for a 2D and 3D numerical investigation on the influence of pin geometry, comparing different pin shapes in terms of their influence upon the material flow and welding forces on the basis of both stick and slip conditions at the tool/work-piece interface. It was only the tool pin that was modeled. Several different tool shapes were considered. The modeling result showed that the difference between the result corresponding to slip and stick conditions was small and the pressure and forces were similar. In spite of the good obtained results, the accuracy of the analysis was limited by the assumption of isothermal conditions. Midling [130] and Russell and Sheercliff [151] investigated the effect of tool shoulder of the pin tool on the heat generation during the FSW operation. Generally, those early flow models and others (e.g. Askari et al. [16]) were uncoupled or sequentially coupled to the heat solvers, and limited by the computational power and software capabilities of that time.

Thermo-mechanical modeling More recently, a coupled thermomechanical modeling and simulation of the FSW process can be found in Zhu and Chao [187], Jorge Jr. and Balancín [107] or De Vuyst et al. [67], [66]. Zhu et. al [187] used a 3D nonlinear thermal and thermo-mechanical numerical model using the finite element analysis code WELDSIM. The objective was to study the variation of transient temperature and residual stress in a friction stir welded plate of 304L stainless steel. Based on the experimental records of transient temperatures, an inverse analysis method for thermal nu-

merical simulation was developed. After the transient temperature field was determined, the residual stresses in the welded plate were calculated using a three-dimensional elasto-plastic thermo-mechanical model. In this model the plastic deformation of the material was assumed to follow the Von Mises yield criterion and the associated flow rule.

In a more sophisticated way, De Vuyst et al. [67], [66] used the coupled thermo-mechanical FE code MORFEO to simulate the flow around tools of simplified geometry. The rotation and advancing speed of the tool were modeled using prescribed velocity fields. An attempt to consider features associated to the geometrical details of the probe and shoulder, which had not been discretized in the FE model in order to avoid very large meshes, was taken into account using additional velocity boundary conditions. In spite of that, the mesh used resulted to be large: a mesh of roughly 250,000 nodes and almost 1.5 million of linear tetrahedral elements was used. A Norton-Hoff rigid-visco-plastic constitutive equation was considered, with averaged values of the consistency and strain rate sensitivity constitutive parameters determined from hot torsion tests performed over a range of temperatures and strain rates. The computed streamlines were compared with the flow visualization experimental results obtained using copper marker material sheets inserted transversally or longitudinally to the weld line. The simulation results correlated well when compared to markers inserted transversely to the welding direction. However, when compared to a marker inserted along the weld center line only qualitative match could be obtained. The correlation could have been improved by modeling the effective weld thickness of the experiment, using a more realistic material model, for instance, by incorporating a yield stress or temperature dependent properties, more exact prescription of the velocity boundary conditions or refining the mesh in specific zones, for instance, under the probe. The authors concluded that it was essential to take into account the effects of the probe thread and shoulder thread in order to get realistic flow fields.

Fourment [79] performed the simulation of transient phases of FSW with FEM using an ALE formulation, in order to take the large deformation of a 3D coupled thermo-mechanical model into account. This method permitted both transient and steady state analysis. The formulation was developed in [80] and [92] to simulate the different stages of the FSW process. Assidi [18] presented a 3D FSW simulation based on friction models calibration using Eulerian and ALE formulation. An interesting comparison of the heat energy generated by the FSW between numerical methods and experimental data

was presented in Dong et al. [71] and Chao et al. [39].

In [39], Chao used a FE formulation to model the heat transfer of the FSW process in two boundary values problems: a steady state problem for the tool and transient one for the work-piece. To validate the result, the temperature evolution was recorded in the tool and in the work-piece. The heat input from the tool shoulder was assumed to be linearly proportional to the distance from the center of the tool due to heat generation by friction. To model the work-piece the code WELDSIM was used. It was a transient, nonlinear, 3D FE code. In this model only half the work-piece was modeled due to symmetry meaning that the advancing and retreating sides of the weld were not differentiated. The conclusions from this work indicated that 95 % of the heat generated goes into the work-piece and only 5% goes to the tool. It gave a very high heat efficiency estimate.

Global level modeling Most of the above-mentioned works were performed at global level. These studies typically analyzed the effect of the welding process on the structural behavior in terms of distortions, residual stresses or weakness along the welding line, among others. As the simulations carried out at global level consider the generated heat as input parameter, several techniques were used to determine the heat input to the model. One way was to measure the temperature experimentally, and adjust the heat input of the model till the numerical and experimental temperature profiles match [167], [168], [169], [37], [38], [59]. Another technique involved estimating the power input analytically and then artificially limiting the peak temperature [167], [82] or introducing latent heat effects [167], [168] to avoid over-predicting the weld temperature. The most satisfactory approach involved measuring the weld power experimentally and using this as an input to the model [122], [163], [111], [112], [113].

Khandkar et al. [112] used a finite element method based on a 3D thermal model to study the temperature distributions during the FSW process. The moving heat source generated by the rotation and linear traverse of the pin-tool was correlated to input torque data obtained from experimental investigation of butt-welding. The moving heat source included heat generation due to torques at the interface between the tool shoulder and the work-piece, the horizontal interface between the pin bottom and the work-piece, and the vertical interface between the cylindrical pin surface and the work-piece. Temperature-dependent properties of the weld-material were used for the

numerical modeling.

In Khandkar et al. [113] and Hamilton et al. [95] a torque-based heat input was used. Various aluminium alloys were included into the model and the maximum welding temperature could be predicted from tool geometry, welding parameters and material parameters. The thermal model involved an energy-slip factor which was developed by a relationship between the solidus temperature and the energy per unit length of the weld. In Khandkar et al. latest models, the thermal models were coupled with the mechanical behavior and thereby not only the heat transport was modeled, the residual stress was also an outcome of the model [114].

Reynolds et al. used two models in [147] to explain the FSW process. The first was a thermal model to simulate temperature profiles in friction stir welds. The total torque at the shoulder was divided into shoulder, pin bottom and vertical pin surface. The required inputs for the model were total input power, tool geometry, thermo-physical properties of the material being welded, welding speed and boundary conditions. The output from the model could be used to rationalize observed hardness and microstructure distributions. The second model was a fully coupled, two-dimensional fluid dynamics based model that was used to make parametric studies of variations in properties of the material to be welded (mechanical and thermo-physical) and variations in welding parameters. This was done by a non slip boundary condition at the tool work-piece interface. The deformation behavior was based on deviatoric flow stress using the Zener-Hollomon parameter. Results from this model provided insight regarding the effect of material properties on friction stir weldability and on potential mechanisms of defect formation.

Local level modeling Since the temperature is crucial in the FSW simulation, the heat source needs to be modeled accurately. This consideration obliges the researchers to study the process at the local level where the simulation is concentrated on the stirring zone. For this type of simulation, the heat power is assumed to be generated either by the visco-plastic dissipation or by the friction at the contact interface. At this level the majority of the process phenomena can be analyzed: the relationship between rotation and advancing speed, the contact mechanisms, the effect of pin shape, the material flow within stir zone, the size of the stir zone and the corresponding consequences on the microstructure evolution, etc.

Most models of FSW consider the FEM in a Lagrangian mesh [125],

[88] and [83], which is used to study the process globally and to predict the weld temperature and deformation structure. However, the number of simulations using other numerical methods such as finite volume or other kinematic frameworks such as Eulerian or ALE is also considerable.

In the model by Maol and Massoni [125] (FEM with a Lagrangian mesh), the material was assumed to be visco-plastic, with temperature-dependent properties. A frictional interface was used between the two parts and its value was determined experimentally from the pressure and velocity between the two parts. Bendzsak and North [24] used the finite volume method to predict the flow field in the fully plasticized region of a friction weld. Similar and dissimilar welds were analyzed. In the similar welds the viscosity was found from a heuristic relationship, which was independent of temperature. The dissimilar welds used a transient thermal model, a complex viscosity relationship and an Eulerian-Lagrangian mesh.

A thermo-mechanical model for FSW was proposed by Dong et al. [72]. There, an axis-symmetrical FE Lagrangian formulation was used. Ulysse in [178] modeled 3D FSW for aluminium thick plates. Forces acting on the tool were studied for various welding and rotational speeds. The deviatoric stress tensor was used by Ulysse to model the stir-welding process using 3D visco-plastic modeling. Parametric studies were conducted to determine the effect of tool speed on plate temperatures and to validate the model predictions by comparing with available measurements. In addition, forces acting on the tool were computed for various welding and rotational speeds. It was found that pin forces increased with increasing welding speeds, but the opposite effect was observed for increasing rotational speeds.

Askari et al. [17] used the CTH finite volume hydrocode coupled to an advection-diffusion solver for the energy balance equation. This model predicts important fields like strain, strain rate and temperature distribution. The elastic response was taken into account in this case. The results proved encouraging with respect to gaining an understanding of the material flow around the tool. However, simplified friction conditions were used. They used particle tracking and the mixing fraction to visualize the flow. The mixing fraction determines the ratio of advancing to retreating side material in the welded joint. These techniques enabled very impressive flow visualization, with the large dispersion of material that occurs with an advancing side marker being correctly predicted. The work also predicted that material, particularly that starting on the advancing side, flows more than one revolution around the tool.

Xu et al. [180] used finite element models to describe the material flow around the pin. This was done by using a solid mechanical 2D FE model. It included heat transfer, material flow, and continuum mechanics. The pin was included but not the threads of the pin. Xu and Deng [181], [182] developed a 3D finite element procedure to simulate the FSW process using the commercial FEM code ABAQUS, focusing on the velocity field, the material flow characteristics and the equivalent plastic strain distribution. The authors used an ALE formulation with adaptive meshing and considered large elasto-plastic deformations and temperature dependent material properties. However, the authors did not perform a fully coupled thermo-mechanical simulation, super imposing the temperature map obtained from the experiments as a prescribed temperature field to perform the mechanical analysis. The numerical results were compared to experimental data available, showing a reasonable good correlation between the equivalent plastic strain distributions and the distribution of the microstructure zones in the weld. They examined the velocity gradient around the pin and found that it was higher on the advancing than retreating side and higher in front than behind the pin. Maps of the strain on the transverse cross section were compared against typical weld macrosections.

Seidel and Reynolds [158] also used the CFD commercial software FLUENT to model the 2D steady-state flow around a cylindrical tool. The paper describes the progressive development of a finite volume model in FLUENT that used a visco-plastic material whose viscous properties were based on the Sellars-Tegart relationship. Even though the model was 2D, heat generation and conduction were included. To avoid over-predicting the weld temperature, the viscosity was reduced by 3 orders of magnitude near the solidus. The model correctly predicted material flow around the retreating side of the tool.

Bendzsak et al. [21], [22] used the Eulerian code Stir3D to model the flow around a FSW tool, including the tool thread and tilt angle in the tool geometry and obtaining complex flow patterns. The temperature effects on the viscosity were neglected. They used the finite volume method to predict the flow field in the fully plasticized region of a friction weld. Similar and dissimilar welds were analyzed. In the similar welds the viscosity was found from a heuristic relationship, which was independent of temperature. The dissimilar welds used a transient thermal model, a complex viscosity relationship and an Eulerian-Lagrangian mesh.

Schmidt and Hattel [154] presented a 3D fully coupled thermo-mechanical

FE model in ABAQUS/Explicit using the ALE formulation and the Johnson-Cook material law. The flexibility of the FSW machine was taken into account be connecting the rigid tool to a spring. The work-piece was modeled as a cylindrical volume with inlet and outlet boundary conditions. A rigid back-plate was used. The contact forces were modeled using a Coulomb friction law, and the surface was allowed to separate. Heat generated by friction and plastic deformation were considered. The simulation modeled the dwell and weld phases of the process. A constant contact conductance was used everywhere under the sheet. They used the generated heat from three different areas, the shoulder, pin and pin tip, and used both sticking and sliding conditions. Despite the wealth of information that this model can provide (e.g. material velocity, plastic strains, and temperatures across the weld), a major shortcoming for it was the long processing time for reaching the steady-state (14 days on a 3 GHz Pentium PC to reach only 10 seconds of model time).

The model developed by Chen and Kovacevic in [42] uses the commercial FEM software ANSYS for a thermo-mechanically coupled Lagrangian finite element model of aluminium alloy AA-6061-T6. The welding tool was modeled as a heat source. The model only included the shoulder and so the effect of the pin was ignored. This simple model severely limited the accuracy of the stress and force and the strain rate dependence was not included in the material model. However, the authors were able to investigate the effect of the heat moving source on the work-piece material. Finally the model predicted the welding forces in the x, y and z directions.

Nikiforakis [139] used a finite difference method to model the FSW process. Despite the fact that he was only presenting 2D results, the model proposed had the advantage of minimizing calibration of model parameters, taking into account a maximum of physical effects. A transient and fully coupled thermo-fluid analysis was performed. The rotation of the tool was handled through the use of the overlapping grid method. A rigid-visco-plastic material law was used and sticking contact at the tool work-piece interface was assumed. Hence, heating was due to plastic deformation only.

Heurtier et al. [96] used a 3D semi-analytical coupled thermo-mechanical FE model to simulate FSW processes. The model uses an analytical velocity field and considers heat input from the tool shoulder and plastic strain of the bulk material. Trajectories, temperature, strain, strain rate fields and micro-hardness in various weld zones are computed and compared to experimental results obtained on a AA 2024-T351 alloy FSW joint.

Kinematic framework Among the distinctive local level studies, Cho et al. [53] used an Eulerian approach including thermomechanical models without considering the transient temperature in simulation. The strain hardening and texture evolution in the friction stir welds of stainless steel was studied in this paper. A Lagrangian approach with intensive re-meshing was employed in [43] while similar approaches were applied in [29] and [30], which are not numerically efficient.

Buffa et al. [29] using the commercial FE software DEFORM-3D, proposed a 3D Lagrangian, implicit, coupled thermo-mechanical numerical model for the simulation of FSW processes, using a rigid-visco-plastic material description and a continuum assumption for the weld seam. The proposed model is able to predict the effect of process parameters on process variables, such as the temperature, strain and strain rate fields, as well as material flow and forces. Reasonable good agreement between the numerically predicted results, on forces and temperature distribution, and experimental data was obtained. The authors found that the temperature distribution about the weld line is nearly symmetric because the heat generation during FSW is dominated by rotating speed of the tool, which is much higher than the advancing speed. On the other hand, the material flow in the weld zone is non symmetrically distributed about the weld line because the material flow during FSW is mainly controlled by both advancing and rotating speeds.

Nandan et al. in [134] and [136] employed a control volume approach for discretization of the FSW domain. They investigated visco-plastic flow and heat transfer during friction stir welding in mild steel. The temperature, cooling rates and plastic flows were solved by the equations of conservation of mass, momentum and energy together with the boundary conditions. In this model the non-Newtonian viscosity was determined from the computed values of strain rate, temperature and material properties. Temperatures and total torque was compared with experimental values showing good agreement. The computed temperatures were in good agreement with the corresponding experimental values.

Aspects that are ignored by most authors are the effect of convective heat flow due to material deformation and the asymmetry of heat generation due to the much higher pressure at the back of the shoulder. The former requires a prediction of the material flow around the tool, which is difficult to implement in most (non-fluid) solvers, which only predict weld temperature.

Recently, Assidi et al. in [19] used an ALE formulation implemented into the Forge3® software with a splitting approach and an adaptive re-

meshing scheme based on error estimation. In [31] the residual stresses in a 3D FE model were predicted for the FSW simulation of butt joints through a single block approach. The model was able to predict the residual stresses by considering only thermal actions.

Santiago et al. [153] developed a simplified computational model taking into account the real geometry of the tool, i.e. the probe thread, and using an ALE formulation. They considered also a simplified friction model to take into account different slip/stick conditions at the pin shoulder/work-piece interface.

The more recent works performed in this direction are those presented in this thesis. Agelet de Saracibar et al. ([5], [6]), Agelet de Saracibar et al. ([7], [8]), Chiumenti et al. [50], and Dialami et al. ([68], [69]) used a sub-grid scale finite element stabilized mixed velocity/pressure/temperature formulation for coupled thermo-rigid-plastic models, using Eulerian and Arbitrary Lagrangian Eulerian (ALE) formalisms, for the numerical simulation of FSW processes. They used ASGS and OSGS methods and quasi-static sub-grid scales, neglecting the sub-grid scale pressure and using the finite element component of the velocity in the convective term of the energy balance equation. Chiumenti et al. [50], Dialami et al. [68], and Chiumenti et al. [51] developed an apropos kinematic framework for the numerical simulation of FSW processes and compared with a solid approach in [32]. A combination of ALE, Eulerian and Lagrangian descriptions at different zones of the computational domain and an efficient coupling strategy was proposed. The resulting apropos kinematic setting efficiently permitted to treat arbitrary pin geometries and facilitates the application of boundary conditions. The formulation was implemented in an enhanced version of the finite element code COMET [36] developed by the authors at the International Centre for Numerical Methods in Engineering (CIMNE). Chiumenti et al. [51] used a novel stress-accurate FE technology for highly nonlinear analysis with incompressibility constraints typically found in the numerical simulation of FSW processes. They used a mixed linear piece-wise interpolation for displacement, pressure and stress fields, respectively, resulting in an enhanced stress field approximation which enables for stress accurate results in nonlinear computational mechanics.

1.2.4 Industrial background of SMD

Two of the most used processes for manufacturing structural components are casting and forging. The forged component typically has to be manufactured substantially oversized to allow for final machining of the peripheral features. Machining removes a great amount of component volume. Since the materials used sometimes are expensive and with high strength, the process results in a costly and time consuming procedure. Casting creates a component much closer to the final shape, despite of less qualified material integrity comparing to forging. Casting is expensive and only justified for medium or large series. There are also limitations in the design of the component, transitions of thicknesses must not be too sharp and the ratio between the thickest and thinnest section must not be too large. New manufacturing processes are currently being developed to replace traditional casting processes, particularly for special alloys and short series.

The Shaped Metal Deposition (SMD) process yields high structural integrity, produced with a minimum of scrap. SMD is one of the welding procedures used to generate prototypes of metal parts. It is a manufacturing technology similar to the multi-pass welding but with the aim to build up features such as lugs and flanges on fabricated components with wanted geometry (Figure 1.9). The material is melted using a heat source, e.g. a tungsten electrode or laser, and when the weld material solidifies it builds up the feature. It creates different layers of filler material on a substrate following a predefined welding path to fabricate the desired geometry without the need for tooling (Figure 1.10). SMD involves a moving heat source and a filler material to build features layer-by-layer. Each layer experiences repeatedly heating and cooling with high rates up to maximum temperatures, which may depend on the time and location. The temperature field developed during SMD depends on many welding parameters, such as the arc power, welding speed, welding sequences and environmental conditions. During the deposition of a new layer, some of the previous layers are re-melted and a continuous change in the microstructure during the full process is induced. SMD results in a unique morphology and in microstructures, usually not achievable by conventional fabrication techniques [20]. The advantage of this process is that the material is created where it needs to be on the component while the quality can be assured. It is built usually in the shortest time possible and with minimal post-machining. It is a reliable method for fabricating local, complex features in large components.

Figure 1.9: Experimental setting for a SMD test (Casting of Large Ti structures (COLTS), FP7 - Aeronautics and Air Transport (AAT) - 2010 - RTD-CHINA)

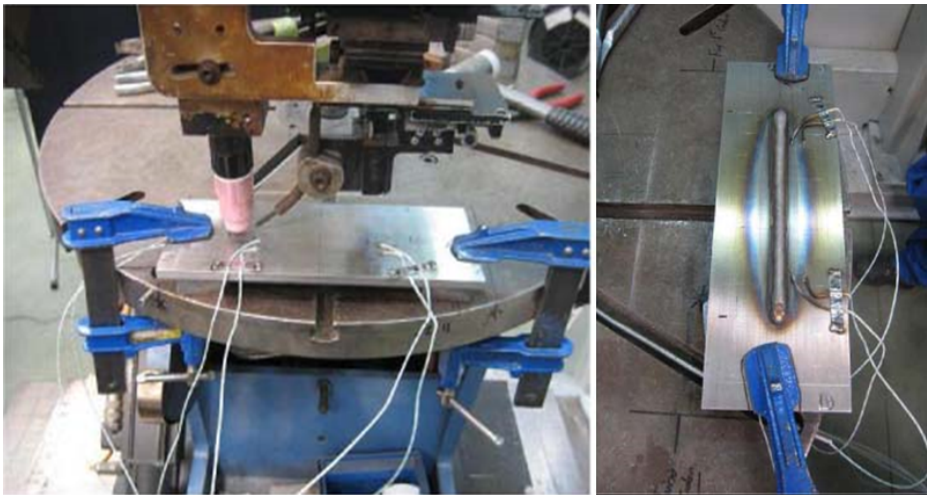

Figure 1.10: Experimental setting for a 12 layers deposition (Casting of Large Ti structures (COLTS), FP7 - Aeronautics and Air Transport (AAT) - 2010 - RTD-CHINA)

The technology was initially developed by Rolls-Royce plc, but was not widely adopted for commercial production. This innovative technique is of great interest due to the possibility of employing standard welding equipment without the need for extensive new investment; however it is less studied in comparison with other welding processes. This type of manufacturing process is of particular interest nowadays in aerospace industry to build components using titanium or nickel-based alloys. SMD can be applied for any material which can be welded and is currently under investigation for different metals, such as Ni alloys [55], steels [166] and Ti alloys ([110], [40], [41], [20]).

In SMD, the accuracy of the component depends on the thermal stresses induced during the welding process. The appropriate control of heat transfer during material deposition reduces residual stresses and component distortion. Process parameters that give rise to successfully manufactured components are usually determined experimentally by trial and error, a very costly and time-consuming procedure. In practice, the costly and time consuming trial-and-error procedures are commonly performed, based on the previous knowledge and experience. Up to now, the number of experimental investigations on SMD is much higher than numerical studies. However, the interest toward numerical investigations is growing fast. It would be useful to determine the set of parameters that results in less piece-work distortion with fewer residual stresses and appropriate micro-structural properties. The numerical simulation of the process is an efficient alternative for optimization of the SMD strategy and for studying the influence of process parameters on heat transfer during welding processes. Simulation of multi-pass welding and particularly SMD poses several challenges to the modeler in addition to the usual challenges in modeling of welding. There are ad-hoc numerical aspects such as, element activation techniques to model the added material during the deposition and heat source models capable of reproducing the specific heat source.

1.2.5 Experimental and numerical modeling of SMD

Various researchers have focused their work on different topics related to SMD ranging from the monitoring the welding arc and controlling the deposition to thermo-mechanical or metallurgical modeling.

SMD was patented by Rolls-Royce using Tungsten insert gas (TIG) welding technique or laser heat sources with various consumables. Researchers also investigated variants of these ([26], [55]) including the use of an electron

beam or conventional arc welding as possible heat source for deposition [126]. Clark et al. [55] investigated the metal insert gas (MIG) process for SMD. It resulted to be a feasible method for fabrication of local, complex features in aerospace components. The MIG welding offered high deposition rates with a relatively low investment cost. The productivity and quality of the process was diminished as the use of a consumable electrode in MIG welding increased the risk of spatter.

A moving heat flux on a 3D geometry is considered in the mathematical model proposed by Rosenthal [149]. A Gaussian power distribution for a circular welding pool is a better approximation of the energy input (Pavelec et al. [145]). The double ellipsoidal power density distribution presented by Goldak et al. [89] is the most sophisticated model currently proposed. In their work, the double-ellipsoidal heat source model is used to represent the TIG-wash steps and is usually performed in the literature for welding without filler material or a single-pass welding. Based on observations of the shape of the liquid pool on subsequent layers, the double-ellipsoidal heat source model is replaced by a constant heat power density throughout the newly added material and the thermal conductivity is artificially increased to account for heat convection. Fachinotti et al. [77] assumed that the melt flow is affected by the direction of the deposition and consequently, the conductivity should be increased mainly in this direction. Both improvements contribute to simplify the liquid pool using a heat conduction model, i.e. without the high cost of modeling the melt flow.

The techniques for element activation corresponding to inserted filler material can be classified into two categories: the quiet and inactive approaches. The concepts were introduced and compared by Lindgren et al. [121].

Multi-dimensional thermal, mechanical and metallurgical models of the deposition process were developed to predict process conditions and further optimization ([11], [12]). The mechanical model was based on a standard FE formulation limited to the solid domain but with full consideration of yielding (element distortion) and the dependence of the material properties on the temperature evolution of the part. The model was solved with hexahedral elements, tri-linear interpolation of displacements and constant interpolation of mean stresses. This model was able to predict the substrate distortion and residual stresses that occur during the SMD process.

The thermal model used a double ellipsoidal heat source [74] to represent the TIG torch. A FE formulation that considers phase change was developed [12] and was solved using linear tetrahedral elements to account for the

liquid/solid phase change. The 3D FE model of SMD developed by Anca et al. [12], was restricted to the deposition analysis of only four layers with a poor mesh along the thickness of the deposited layers. The geometry of each layer was properly described. Basically, they focused on the determination of the distortion of the component. A satisfactory result was obtained comparing to the experiments. The evolution of temperature during SMD was also modelled using FE analysis [75]. The numerical simulation was performed using a 2D cross-section FE model. Making this assumption the whole time interval of the SMD build (2-3 h) could be considered with small time-steps (0.1 s). The temperature field predicted using the FE model was correlated with macro-meso and micrographical observations. The model was able to predict successfully the extent of the top region, where the built material was characterized by a finer microstructure. The evolution of the microstructure during SMD was also modelled [76]. The model developed not only took into account the temperature evolution but also the kinetics of the different solid phase transformations. Ti-6Al-4V alloy is the target material used in this work. Numerical results were compared to micrographs of SMD material deposited with different parameters. There was good agreement between experimental observations and model predictions.

Many layered manufacturing processes including SMD are accompanied by the development of residual stresses. These stresses arise from the contraction associated with the deposition of a layer. These stresses cause distortions and possibly failure by layer delamination or cracking. Many authors have investigated these stresses. Karapatis et al. [109] and Dalgarno et al. [64] investigated residual stresses in SLS. Chin et al. [44], [45] and Klingbeil et al. [117], [118] investigated residual stresses in metal parts produced using shaped deposition manufacturing (SDM). Through FE modeling and experimentation they determined that substrate preheating and rigid bolting of the substrate reduces the resulting part distortion. Nickel et al. [138] modelled the residual stresses generated in parts produced by SDM using the finite element method (FEM). In SDM, a piece was produced by depositing a powdered metal onto a substrate and heating it locally with a laser heat source. The material deposition process was not modeled.

Mughal et al. [133] obtained the residual stress and distortion in solid freeform fabrication processes by direct metal deposition using metal arc welding. They used a 2D FE thermo-mechanical model. In their approach, the filler material was modeled by assigning negligible material properties to those elements that had not yet been introduced to the substrate. This

technique was not accurate as the results depended on the appropriate choice of these fictitious material properties. Alimardani et al. [10] studied the 3D multilayer solid freeform fabrication process considering only elastic strains, and neglecting the plasticity effects. Lindgren et al. [121] analyzed and compared the so-called quiet and inactive elements approaches for multipass welding process. Although both approaches gave similar results, they reported that the inactive approach required less computational effort than the first one.

The more recent work in this direction is presented in this thesis. Chiumenti et al. [49] adopted a fully coupled thermomechanical solution including phase-change phenomena defined in terms of both latent heat release and shrinkage effects. Temperature evolution as well as residual stresses and distortions, due to the successive welding layers deposited, were accurately simulated coupling the heat transfer and the mechanical analysis.

1.3 Outline

The following chapters outline the framework on which the work in this thesis is based.

In Chapter 2 the thermal problem for the simulation of the welding process at both local and global level is formulated. The thermal problem is governed by the enthalpy based balance of energy equation. Heat generation via viscous dissipation as well as frictional heating due to the contact is taken into account. Thermal convection and radiation boundary conditions are also considered. The weak form of the governing equation is presented.

In Chapter 3 the mechanical problem for the simulation of the welding process is formulated. The mechanical problem is described by the balance of momentum equation. The weak form of the governing equations are presented.

The material behavior is either thermo-elasto-visco-plastic (global level analysis) or thermo-rigid-visco-plastic (local level analysis). The features and peculiarities of each one of these constitutive models in the context of welding are highlighted. Two alternative rigid-visco-plastic constitutive models are presented to deal with the extremely large deformation rates occurring in FSW: Norton-Hoff and Sheppard-Wright. Both models are coupled with the temperature field to consider the thermal softening behavior of the material during the stirring process. The thermo-elasto-visco-plastic constitutive

model used to characterize the material behavior for SMD process includes isotropic hardening and thermal softening. A smooth transition from liquid-like phase to solid including thermal shrinkage, passing through the so-called mushy zone where the phase transformation takes place, is considered.

Chapter 4 describes the discrete FE modeling and sub-grid scale stabilization to deal with incompressibility and heat convection dominated problems. The multiscale stabilization method is introduced and an approximation of the sub-grid scale variables together with the stabilization parameters is given. Algebraic Sub-grid Scale (ASGS) and Orthogonal Sub-grid Scale (OSGS) methods for mixed velocity, pressure and temperature linear elements are used. It is shown how the classical GLS and SUPG methods can be recovered as a particular case of the ASGS method.

Chapter 5 describes the FE technology used to simulate the process of filler metal addition in multi-pass welding and SMD. The strategy adopted for an ad-hoc element activation procedure is presented allowing for switching on the elements according to the welding path defined by the user.

Chapter 6 is devoted to the description of the proposed kinematic framework to simulate the FSW process. A novel numerical strategy to model FSW is presented. Using the Arbitrary-Lagrangian-Eulerian kinematic framework, the overall computational domain is divided into sub-domains associating an apropos kinematic framework to each one of them. A combination of ALE, Lagrangian and Eulerian formulations for the different domain parts is proposed. Coupling between each domain is explained in detail including the friction contact. The strategy adopted to deal with an accurate definition of the boundary conditions is presented.

Chapter 7 deals with the visualization of material flow during the welding process. A particle tracing technique is used, to visualize the trajectories of any material points. This method can be naturally applied to the simulation of the material flow in welding simulations. The trajectories of the material points are integrated from the velocity field obtained in the simulation at the post-process level.

Chapter 8 summarizes the work and provides a critical overview of the goals achieved in the simulation of welding processes. Innovative features of the work are highlighted. Conclusions are drawn with regard to the fields of application and the intrinsic limits of the presented methods. Steps for future developments are also outlined.

All the formulations and algorithms were implemented by the author within COMET (COupled MEchanical and Thermal analysis) finite element

code, which is a program for coupled thermo-mechanical analysis developed at CIMNE.

These chapters are the compendium of the following publications attached as appendices:

- "An apropos kinematic framework for the numerical modeling of Friction Stir Welding", Dialami N., Chiumenti M., Cervera M. and Agelet de Saracibar C., Computers and Structures, 117 (2013) 48–57.
- "Numerical Modeling of Friction Stir Welding Processes", Chiumenti M., Cervera M., Agelet de Saracibar C. and Dialami N., Computer Methods in Applied Mechanics and Engineering, 254 (2013) 353–369.
- "Material Flow Visualization in Friction Stir Welding via Particle Tracing", Dialami N., Chiumenti M., Cervera M., Agelet de Saracibar C. and Ponthot J.-P., International Journal of Metal Forming, DOI: 10.1007/s12289-013-1157-4.
- "Computational modeling and sub-grid scale stabilization of incompressibility and convection in the numerical simulation of friction stir welding processes", Agelet de Saracibar C., Chiumenti M., Cervera M., Dialami N. and Seret A., Archives of Computational Methods in Engineering, 21(1) (2014), in press.
- "Finite element modeling of multi-pass welding and shaped metal deposition processes", Chiumenti M., Cervera M., Salmi A., Agelet de Saracibar C., Dialami N. and Matzui K., Computer Methods in Applied Mechanics and Engineering, 199 (2010) 2343-2359.
- "Comparison of a fluid and a solid approach for the numerical simulation of Friction Stir Welding with a non-cylindrical pin", Bussetta P., Dialami N., Boman R., Chiumenti M., Agelet de Saracibar C., Cervera M. and Ponthot J.-P., Steel research international, DOI: 10.1002/srin. 201300182.
- "Numerical simulation and visualization of material flow in friction stir welding via particle tracing", Dialami N., Chiumenti M., Cervera M., Agelet de Saracibar C. and Ponthot J.-P. and Bussetta P. In Idelsohn S. (Ed.) Numerical Simulations of Coupled Problems in Engineering, Springer publisher (2014), in press.

Chapter 2

Thermal problem

In this chapter, the general framework for the description of the thermal problem in the welding process is presented. The governing equation representing the thermal problem is the *balance of energy* equation. This equation controls the temperature and solidification evolution and can be stated as ([2], [34], [48]):

$$\rho_o \frac{dh}{dt} = \dot{R} - \boldsymbol{\nabla} \cdot \mathbf{q} \tag{2.1}$$

where ρ_o, h, $\dot{R}$ and $\mathbf{q}$ are the density at the reference configuration, the specific enthalpy function (accumulated energy in the system), the volumetric heat source introduced into the system (by plastic dissipation, magnetic induction, Electron Beam (EB), laser, etc) and the heat flux, respectively.

The enthalpy, $h\left(T, f_L\right)$, is defined as a function of temperature, T, and liquid fraction function, f_L, if the phase change transformation is taken into account. Therefore, it can be written

$$\rho_o \frac{dh}{dt} = \rho_o \frac{\partial h}{\partial T}\frac{dT}{dt} + \rho_o \frac{\partial h}{\partial f_L}\frac{df_L}{dt} = \rho_o c \frac{dT}{dt} + \rho_o \mathcal{L}_{PC}\frac{df_L}{dt} \tag{2.2}$$

where c is the specific heat and $\mathcal{L}_{PC}$ is the latent heat of the phase transformation. In the case of phase change, the latent heat is released (or absorbed) according to the liquid fraction evolution. Definition for this function can be stated as (Figure 2.1)

$$f_L\left(T\right) = \begin{cases} 0 & \text{if} \quad T \geq T_L \\ 0 < f_L\left(T\right) < 1 & \text{if} \quad T_S < T < T_L \\ 1 & \text{if} \quad T \leq T_S \end{cases} \tag{2.3}$$

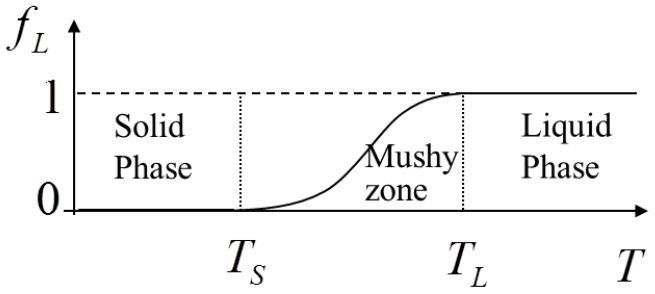

Figure 2.1: Liquid fraction function vs. temperature

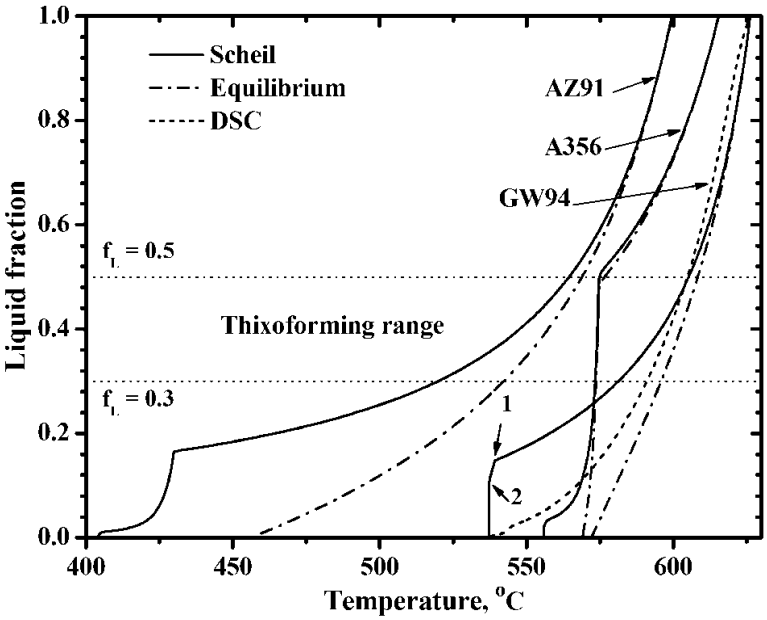

Figure 2.2: Liquid fraction versus temperature curves for GW94 alloy, AZ91 magnesium alloy and A356 aluminium alloy.

where T_L and T_S are the liquid and solid temperatures, respectively. The solid fraction function is defined as:

$$f_S(T) = 1 - f_L(T) \tag{2.4}$$

Figure 2.2 represents the solidification curves of the GW94 alloy calculated under Scheil and equilibrium conditions together with AZ91 magnesium alloy and A356 aluminium ([84]).

Taking this into account, the final expression of the balance of energy equation used to solve the thermal problem can be stated as

$$\rho_o \hat{c} \frac{dT}{dt} = \dot{R} - \boldsymbol{\nabla} \cdot \mathbf{q} \tag{2.5}$$

where

$$\hat{c} = c + \mathcal{L}_{PC} \frac{df_L}{dT}$$

Depending on the aim of the analysis, whether it is local or global, there are different definitions for the heat source, $\dot{R}$. The heat source $\dot{R}$ can be originated by:

- Power dissipated through plastic deformation (i.e. local analysis for FSW).
- External heat sources such as EB, laser, arc power, etc (i.e. global analysis for SMD).

In global level analysis, the heat source, $\dot{R}$, is the (known) input for the system. The heat source distribution can be defined with different degrees of sophistication: as a Gaussian power distribution typically used for EB welding (Figure 2.3) or by the double ellipsoidal power density distribution as in arc welding analysis (Figure 2.4).

There are some difficulties from the numerical point of view to adopt such a detailed power distribution. The mesh density used to discretize the geometry is not usually fine enough to define a complex welding pool shape or even a non-uniform heat source. This is however possible if the simulation of the welding pool is the objective itself as for the local level analysis.

In the case of the FSW process, the heat source introduced into the system is due to the mechanical dissipation and it is computed as a function of the plastic strain rate, $\dot{\mathbf{e}}$, and the deviatoric stresses, $\mathbf{s}$, as:

$$\dot{R} = \gamma \mathbf{s} : \dot{\mathbf{e}} \tag{2.6}$$

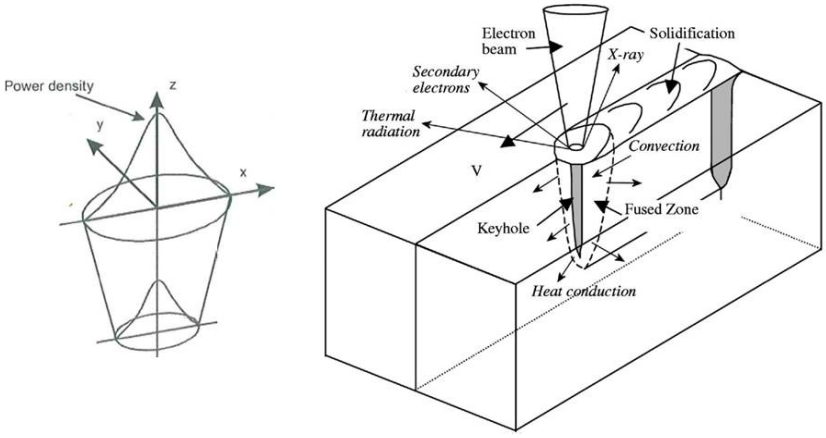

Figure 2.3: Gaussian power distribution in EBW

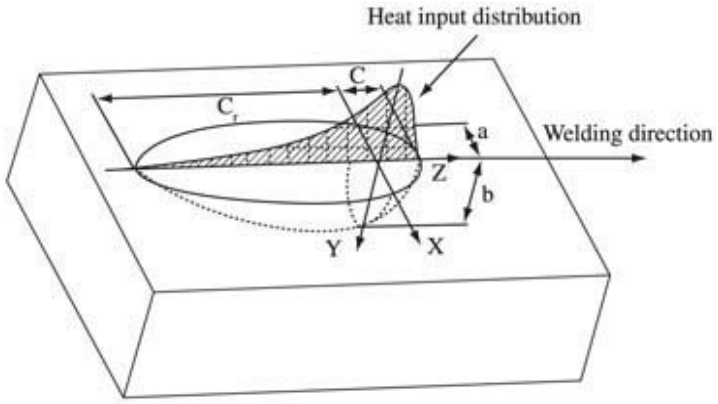

Figure 2.4: Schematic model for double ellipsoid heat source.

where $\gamma \simeq 90\%$ is the fraction of the total plastic energy converted into heat. When studying the EB welding process or SMD, the dissipation rate per unit of volume can be neglected in front of the heat power of the electron beam or in front of the heat flux generated by the thermal gradient between the melted material and the component.

2.1 Thermal problem at the global level

At the global level, the Lagrangian framework is used to describe the thermal problem. According to this framework, the material time derivative is:

$$\frac{d\left(\circ\right)}{dt} = \frac{\partial\left(\circ\right)}{\partial t} \tag{2.7}$$

Therefore, the Eq. (2.5) can be rewritten as

$$\rho_o \hat{c} \frac{\partial T}{\partial t} = \dot{R} - \boldsymbol{\nabla} \cdot \mathbf{q} \tag{2.8}$$

Applications of the global level analysis on the welding of a turbine and a tube can be seen in Figure 2.5 and 2.6, respectively.

2.2 Thermal problem at the local level

At the local level, where the focus of the simulation is the heat affected zone (fixed in the space together with the reference frame), the Eulerian framework is considered. According to this kinematic setting, the material time derivative is expressed as

$$\frac{d\left(\circ\right)}{dt} = \frac{\partial\left(\circ\right)}{\partial t} + \mathbf{v} \cdot \boldsymbol{\nabla}\left(\circ\right) \tag{2.9}$$

where $\mathbf{v}$ is the velocity. Therefore, the Eq. (2.5) can be rewritten as

$$\rho_o \hat{c} \left(\frac{\partial T}{\partial t} + \mathbf{v} \cdot \boldsymbol{\nabla} T \right) = \dot{R} - \boldsymbol{\nabla} \cdot \mathbf{q} \tag{2.10}$$

The convective term is responsible for the transport of the energy produced by the material movement based on the velocity field. Note that, $\mathbf{v} \cdot \boldsymbol{\nabla} T$ transports the temperature in the velocity field direction.

Application of the local level analysis in FSW process can be seen in Figure 2.7.

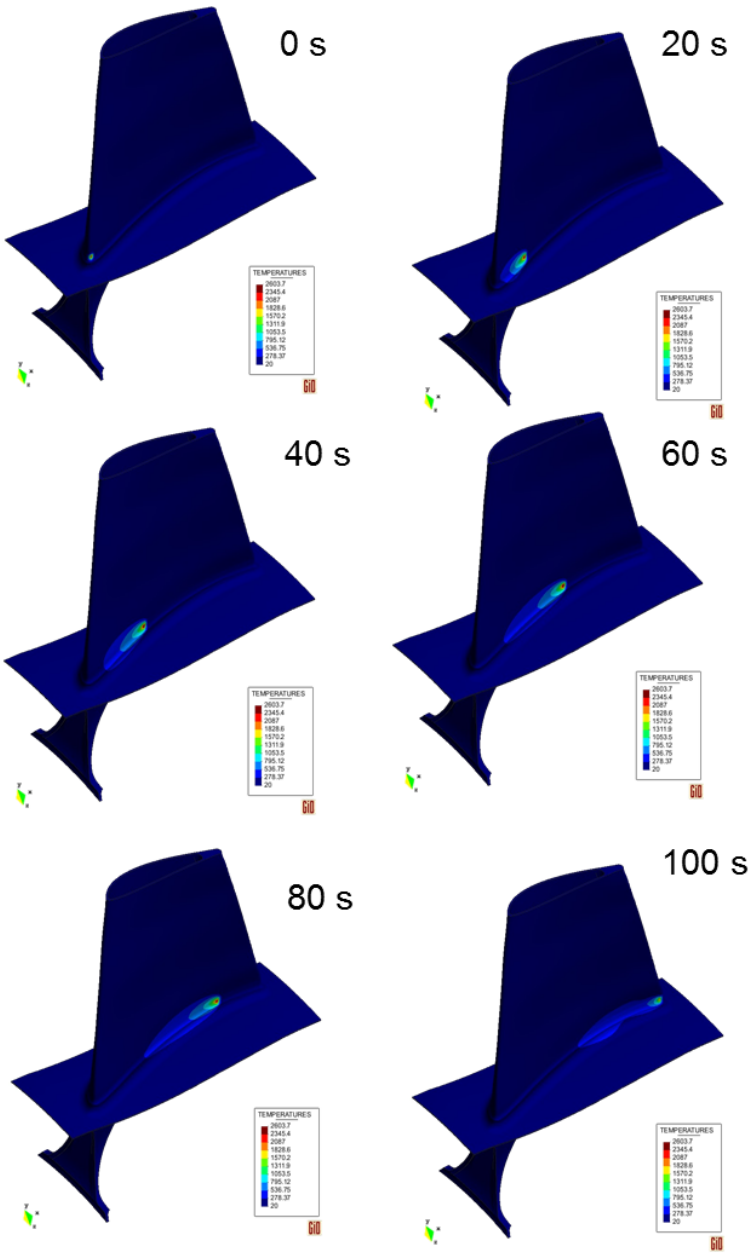

Figure 2.5: Temperature evolution in a turbine (SMD process)

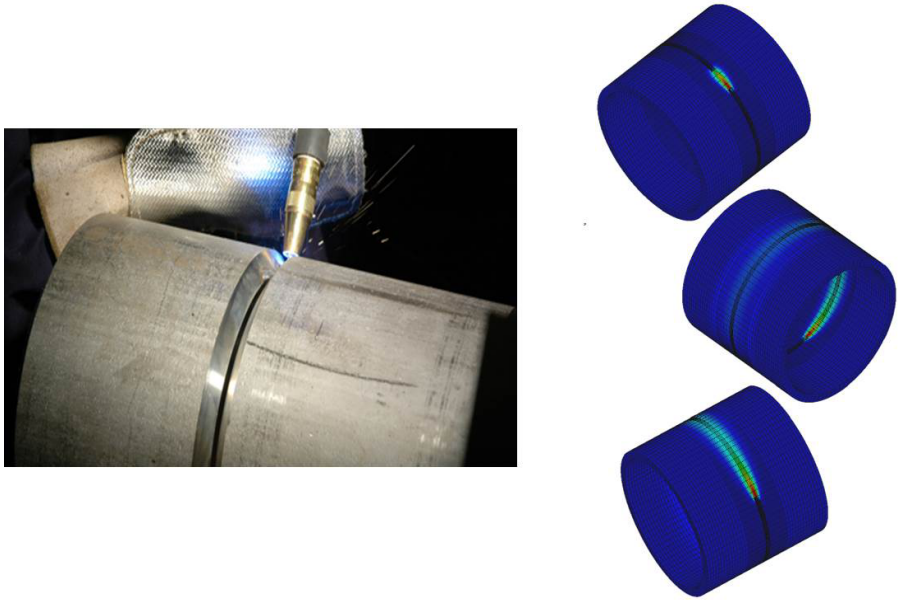

Figure 2.6: Temperature evolution in a tube welding

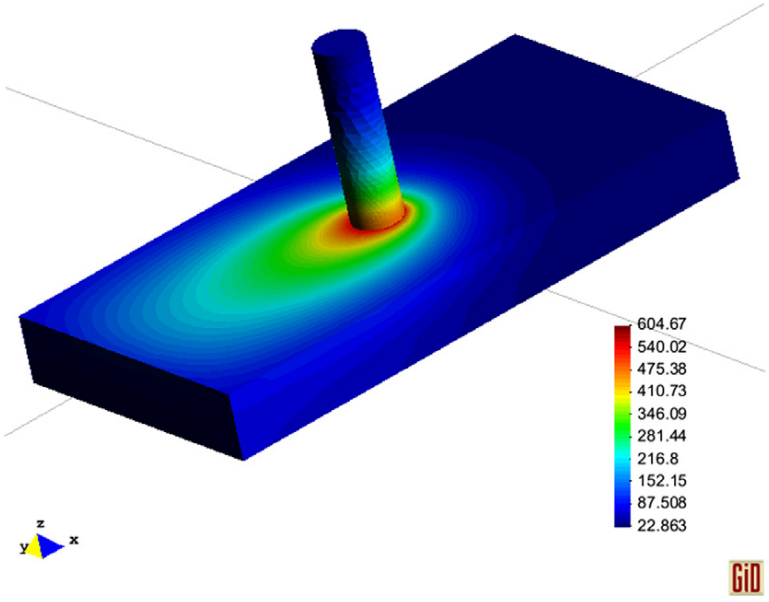

Figure 2.7: Temperature contour field in FSW process.

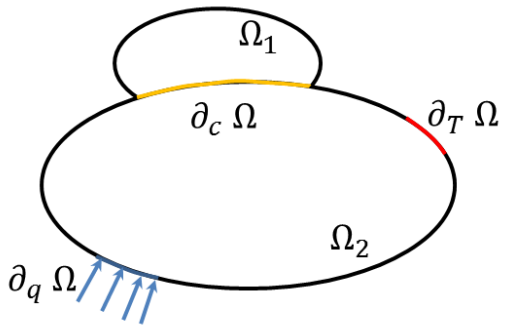

Figure 2.8: Thermal boundary condition

2.3 Boundary conditions

Let us denote by Ω an open and bounded domain. The boundary $\partial\Omega$ can be split into $\partial\Omega_q$ and $\partial\Omega_T$ such that $\partial\Omega = \partial\Omega_q \cup \partial\Omega_T$, where fluxes (on $\partial\Omega_q$) and temperatures (on $\partial\Omega_T$) are prescribed for the heat transfer analysis as (Figure 2.8)

$$\begin{aligned} \mathbf{q}\cdot\mathbf{n} &= \bar{q} \ \text{ on } \ \partial\Omega_q \\ T &= \bar{T} \quad \text{on } \ \partial\Omega_T \end{aligned} \tag{2.11}$$

The initial condition for the transient thermal problem in terms of the initial temperature field is: $T\,(t=0) = T_o$.

On free surfaces, the heat flux is dissipated through the boundaries to the environment by heat convection, expressed by Newton's law as:

$$q_{conv} = h_{conv}(T - T_{env}) \tag{2.12}$$

where h_{conv} is the heat transfer coefficient by convection, T_{env} is the surrounding environment temperature and T is the temperature of the body surface.

Another heat dissipation mechanism is heat loss due to radiation. Heat radiation flux is computed using the Stefan-Boltzmann law:

$$q_{rad} = \sigma_0 \varepsilon (T^4 - T_{env}^4) \tag{2.13}$$

where σ_0 is the Stefan–Boltzmann constant and ε is the emissivity factor. For high temperatures, radiation is a dominant mechanism and it is the only phenomenon in vacuum as for EB welding.

It must be pointed out that the radiation heat flux can be neglected out of the heat affected zone. This means that in global analysis its effect can be considered by modifying the efficiency parameter of the heat source without loss of accuracy.

2.4 Thermal constitutive model

Heat transfer by conduction involves transfer of energy within a material without material flow. The thermal constitutive model for conductive heat flux is defined according to the isotropic conduction law of Fourier. It is computed in terms of the temperature gradient, ∇T, and the (temperature dependent) thermal conductivity, k, as:

$$\mathbf{q} = -k\,\nabla T \tag{2.14}$$

Remark 1 *Even if the heat conduction drives the solidification and cooling evolution due to the high conductivity of the metallic materials, radiation and convection heat fluxes are the most important boundary condition of the problem, especially at the highest temperatures of the welding process.*

2.4.1 Thermal contact model

On the contact surface $\partial\Omega_c \subset \partial\Omega_q$, the thermal exchange by conduction between two bodies in contact is expressed by the following equation (Newton's law):

$$q_{cond} = h_{cond}(T_1 - T_2) \tag{2.15}$$

where h_{cond} is the heat transfer coefficient by conduction (HTC), T_1 is the surface temperature of the first body in contact and T_2 is the surface temperature of the second body. The coefficient h_{cond} depends on the contact pressure at the interface or the gap formed between the surfaces in contact due to thermal contraction of the body during cooling.

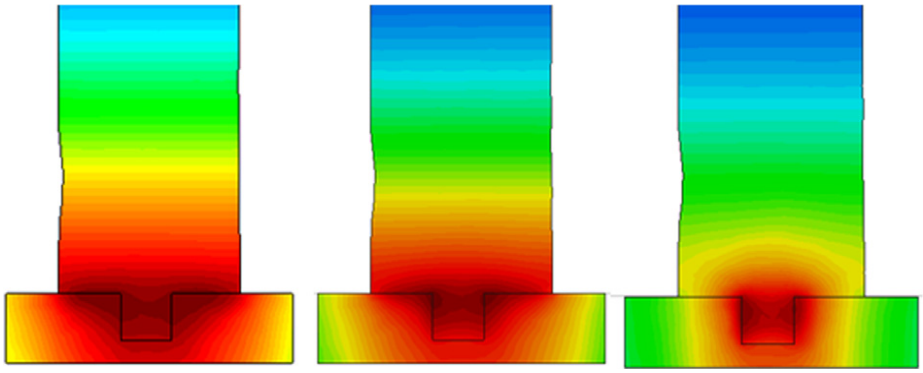

Figure 2.9: Temperature contour field from left to right with fully stick, stick/slip and fully slip condition.

2.5 Friction model

The thermal exchanges at the contact boundary can also result from a friction type dissipation process (Figure 2.9). The heat generated by frictional dissipation at the contact interface is absorbed by the two bodies in contact according to their respective thermal diffusivity. In this section the frictional contact is described by two models: Coulomb's law used when Lagrangian setting is considered in global studies; and Norton's law considered when Eulerian/ALE setting is used in local studies.

2.5.1 Coulomb's friction law

Adopting the classical friction model based on *Coulomb's law*, the so called *slip function* is defined as [9]:

$$\phi\left(\mathbf{t}_N, \mathbf{t}_T\right) = \|\mathbf{t}_T\| - \eta \|\mathbf{t}_N\| \leq 0 \tag{2.16}$$

where $\eta\left(T, \Delta\mathbf{u}_c\right)$ is the friction coefficient, which can result in a nonlinear function of temperature and slip displacement $\Delta\mathbf{u}_c$. $\mathbf{t}_N$ and $\mathbf{t}_T$ are the normal and tangential components of the traction vector, $\mathbf{t}_c = \boldsymbol{\sigma} \cdot \mathbf{n}$, at the contact interface, respectively:

$$\mathbf{t}_N = (\mathbf{n} \otimes \mathbf{n}) \cdot \mathbf{t}_c = (\mathbf{t}_c \cdot \mathbf{n})\,\mathbf{n} \tag{2.17}$$

$$\mathbf{t}_T = (\mathbf{I} - \mathbf{n} \otimes \mathbf{n}) \cdot \mathbf{t}_c = \mathbf{t}_c - \mathbf{t}_N \tag{2.18}$$

where $\mathbf{n}$ is the unit vector normal to the contact interface.

This given, both stick and slip mechanisms can be recovered using the unified format:

$$\|\mathbf{t}_T\| = \varepsilon_T \left(\|\Delta\mathbf{u}_T\| - \dot{\gamma}\frac{\partial\phi}{\partial\|\mathbf{t}_T\|} \right) = \varepsilon_T \left(\|\Delta\mathbf{u}_T\| - \dot{\gamma} \right) \tag{2.19}$$

together with the Kuhn-Tucker conditions defined in terms of the slip function, ϕ, and the slip multiplier, $\dot{\gamma}$, as:

$$\begin{aligned} \phi &\leq 0 \\ \dot{\gamma} &\geq 0 \\ \phi\dot{\gamma} &= 0 \end{aligned} \tag{2.20}$$

where ε_T is a penalty parameter (regularization of the Heaviside function).

$\Delta\mathbf{u}_T$ and $\Delta\mathbf{u}_N$ are the tangential and the normal components of the total relative displacement, $\Delta\mathbf{u}_c$, computed as:

$$\Delta\mathbf{u}_T = (\mathbf{I} - \mathbf{n}\otimes\mathbf{n}) \cdot \Delta\mathbf{u}_c \tag{2.21}$$

$$\Delta\mathbf{u}_N = \Delta\mathbf{u}_c - \Delta\mathbf{u}_T \tag{2.22}$$

- The *sliding condition* allows for relative slip between the contact surfaces. The tangential traction vector, $\mathbf{t}_T$, is computed from 2.16 assuming $\phi = 0$, as:

  $$\mathbf{t}_T = \eta \|\mathbf{t}_N\| \frac{\Delta\mathbf{u}_T}{\|\Delta\mathbf{u}_T\|} \tag{2.23}$$

  The normal traction vector is obtained with a further penalization as:

  $$\mathbf{t}_N = \varepsilon_N \Delta\mathbf{u}_N \tag{2.24}$$

  where ε_N is the normal penalty parameter (not necessarily equal to ε_T), which enforces non-penetration in the normal direction.

- The *stick condition* is obtained for $\dot{\gamma} = 0$, when the contact surfaces are sticked to each other and there is no relative slip between them. The tangential traction vector reads:

  $$\mathbf{t}_T = \varepsilon_T \Delta\mathbf{u}_T \tag{2.25}$$

  while the normal component of the traction vector is given by Eq. (2.24).

Remark 2 *The choice of the penalty parameters is complicated. The larger they are, better they approximate the Heaviside (step) function. However, large penalty parameters lead to ill-conditioning of the solution matrix.*

2.5.2 Norton's friction law

The relative velocity between two bodies in contact is the cause of heat generation by friction. This is one of the key mechanisms of generating heat in the FSW process. When the driving variable is the velocity field, $\mathbf{v}$, it is very convenient to use a Norton type friction law.

The tangential component of the traction vector at the contact interface, $\mathbf{t}_T$, is defined as:

$$\mathbf{t}_T = \eta_{eq}\mathbf{n}_T = a\left(T\right)\left\|\Delta\mathbf{v}_T\right\|^q \mathbf{n}_T \tag{2.26}$$

where $\eta_{eq}\left(T, \Delta\mathbf{v}_T\right) = a\left(T\right)\left\|\Delta\mathbf{v}_T\right\|^q$ is the equivalent friction coefficient. $a\left(T\right)$ is the (temperature dependent) material consistency, $0 \leq q \leq 1$ is the strain rate sensitivity and $\mathbf{n}_T = \dfrac{\Delta\mathbf{v}_T}{\left\|\Delta\mathbf{v}_T\right\|}$ is the tangential unit vector, defined in terms of the relative tangential velocity at the contact interface.

This given, the heat flux generated by Norton's friction law reads:

$$\begin{aligned} \mathbf{q}_{frict}^{(1)} &= -\varsigma^{(1)}\mathbf{t}_T \cdot \Delta\mathbf{v}_T = -\varsigma^{(1)} a\left(T\right)\left\|\Delta\mathbf{v}_T\right\|^{q+1} \\ \mathbf{q}_{frict}^{(2)} &= -\varsigma^{(2)}\mathbf{t}_T \cdot \Delta\mathbf{v}_T = -\varsigma^{(2)} a\left(T\right)\left\|\Delta\mathbf{v}_T\right\|^{q+1} \end{aligned} \tag{2.27}$$

The total amount of heat generated by the friction dissipation is split into the fraction absorbed by the bodies in contact. The amount of heat absorbed by the first body, $\varsigma^{(1)}$, and by the second body, $\varsigma^{(2)}$, depends on the thermal diffusivity, $\alpha = \dfrac{k}{\rho_0 c}$, of the two materials in contact as:

$$\begin{aligned} \varsigma^{(1)} &= \frac{\alpha^{(1)}}{\alpha^{(1)} + \alpha^{(2)}} \\ \varsigma^{(2)} &= \frac{\alpha^{(2)}}{\alpha^{(2)} + \alpha^{(1)}} \end{aligned} \tag{2.28}$$

The more diffusive is the material of one part in comparison with the other part, the more heat is absorbed by it.

2.6 Weak form of the thermal problem

Considering Eqs. (2.8) and (2.14), the weak form of the thermal problem at global level is defined over the integration domain Ω and its boundary $\partial\Omega$ as:

$$\int_{\Omega} \left(\left[\rho_o \hat{c} \frac{\partial T}{\partial t} \right] \ \delta T \right) dV + \int_{\Omega} \left[k \nabla T \cdot \nabla \left(\delta T \right) \right] \ dV = W_{ther} \qquad \forall \delta T \tag{2.29}$$

where δT is the test function of the temperature field, while the thermal work, W_{ther}, is defined as:

$$W_{ther} = \int_{\Omega} \left(\dot{R} \ \delta T \right) \ dV - \int_{\partial\Omega q} \left(\bar{q} \delta T \right) dS - \int_{\partial\Omega_c} \left(q_c \delta T \right) dS \tag{2.30}$$

Similarly, considering Eqs. (2.10) and (2.14), the weak form of the problem at local level is written as

$$\int_{\Omega} \left(\left[\rho_o \hat{c} \left(\frac{\partial T}{\partial t} + \mathbf{v} \cdot \boldsymbol{\nabla} T \right) \right] \ \delta T \right) dV + \int_{\Omega} \left[k \nabla T \cdot \nabla \left(\delta T \right) \right] \ dV = W_{ther} \qquad \forall \delta T \tag{2.31}$$

2.7 Discrete weak form of the thermal problem

In the framework of the standard Galerkin finite element method, the discrete counterpart of the weak form for the thermal problem can be written as

- Global form

$$\int_{\Omega} \left[\left(\rho_o \hat{c} \frac{\partial T_h}{\partial t} \right) \ \delta T_h \right] \ dV + \int_{\Omega} k \nabla T_h \cdot \boldsymbol{\nabla} \left(\delta T_h \right) dV \ = W_{ther}^{ext} \left(\delta T_h \right) \qquad \forall \delta T_h \tag{2.32}$$

- Local form

$$\int_{\Omega} \left[\left(\rho_o \hat{c} \left(\frac{\partial T_h}{\partial t} + \mathbf{v}_h \cdot \boldsymbol{\nabla} T_h \right) \right) \delta T_h \right] dV \tag{2.33}$$
$$+ \int_{\Omega} k \nabla T_h \cdot \boldsymbol{\nabla} \left(\delta T_h \right) dV = W_{ther}^{ext} \left(\delta T_h \right) \qquad \forall \delta T_h$$

  where T_h is the discrete temperature field.

2.8 Paper contributions

The main contributions of the work briefly presented in this chapter have been published in the research papers attached. More in detail:

- The description of the thermal problem in the Lagrangian framework is presented in paper (E). The final industrial application at global level is SMD. Details about the corresponding heat source definition are presented there.

- The thermal problem conveniently expressed in the Eulerian framework for local analysis is presented in papers (A) and (B). The final industrial application is FSW. Details about heat generation by frictional effects and plastic dissipation are also discussed there.

Chapter 3

Mechanical problem

In this chapter, the general framework for the description of the mechanical problem in welding processes is presented. This framework is developed both for local and global analysis. In global level analyses, the effect of a moving heat source on the entire structure is studied. The heat source is introduced into the system and moves along the weld line while the structure is fixed. In this case the Lagrangian framework is used for the definition of the problem, as the reference frame is attached to the structure. The moving heat source generates thermal deformation in the structure. Therefore, definition of the problem in terms of displacements is a natural choice for the computation of the mechanical problem. On the other side, in local level analysis, the focus of the study is the heat affected zone. The heat source is fixed together with the reference frame while the structure moves with the imposed velocity (relative movement). In this case, the Eulerian model is a suitable choice and the problem can be conveniently defined in terms of the velocity field.

In both cases, assuming quasi-static condition, the local form of the *balance of momentum equation,* also known as *Cauchy's equation of motion,* is given by

$$\boldsymbol{\nabla} \cdot \boldsymbol{\sigma} + \rho_o \mathbf{b} = 0 \tag{3.1}$$

where $\boldsymbol{\sigma}$ is the Cauchy's stress tensor, $\mathbf{b}$ is the body forces vector per unit of volume, ρ_o is the density in the reference configuration and $\boldsymbol{\nabla} \cdot (\circ)$ is the divergence operator.

In the case of metallic materials where the behavior of inelastic (plastic) strains is isochoric (plastic deformations are deviatoric), it is convenient to

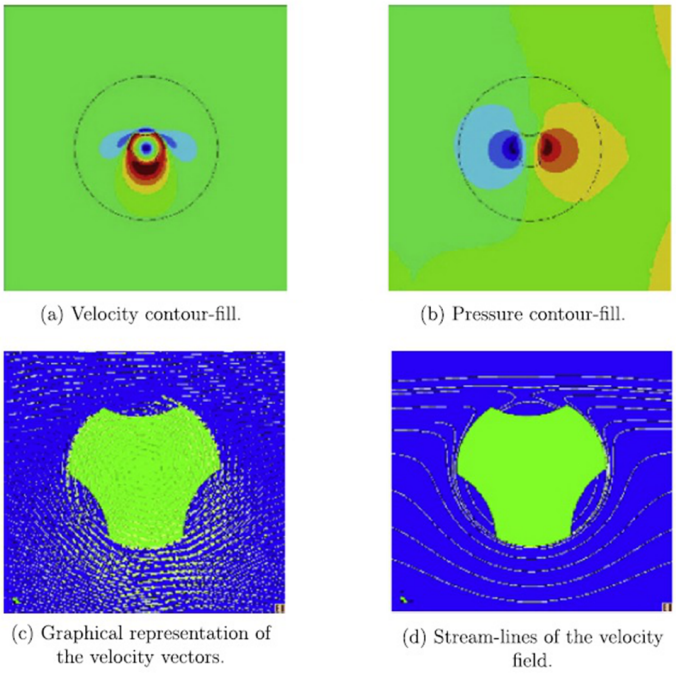

(a) Velocity contour-fill.

(b) Pressure contour-fill.

(c) Graphical representation of the velocity vectors.

(d) Stream-lines of the velocity field.

Figure 3.1: Mechanical results in a FSW process.

split the stress tensor, $\boldsymbol{\sigma}$, into volumetric and deviatoric parts:

$$\boldsymbol{\sigma} = p\mathbf{I} + \mathbf{s} \tag{3.2}$$

where $p = \frac{1}{3}\mathrm{tr}\left(\boldsymbol{\sigma}\right)$ is the pressure and $\mathbf{s} = \mathrm{dev}\left(\boldsymbol{\sigma}\right)$ is the stress deviator. The split is valid for both the compressible and incompressible cases. Similarly, the strain tensor, $\boldsymbol{\varepsilon}$, can be split into volumetric, e_{vol}, and the deviatoric, $\mathbf{e}$, parts.

$$\boldsymbol{\varepsilon} = \frac{1}{3}e_{vol}\mathbf{I} + \mathbf{e} \tag{3.3}$$

Therefore, the local form of the mechanical problem can be stated as:

$$\boldsymbol{\nabla} \cdot \mathbf{s} + \boldsymbol{\nabla} p + \rho_o \mathbf{b} = \mathbf{0} \tag{3.4}$$

where p and $\mathbf{s}$ are defined according to the constitutive equations selected for the local or global analysis, respectively.

Figure 3.1 shows the mechanical results in a FSW process.

3.1 Constitutive model

According to the general perspective of this thesis, which studies the welding process at both local and global level, this section is divided into two parts: the first part describes the mechanical constitutive equations used at global level; the second part is devoted to the description of the mechanical constitutive model used at the local level.

3.1.1 Mechanical constitutive model at global level

When the effects induced by the welding process on the structural behavior are the target of the study, the global level study is preferred. These effects are distortions, residual stresses or weaknesses along the welding line, among others and the displacement field is the driving variable.

At global level, on one side, the stress deviator, $\mathbf{s}(\mathbf{u}, T)$, is generally defined through the constitutive equation as a function of displacements $\mathbf{u}$ and temperature T. In a typical welding process, the heat source moves along the welding path and the temperature range varies from room temperature to very high temperatures above the melting point. Consequently, the material behavior changes from elasto-plastic (at room temperature) to pure viscous (above the melting point). This evolution can be defined by a thermo-elasto-visco-plastic constitutive model, which includes both isotropic hardening and thermal softening. Close to the melting point, the viscous behavior dominates and the elastic limit gradually decreases until vanishing above liquidus temperature. Therefore, visco-plastic models can be used to simulate the liquid-like behavior. The transition from the solid phase to the liquid-like behavior is driven by the temperature dependency of the material properties and can be forced during the phase change transformation.

The idea is to introduce a unique model valid for all the phases of the material starting from solid, passing through the mushy zone until the liquid-like phase (Figure 3.2).

Figure 3.3 represents the phase diagram for Nickel-alloy 718.

To this end, the material is characterized by a thermo-elasto-visco-plastic constitutive model controlled by the solid fraction function $f_S(T)$. It can be written as:

$$p = \hat{K}\, e^e = \hat{K}\ \left(e - e^\theta\right) = \hat{K}\ \left(\nabla \cdot \mathbf{u} - e^\theta\right) \tag{3.5}$$

$$\mathbf{s} = \hat{G}\mathbf{e}^e = 2\,\hat{G}\,\mathrm{dev}\left(\ \boldsymbol{\varepsilon} - \boldsymbol{\varepsilon}^{vp}\right) = 2\,\hat{G}\,\mathrm{dev}\left(\ \boldsymbol{\nabla}^s\mathbf{u} - \boldsymbol{\varepsilon}^{vp}\right) \tag{3.6}$$

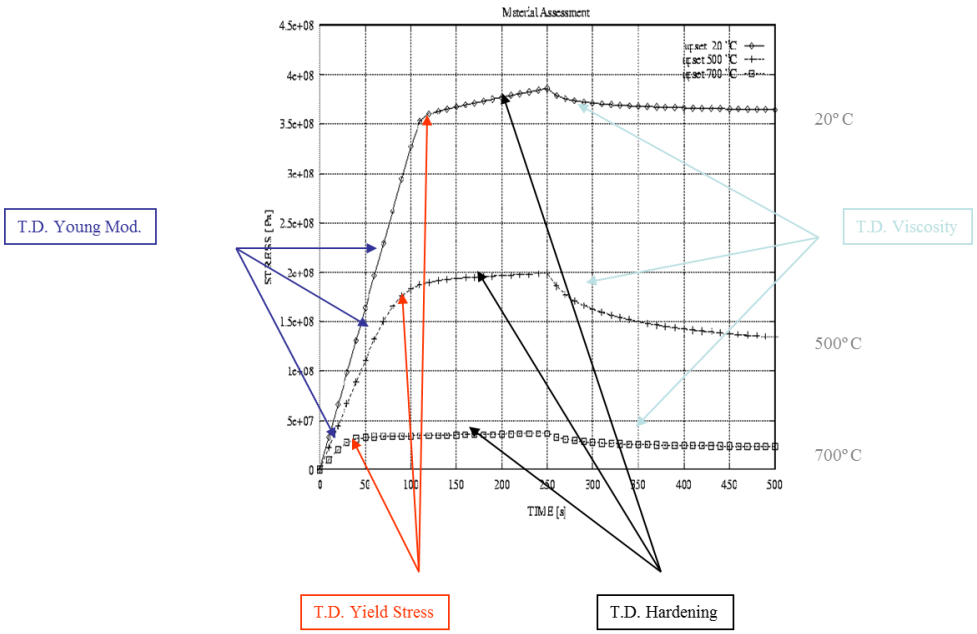

Figure 3.2: Temperature-dependent (T.D.) material's assessment.

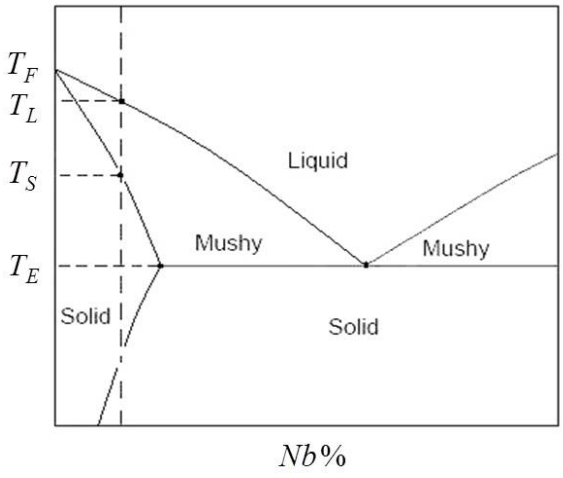

Figure 3.3: Phase diagram for Nickel alloy-718.

where $\hat{K}(T) = \dfrac{K(T)}{f_S(T)}$ is a modified bulk modulus, which controls the material compressibility and $\hat{G} = \dfrac{G(T)}{f_S(T)}$ is a modified shear modulus. Deformations e^{θ}, e^{e} and $\mathbf{e}^{e}$ are the volumetric thermal deformation, the elastic volumetric strain and the elastic deviatoric strain, respectively. The volumetric thermal deformation, $e^{\theta}(T)$, is defined as

$$e^{\theta}(T) = \begin{cases} 0 & \text{if} \quad T \geq T_L \\ e^{pc}(T) & \text{if} \quad T_S < T < T_L \\ e^{cool}(T) & \text{if} \quad T \leq T_S \end{cases} \tag{3.7}$$

where T_L and T_S are the *liquidus* and *solidus* temperatures, respectively.

The plastic response depends on the definition of the visco-plastic potential $\Phi(\mathbf{s}, q, T)$

$$\Phi(\mathbf{s}, q, T) = \|\mathbf{s}\| - R(q, T) \tag{3.8}$$

there $R(q, T)$ is the radius of the yield surface defined according to the Von Mises yield criterion, including isotropic hardening combined with thermal softening effects:

$$R(q, T) = \sqrt{\frac{2}{3}} \left[\sigma_0(T) - q\right] f_S(T) \tag{3.9}$$

where the state variable q is defined as a function of the isotropic strain hardening variables, ξ as

$$\begin{aligned} q \;=\; & -f_S(T) \left[\sigma_\infty - \sigma_o\right] \left[1 - exp(\delta\xi)\right] \\ & -f_S(T)\, H\, \xi \end{aligned} \tag{3.10}$$

where σ_o is the initial flow stress, σ_∞ is the saturation hardening limit, H and δ are the linear and exponential isotropic hardening coefficients, respectively, and f_S is the solid fraction function.

Figure 3.4 shows the temperature-dependent material property for Nickel-alloy 718.

According to the principle of maximum plastic dissipation, the evolution laws for the plastic variables can be obtained as

$$\dot{\mathbf{e}} \;=\; \gamma^{vp}\, \mathbf{n} \tag{3.11}$$

$$\dot{\xi} \;=\; \gamma^{vp} \sqrt{\frac{2}{3}} \tag{3.12}$$

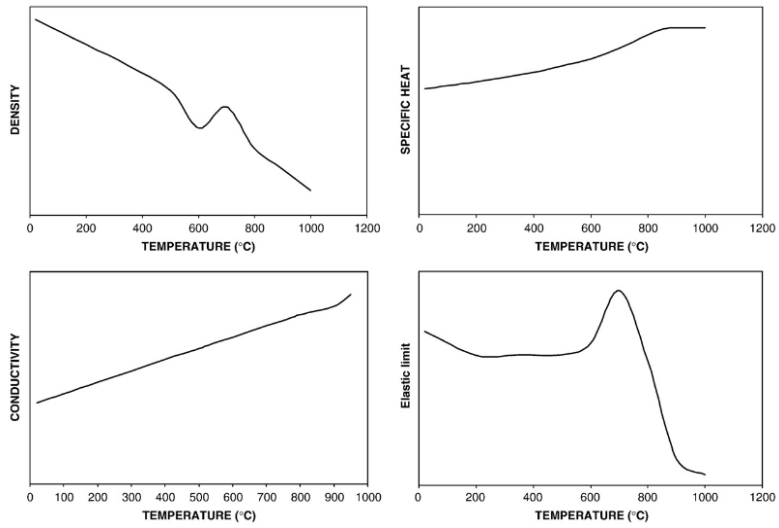

Figure 3.4: Temperature dependent density and elastic limit for Nickel-alloy 718.

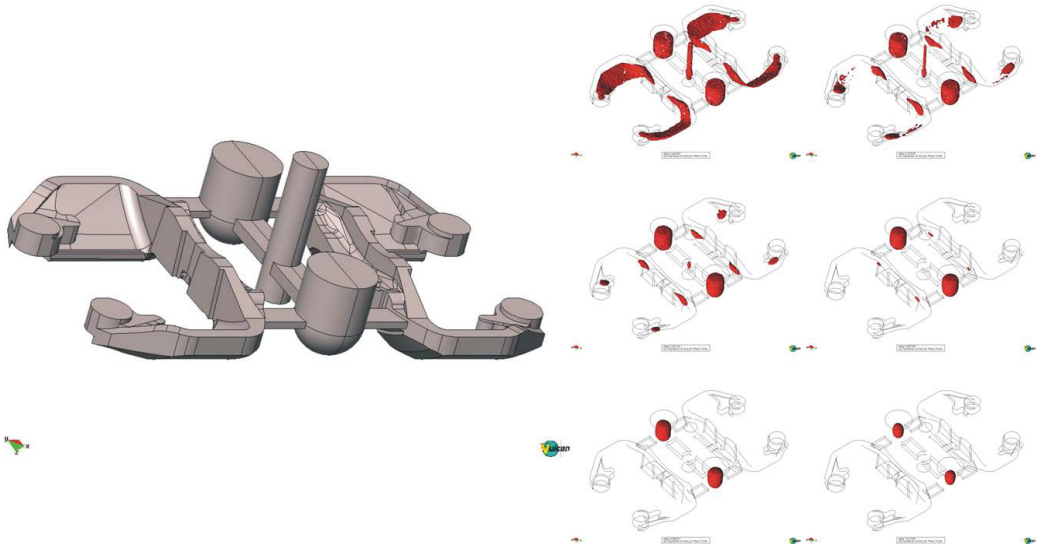

Figure 3.5: Solid fraction evolution in a gravity casting process.

where $\dot{\xi}$ is the isotropic strain-hardening variable, $\mathbf{n} = \dfrac{\mathbf{s}}{\|\mathbf{s}\|}$ is the unit normal to the yield surface and $\gamma^{vp} = \left\langle \dfrac{\Phi(\mathbf{s}, q, T)}{\eta} \right\rangle$ is the visco-plastic parameter when a rate-dependent evolution law is assumed. $\eta(T)$ is the plastic viscosity associated to the visco-plastic model.

Figure 3.5 shows the solid fraction evolution in a gravity casting process [48].

Remark 3 *The split format assumed for the stress tensor is very convenient when using mixed* $\mathbf{u}/p$ *formulations to overcome the volumetric locking that occurs when approaching the incompressibility limit* ($K \to \infty$) *(See chapter 4).*

Solid phase

The material behavior below the solidus temperature can be characterized by a thermo-elasto-visco-plastic constitutive model. In this case the solid fraction is $f_S(T_S) = 1$. Therefore,

$$p = K \left(\nabla \cdot \mathbf{u} - e^{\theta} \right) \tag{3.13}$$

$$\mathbf{s} = 2G \operatorname{dev}\left(\boldsymbol{\nabla}^s \mathbf{u} - \boldsymbol{\varepsilon}^{vp} \right) \tag{3.14}$$

The volumetric thermal deformation, e^{θ} , is computed adding the thermal shrinkage during the phase change, e^{pc}, to the thermal deformation during the cooling phase, e^{cool} , as follows:

$$\begin{aligned} e^{\theta} &= e^{cool} + e^{pc} \\ &= \frac{\rho_S - \rho_L}{\rho_S} + 3\left[\alpha(T)(T - T_{ref}) - \alpha(T_0)(T_0 - T_{ref})\right] \end{aligned} \tag{3.15}$$

where $\alpha(T)$ is the thermal expansion coefficient, $\rho_S = \rho(T_S)$ and $\rho_L = \rho(T_L)$ are the material density at solidus and liquidus temperature, respectively.

Mushy phase

In this range the material transforms from liquid to solid or vice-versa and the solid fraction is $0 < f_S(T) < 1$.

The volumetric thermal deformations is computed as the thermal shrinkage during the phase change:

$$e^{\theta} = e^{pc} = \frac{\rho(T) - \rho_L}{\rho_S} \tag{3.16}$$

Observe that when $T = T_L$ the thermal deformation disappears. The radius of the Von Mises yield surface (Eq. (3.9)) is forced to vanish by the solid fraction when reaching to the liquid-like phase. This enforces a rigid-visco-plastic behavior when the material is liquid while restoring the standard elasto-visco-plastic model when the material solidifies.

Liquid-like phase

In this phase, the solid fraction is $f_S(T_L) = 0$. The radius of the Von Mises yield surface vanishes ($R(q,T) = 0$) and, therefore, the visco-plastic potential $\Phi(\mathbf{s}, q, T)$ degenerates into a purely-viscous potential

$$\Phi(\mathbf{s}) = \|\mathbf{s}\| \tag{3.17}$$

As a consequence, the visco-plastic multiplier transforms into

$$\gamma^{vp} = \frac{\|\mathbf{s}\|}{\eta} \tag{3.18}$$

Therefore, it is possible to obtain a viscous relationship between the deviator of the stress tensor, $\mathbf{s}$, and the visco-plastic strain rate, $\dot{\boldsymbol{\varepsilon}}^{vp}$, governed by the viscous parameter, η, as $\mathbf{s} = \eta\gamma^{vp}\mathbf{n} = \eta\,\dot{\mathbf{e}}$.

In this phase, the material behavior is purely deviatoric ($K \to \infty$ and $e^{\theta} = 0$) and a rigid-visco-plastic constitutive model is recovered.

$$\begin{cases} \nabla \cdot \mathbf{u} = 0 \\ \mathbf{s} = \eta\,\dot{\mathbf{e}} = \eta\,\dot{\boldsymbol{\varepsilon}} \end{cases} \tag{3.19}$$

The visco-plastic strain rate is the total strain rate $\dot{\boldsymbol{\varepsilon}} = \dot{\mathbf{e}}$, as neither thermal deformations nor elastic strains ($G \to \infty$) exist.

3.1.2 Mechanical constitutive model at local level

When the welding pool is the focus of the study, the local level analysis in Eulerian format is preferred. The stress deviator $\mathbf{s}(\mathbf{v}, T)$ is defined as a function of temperature, T, and the velocities, $\mathbf{v}$, rather than displacements. The constitutive laws are typically formulated in terms of strain-rate rather than strain. For instance in case of FSW, the process is characterized by very high strain rates as well as a wide temperature range going from the environmental temperature to the melting point. Hence, instead of a thermo-elasto-visco-plastic model (generally adopted for metals in the Lagrangian formulation), a thermo-rigid-visco-plastic behavior is usually introduced within an Eulerian/ALE framework.

When the problem is defined in terms of velocities, the strain rate tensor is obtained as $\dot{\boldsymbol{\varepsilon}} = \nabla^s \mathbf{v}$. The split into volumetric and deviatoric parts results in:

$$\dot{\boldsymbol{\varepsilon}} = \frac{1}{3}\dot{e}_{vol}\mathbf{I} + \dot{\mathbf{e}} \tag{3.20}$$

where $\dot{e}_{vol}$ and $\dot{\mathbf{e}}$ are the volumetric and the deviatoric parts of the strain rate tensor, respectively.

The incompressibility constraint is often adopted by assuming that the volumetric changes, including thermal deformation, are negligible in comparison with elasto-plastic (deviatoric) deformation:

$$\dot{e}_{vol} = \boldsymbol{\nabla} \cdot \mathbf{v} \cong 0 \tag{3.21}$$

so that $\dot{\mathbf{e}} = \dot{\boldsymbol{\varepsilon}} = \nabla^s \mathbf{v}$.

According to the split of the stress tensor introduced in Eq. (3.2), different rate-dependent constitutive models can be used for modeling the welding process in this phase. The constitutive models are usually defined by the relationship between the deviatoric parts of the stress and the strain rate, $\dot{\mathbf{e}}$. This reduces into the definition of visco-plastic constitutive models of the form:

$$\mathbf{s} = \eta\, \dot{\mathbf{e}} = 2\overline{\mu}\dot{\mathbf{e}} \tag{3.22}$$

where $\overline{\mu}$ is the effective viscosity coefficient of the material. The following additive decomposition of the deviatoric strain rate is assumed:

$$\dot{\mathbf{e}} = \dot{\mathbf{e}}^e + \dot{\mathbf{e}}^{vp} \tag{3.23}$$

where $\dot{\mathbf{e}}^e$ and $\dot{\mathbf{e}}^{vp}$ are the elastic and visco-plastic parts, respectively. In FSW, the elastic part of the strain tensor, $\dot{\mathbf{e}}^e$, is negligible compared with

(a)	$\overline{\mu} = \mu$	Newtonian model
(b)	$\overline{\mu} = \mu \left(\sqrt{2}\,\|\dot{\boldsymbol{\varepsilon}}\|\right)^{(m-1)}$	Power-law model [179]
(c)	$\overline{\mu} = \mu_\infty + (\mu_0 - \mu_\infty)\left(\dfrac{\sinh^{-1}\left(\sqrt{2}\,\|\dot{\boldsymbol{\varepsilon}}\|\,\gamma\right)}{\sqrt{2}\,\|\dot{\boldsymbol{\varepsilon}}\|\,\gamma}\right)$	Powell–Eyring model [146]
(d)	$\overline{\mu} = \mu_\infty + (\mu_0 - \mu_\infty)\left(\dfrac{1}{1+\left(\sqrt{2}\,\|\dot{\boldsymbol{\varepsilon}}\|\,\gamma\right)^m}\right)$	Cross model [63]
(e)	$\overline{\mu} = \mu_\infty + (\mu_0 - \mu_\infty)\left(1+\left(\sqrt{2}\,\|\dot{\boldsymbol{\varepsilon}}\|\,\gamma\right)^2\right)^{\left(\frac{m-1}{2}\right)}$	Carreau model [52]
(f)	$\overline{\mu} = \mu_\infty + (\mu_0 - \mu_\infty)\left(1+\left(\sqrt{2}\,\|\dot{\boldsymbol{\varepsilon}}\|\,\gamma\right)^a\right)^{\left(\frac{m-1}{a}\right)}$	Carreau–Yasuda model [183]

Table 3.1: Various constitutive models for the viscosity.

the visco-plastic component, $\dot{\mathbf{e}}^{vp}$, so that:

$$\dot{\mathbf{e}} \equiv \dot{\mathbf{e}}^{vp} \tag{3.24}$$

This means that the total deformation is visco-plastic and a rigid-visco-plastic model is recovered. The rigid-visco-plastic models can be interpreted as non-Newtonian models where the viscosity $\overline{\mu}$ is a nonlinear function of the strain-rate $\dot{\mathbf{e}}$. Typical constitutive equations used for non-Newtonian modeling are listed in Table 3.1. The coefficients μ_0 and μ_∞ in these models represent the asymptotic values of the viscosity $\overline{\mu}$ at zero and infinite strain-rates, respectively. In the Newtonian case $\overline{\mu} = \mu_0 = \mu_\infty = \mu$.

In the present work, depending on the definition for $\overline{\mu}$, two models are introduced from the groups (b) and (c): Norton-Hoff and Sheppard-Wright constitutive models.

Norton-Hoff model

The Norton-Hoff model was originally introduced by Norton [140] in order to describe the unidimensional creep of steel at high temperature, and extended by Hoff [97] to multi-dimensional situations. This model can be easily characterized by simple mechanical tests and accurately describes the behavior of materials with significant viscous and creep response to loading. The Norton-Hoff model is best suited for the materials that are tough and highly rate sensitive. Therefore, this model can be used in FSW analysis.

According to this constitutive model, the effective viscosity is expressed as a function of the temperature and the equivalent plastic strain rate, $\dot{\bar{\varepsilon}} = \sqrt{2/3}\,\|\dot{\mathbf{e}}^{vp}\| = \sqrt{2/3}\,(\dot{\mathbf{e}}^{vp} : \dot{\mathbf{e}}^{vp})^{1/2}$, as:

$$\bar{\mu} = \mu\left(\sqrt{3}\dot{\bar{\varepsilon}}\right)^{(m-1)} \tag{3.25}$$

where $0 \leq m\,(T) \leq 1$ and $\mu\,(T)$ are the (temperature dependent) rate sensitivity and viscosity parameters, respectively (Figure 3.6 and 3.7). One can Note that:

- $m = 0$ leads to the expression of a rigid plastic constitutive law.

$$\mathbf{s} = \sqrt{2}\mu\mathbf{n} \tag{3.26}$$

  where $\mathbf{n} = \dfrac{\dot{\boldsymbol{\varepsilon}}}{\|\dot{\boldsymbol{\varepsilon}}\|} = \dfrac{\mathbf{s}}{\|\mathbf{s}\|}$ defines the plastic-flow direction.

- $m = 1$ leads to the linear behavior of a Newtonian fluid.

$$\mathbf{s} = 2\mu\dot{\boldsymbol{\varepsilon}} \tag{3.27}$$

  that is, a linear relationship between stresses and strain-rates where the constant of proportionality is the viscosity parameter.

The great advantage of the Norton-Hoff model is its simplicity as it only depends on two (temperature dependent) parameters.

For the majority of metals, the rate-sensitivity parameter is usually within the range $0.1 \leq m \leq 0.3$ which results in a very non-linear (non-Newtonian) material behavior (e.g. aluminium and steel alloys).

The nonlinearity of the Norton-Hoff model increases as m diminishes. In our implementation, to deal with this nonlinearity, m is computed in a series of steps starting from the value $m = 1$ in the first step and reaching its real value at step N. This implies that at each time-step $i < N$ the problem is solved with constitutive rate sensitivity m_i:

$$m_i = 1 - (1 - m) * ((1 - i) / (1 - N))^m \tag{3.28}$$

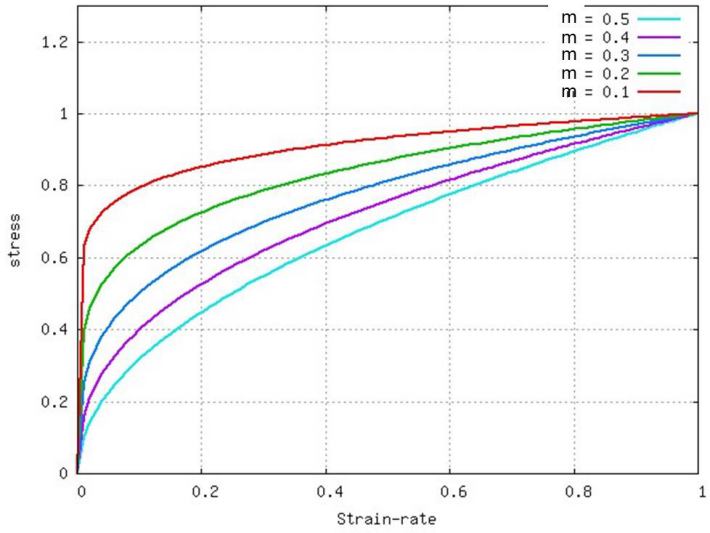

Figure 3.6: Stress vs. strain rate affected by rate sensitivity variation.

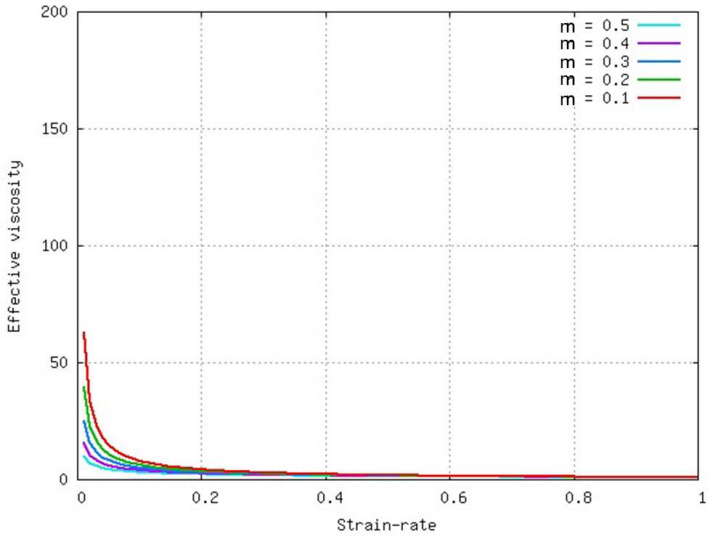

Figure 3.7: Effective viscosity vs. strain rate affected by rate sensitivity variation.

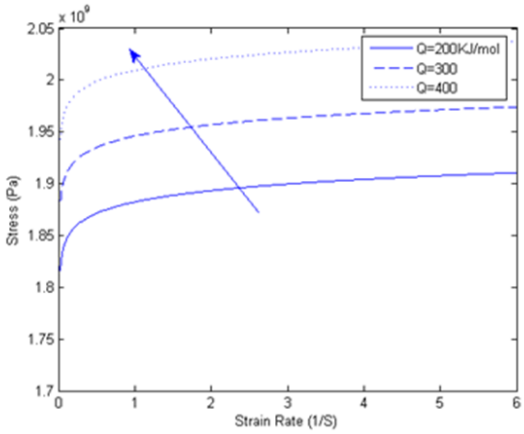

Figure 3.8: Effect of activation energy on stress vs. strain rate.

Sheppard-Wright model

The equation used to describe the flow strength of alloys was introduced initially by Sellars and Tegart [159]. Sheppard and Wright [161] introduced an alternative rigid visco-plastic formulation extending this formulation.

According to the Sheppard-Wright model, the effective viscosity coefficient is defined in terms of effective flow stress σ_e (i.e. norm of deviatoric stress) and effective strain rate $\dot{\bar{\varepsilon}}$ (i.e. norm of deviatoric strain rate) as

$$\bar{\mu} = \frac{\sigma_e}{3\dot{\bar{\varepsilon}}} \tag{3.29}$$

where the effective stress σ_e depends on the strain rate and the temperature field (below the metals solidus temperature) and it is defined as (Figure 3.8)

$$\sigma_e\left(\dot{\bar{\varepsilon}}, T\right) = \frac{1}{\alpha}\sinh^{-1}\left(\left(\frac{Z}{A}\right)^{1/n}\right) = \frac{1}{\alpha}\ln\left[\left(\frac{Z}{A}\right)^{1/n} + \sqrt{1+\left(\frac{Z}{A}\right)^{2/n}}\right] \tag{3.30}$$

where Z, the Zener–Hollomon parameter, represents the temperature compensated effective strain rate [185]

$$Z = \dot{\bar{\varepsilon}}\exp(\frac{Q}{RT}) \tag{3.31}$$

R is the universal gas constant and T is the absolute temperature (in Kelvin). The material constants α, A, n and the apparent activation energy, Q, are derived by fitting experimental response of the material, and are all independent of temperature.

The advantage of the Sheppard-Wright model in comparison with the Norton-Hoff model is the possibility of a better calibration of the material behavior in the entire temperature range from the environment temperature to the melting point.

Remark 4 *Neither Sheppard-Wright nor Norton Hoff model considers thermo-elastic strains. Therefore the proposed constitutive laws cannot predict residual stresses after joining and cooling back to the room temperature. In our opinion, the prediction of residual stresses should be the outcome of the process study at global level where the whole structure is simulated assuming moving heat source obtained from the local based simulation.*

3.2 Weak form of the mechanical problem

The mixed $\mathbf{u}/p$ formulation is the most classical formulation to tackle the incompressible limit (when $K \rightarrow \infty$ in the liquid-like phase), where both displacements and pressures are used as master fields. It is often used for modeling nearly incompressible (Poisson's ratio above 0.49) or completely incompressible material behavior (Poisson's ratio equal to 0.50). The standard irreducible formulation is simply not suitable for incompressible conditions.

The mixed $\mathbf{u}/p$ formulation solves the balance of momentum equation (3.4) and the volumetric part of the constitutive Eq. (3.5) in the weak form. Taking into account that $\mathbf{s}(\mathbf{u})$ is defined as a function of displacement, the weak form of the mixed $\mathbf{u}/p$ mechanical problem at global level is defined over the integration domain Ω and its boundary $\partial\Omega$ as:

$$\begin{cases} \int\limits_{\Omega} \left(\mathbf{s}\left(\mathbf{u}\right) : \nabla^{s}\delta\mathbf{u}\right)\ dV + \int\limits_{\Omega} \left(p\boldsymbol{\nabla}\cdot\delta\mathbf{u}\right)\ dV = W_{mech} & \forall\delta\mathbf{v} \\ \int\limits_{\Omega} \left[\left(\boldsymbol{\nabla}\cdot\mathbf{u}\right)\ \delta p\right]\ dV - \int\limits_{\Omega} \left[\left(e^{\theta} + \dfrac{p}{\hat{K}}\right)\ \delta p\right]\ dV = 0 & \forall\delta p \end{cases} \tag{3.32}$$

where $\delta\mathbf{u}$ and δp are the test functions of the displacement and pressure fields, respectively, while the mechanical work is defined as:

$$W_{mech} = \int_{\Omega} (\rho_o \mathbf{b} \cdot \delta\mathbf{u}) \ dV + \int_{\partial\Omega_\sigma} (\bar{\mathbf{t}} \cdot \delta\mathbf{u}) \ dS \tag{3.33}$$

Definition of the problem in the mixed $\mathbf{u}/p$ format is not obligatory, however it is convenient for including both the compressible and incompressible cases. If $e^\theta \to 0$ and the bulk modulus $K \to \infty$, such as in the fluid phase, the incompressibility condition is recovered: $\boldsymbol{\nabla} \cdot \mathbf{u} = 0$. In this case, the second Eq. (3.32) enforces (in weak sense) the incompressibility condition as a purely kinematic constraint.

Similarly, according to Eqs. (3.4) and (3.21), and taking into account that $\mathbf{s}(\mathbf{v})$ is defined as a function of the velocity field, the weak form of the mixed $\mathbf{v}/p$ mechanical problem at local level is defined over the integration domain Ω and its boundary $\partial\Omega$ as:

$$\begin{cases} \int_{\Omega} (\mathbf{s}(\mathbf{v}) : \nabla^s \delta\mathbf{v}) \ dV + \int_{\Omega} (p\boldsymbol{\nabla} \cdot \delta\mathbf{v}) \ dV = W_{mech} & \forall \delta\mathbf{v} \\ \int_{\Omega} [(\boldsymbol{\nabla} \cdot \mathbf{v}) \ \delta p] \ dV = 0 & \forall \delta p \end{cases} \tag{3.34}$$

where $\delta\mathbf{v}$ is the test function of the velocity field.

3.2.1 Boundary conditions

For the global level analysis, the boundary $\partial\Omega$ is split into $\partial\Omega_\sigma$ and $\partial\Omega_u$, being $\partial\Omega = \partial\Omega_\sigma \cup \partial\Omega_u$ such that the tractions are prescribed on $\partial\Omega_\sigma$ while displacements are specified on $\partial\Omega_u$. The corresponding Neumann and Dirichlet boundary conditions on $\partial\Omega_\sigma$ and $\partial\Omega_u$ are defined as

$$\begin{aligned} \boldsymbol{\sigma} \cdot \mathbf{n} &= \bar{\mathbf{t}} \ \text{ on } \ \partial\Omega_\sigma \\ \mathbf{u} &= \bar{\mathbf{u}} \quad \text{ on } \ \partial\Omega_u \end{aligned} \tag{3.35}$$

Similarly, for the local level analysis, the boundary $\partial\Omega$ is split into $\partial\Omega_\sigma$ and $\partial\Omega_v$, being $\partial\Omega = \partial\Omega_\sigma \cup \partial\Omega_v$ such that the velocities are specified on $\partial\Omega_v$. The corresponding Dirichlet and Neumann boundary conditions on $\partial\Omega_\sigma$ and $\partial\Omega_v$ are defined as

$$\begin{aligned} \boldsymbol{\sigma} \cdot \mathbf{n} &= \bar{\mathbf{t}} \ \text{ on } \ \partial\Omega_\sigma \\ \mathbf{v} &= \bar{\mathbf{v}} \quad \text{ on } \ \partial\Omega_v \end{aligned} \tag{3.36}$$

where $\bar{\mathbf{t}}$, $\bar{\mathbf{u}}$ and $\bar{\mathbf{v}}$ are the prescribed traction, displacement and velocity field, respectively and $\mathbf{n}$ is the unit outward normal to the surface $\partial\Omega_\sigma$.

3.3 Discrete weak form of the mechanical problem

In the framework of the standard Galerkin finite element method, the discrete counterparts of the weak forms for the mechanical problem can be written as

- Global form:

$$\begin{cases} \int\limits_{\Omega} \left(\mathbf{s}_h\left(\mathbf{u}_h\right) : \nabla^s \delta\mathbf{u}_h\right)\ dV + \int\limits_{\Omega} \left(p_h\ \boldsymbol{\nabla}\cdot\delta\mathbf{u}_h\right)\ dV = W^{ext}_{mech}\left(\delta\mathbf{u}_h\right) & \forall\delta\mathbf{u}_h \\ \int\limits_{\Omega} \left[\left(\boldsymbol{\nabla}\cdot\mathbf{u}_h\right)\ \delta p_h\right]\ dV - \int\limits_{\Omega} \left[\left(e^{\theta}\left(T_h\right) + \dfrac{p_h}{\hat{K}}\right)\ \delta p_h\right]\ dV = 0 & \forall\delta p_h \end{cases} \tag{3.37}$$

- Local form:

$$\begin{cases} \int\limits_{\Omega} \left(\mathbf{s}_h\left(\mathbf{v}_h\right) : \nabla^s \delta\mathbf{v}_h\right)\ dV + \int\limits_{\Omega} \left(p_h\ \boldsymbol{\nabla}\cdot\delta\mathbf{v}_h\right)\ dV = W^{ext}_{mech}\left(\delta\mathbf{v}_h\right) & \forall\delta\mathbf{v}_h \\ \int\limits_{\Omega} \left[\left(\boldsymbol{\nabla}\cdot\mathbf{v}_h\right)\ \delta p_h\right]\ dV = 0 & \forall\delta p_h \end{cases} \tag{3.38}$$

  where $\mathbf{u}_h$, $\mathbf{v}_h$, p_h, $\mathbf{s}_h$ and T_h are the discrete counterparts of the respective fields.

3.4 Paper contributions

The main contributions of the work, briefly presented in this chapter, have been published in the research papers attached. More in detail:

- The thermo-elasto-visco-plastic constitutive model used to describe the material behavior from liquid to solid phase passing through the mushy zone is presented in paper (E). In this case the industrial process analyzed correspond to SMD technology.

- The rigid-visco-plastic constitutive equations used to describe the material behavior at very high strain rates and a wide temperature range going from the environmental temperature to the melting point are described in paper (A) and (B). The final industrial application is FSW process for both of them.

- The mixed $\mathbf{u}/p$ formulation used to tackle the incompressible constraint induced by either liquid-like behavior or the deviatoric nature of plastic deformation in a J2 model is presented in paper (E). The final application is SMD process.

- The mixed $\mathbf{v}/p$ formulation used to deal with rigid-visco-plastic material behavior is presented in both papers (A) and (B). The final application is FSW process.

Chapter 4

Stabilization methods

In this chapter, a stabilized finite element formulation based on the Variational Multiscale (VMS) stabilization method is adopted. This stabilization method allows the use of equal order interpolation for the velocity and pressure fields, bypassing the need to satisfy the inf-sup condition (see first section), and avoiding the oscillations arising in convective dominated problems (see second section).

4.1 Pressure stabilization

It is known that the incompressibility constraint or under isochoric strain conditions, the use of an irreducible velocity-based (or displacement-based) formulation leads to pressure locking situations. It must be pointed out that when using a J2-plasticity model (in solid mechanics) or one of the non-Newtonian laws presented in the previous chapter (for the Eulerian framework), it is usual to get an isochoric strain field, that, is most of the deformations are deviatoric and the volumetric part is negligible. The use of a mixed $\mathbf{v}/p$ formulation is a well-known remedy. However, when the standard Galerkin formulation is used, compatible spaces for the pressure and the velocity field have to be considered and they must satisfy the Ladyzhenskaya-Babuška–Brezzi (LBB) stability condition [27].

The LBB compatibility condition restricts the choice of finite element spaces V_h and P_h for velocities (or displacements) and pressure, respectively. It states that in order to obtain a stable formulation, V_h and P_h must be chosen such that the following inf-sup condition is satisfied:

$$\inf_{\delta p_h \in P_h} \sup_{\delta \mathbf{v}_h \in V_h} \frac{(\delta p_h, \nabla \cdot \delta \mathbf{v}_h)}{\|\delta p_h\|_0 \, \|\delta \mathbf{v}_h\|_1} \geq \alpha > 0, \tag{4.1}$$

where parameter α is independent of the mesh size h. If the LBB compatibility condition is satisfied, there exists a unique solution $\mathbf{v}_h \in V_h$ and a $p_h \in P_h$ (determined up to an arbitrary constant in the case of purely Dirichlet boundary conditions).

Unfortunately, standard Galerkin mixed elements with continuous equal order linear velocity/pressure interpolation violate the LBB condition, leading to instabilities in the pressure field and poor numerical performance. Stable formulations can be obtained either by choosing velocity/pressure pairs that satisfies the LBB condition (e.g. P2/P0 [101]) or by using pressure stabilization methods.

Using LBB stable elements, such as the Q2/Q1 (Taylor-Hood element, based upon continuous quadratic velocity, continuous bilinear pressure) or the mini element (continuous linear velocity+bubble function, continuous linear pressure) is difficult in practice, due to the complexity of the associated implementation and lower computational efficiency than that of simplicial elements. Fortunately, there exist possibilities for circumventing the LBB condition, which permit the use of equal order velocity/pressure interpolations, by modifying the original Galerkin problem, adding stabilization terms.

Essentially, in the majority of stabilization methods, the stabilizing terms added to the original Galerkin formulation involve the residual of the balance of momentum equation. These methods are called *residual-based*. A stabilization method is *consistent* if, on convergence, the solution of the modified problem is exactly the solution of the original problem.

The sub-grid method was originally introduced in [104] as a powerful technology known for its enhanced accuracy properties. The exact solution is split into two parts, corresponding to different scales or levels of resolution: the one that can be captured by the finite element mesh (*coarse*) and the other one, called the sub-grid (*finer*) part. While the first one can be resolved by the finite element method, the latter one cannot. The particular approximation used for the sub-grid scale defines the numerical strategy. The solution of the continuous problem contains components from both scales. It is necessary to, somehow, include the effect of both scales in the approximation to get the stable solution of the discrete problem. The aim is to find an approximate solution for the sub-grid scale and to include it into the discrete

finite element solution. The effect of this finer scale can be included, at least locally, to enhance the stability of the pressure in the mixed formulation ([46], [4], [47], [35]).

To this end, the solution space, Ψ, is split into two parts:

$$\Psi = \Psi_h \oplus \tilde{\Psi} \tag{4.2}$$

Ψ_h denotes the finite element solution while $\tilde{\Psi}$, is the one that completes Ψ_h in Ψ and it is called the *sub-grid scale* ([104] and [103]). Accordingly, the velocity and pressure fields of the mixed problem are expressed as (Figure 4.1)

$$\begin{aligned} \mathbf{v} &= \mathbf{v}_h + \widetilde{\mathbf{v}} \\ p &= p_h \end{aligned} \tag{4.3}$$

where $\mathbf{v}_h \in \Psi_h$ is the velocity field of the finite element scale and $\widetilde{\mathbf{v}} \in \tilde{\Psi}$ is

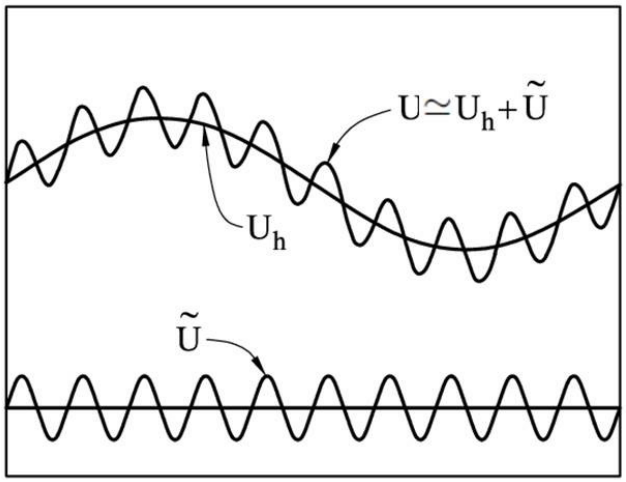

Figure 4.1: Finite element and sub-grid scale parts of the solution $\mathbf{U} = \begin{pmatrix} \mathbf{v} \\ p \end{pmatrix}$

the enhancement of the velocity field belonging to the sub-grid scale. Note that no sub-grid scale contribution is considered for the pressure field. It is reasonable to assume that the sub-grid velocities $\widetilde{\mathbf{v}}$ are sufficiently *small* compared to $\mathbf{v}_h$. They can be viewed as a *high frequency* perturbation of the

finite element field, which cannot be resolved in Ψ_h. It can also be assumed that $\widetilde{\mathbf{v}}$ and its variation $\delta\widetilde{\mathbf{v}}$ vanish on the boundary $\partial\Omega$.

The stress deviator can be similarly decomposed into two different parts:

$$\mathbf{s}(\mathbf{v}) \cong \mathbf{s}_h(\mathbf{v}_h) + \widetilde{\mathbf{s}}(\widetilde{\mathbf{v}}) \tag{4.4}$$

Notice that the stress $\mathbf{s}$ is not a linear function of $\mathbf{v}$ and, therefore, taking $\mathbf{s}_h = \mathbf{s}_h(\mathbf{v}_h)$ and $\widetilde{\mathbf{s}} = \widetilde{\mathbf{s}}(\widetilde{\mathbf{v}})$ is a further approximation.

Different choices are available for the approximation of the velocity sub-grid scales. Two possible options correspond to the ASGS and the OSGS methods.

Using ASGS method, $\widetilde{\mathbf{v}}$ is approximated as $\widetilde{\mathbf{v}} = \tau_v r_h$, where r_h is the residual of the momentum equation in finite element space.

$$r_h = r_h(\mathbf{v}_h, p_h) = \boldsymbol{\nabla}\cdot\mathbf{s}_h + \boldsymbol{\nabla}p_h + \rho_o\mathbf{b} \simeq \boldsymbol{\nabla}p_h \tag{4.5}$$

where $\boldsymbol{\nabla}\cdot\mathbf{s}_h$ vanishes when using linear triangular or tetrahedral elements and the body forces, $\rho_o\mathbf{b}$, are negligible. This given:

$$\widetilde{\mathbf{v}} = \tau_v\boldsymbol{\nabla}p_h \tag{4.6}$$

After substituting into the weak form of both the balance of momentum equation and the constitutive equation, the discrete ASGS stabilized weak form of the mechanical problem for linear elements simplifies to :

$$\begin{cases} \displaystyle\int_\Omega (\mathbf{s}_h : \nabla^s\delta\mathbf{v}_h)\ dV + \int_\Omega (p_h\ \boldsymbol{\nabla}\cdot\delta\mathbf{v}_h)\ dV = W^{ext}_{mech}(\delta\mathbf{v}_h) \quad \forall\delta\mathbf{v}_h \\ \displaystyle\int_\Omega [(\boldsymbol{\nabla}\cdot\mathbf{v}_h)\ \delta p_h]\ dV + \int_\Omega \tau_v(\boldsymbol{\nabla}\delta p_h\cdot\boldsymbol{\nabla}p_h)\,dV = 0 \qquad \forall\delta p_h \end{cases} \tag{4.7}$$

where $\displaystyle\int_\Omega \tau_v(\boldsymbol{\nabla}\delta p_h\cdot\boldsymbol{\nabla}p_h)\,dV$ is the resulting stabilization term to be considered.

A further approximation for the unknown sub-grid space $\tilde{\Psi}$, is the space orthogonal to the finite element space, referred to hereafter as $\Psi_h^\perp$. This means approximating the solution space as $\Psi \simeq \Psi_h \oplus \Psi_h^\perp$. The subsequent stabilization method is called OSGS method, and it has already been successfully applied to several problems in fluid and solid mechanics. According

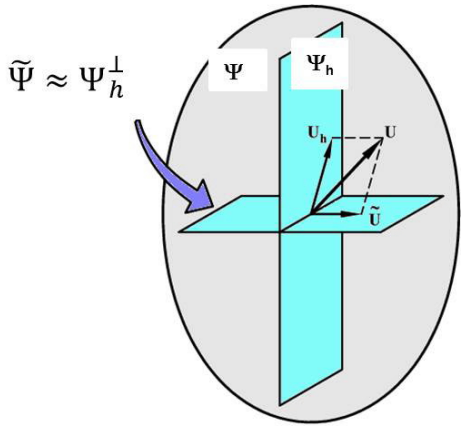

Figure 4.2: Representation of OSGS solution space

to OSGS, $\widetilde{\mathbf{v}}$ is approximated as $\widetilde{\mathbf{v}} = \tau_v P_h^{\perp}(r_h)$, where $P_h^{\perp}$ is the orthogonal projection onto the space orthogonal to the finite element space (Figure 4.2).

The orthogonal projection of a variable $(\cdot)$ can be computed as: $P_h^{\perp}(\cdot) = (\cdot) - P_h(\cdot)$. The resulting discrete OSGS stabilized weak form of the mechanical problem is:

$$\begin{cases} \int\limits_{\Omega} (\mathbf{s}_h : \nabla^s \delta\mathbf{v}_h)\ dV + \int\limits_{\Omega} (p_h\ \boldsymbol{\nabla} \cdot \delta\mathbf{v}_h)\ dV = W_{mech}^{ext}(\delta\mathbf{v}_h) & \forall \delta\mathbf{v}_h \\ \int\limits_{\Omega} [(\boldsymbol{\nabla} \cdot \mathbf{v}_h)\ \delta p_h]\ dV + \int\limits_{\Omega} \tau_v \left[\boldsymbol{\nabla}\delta p_h \cdot (\boldsymbol{\nabla} p_h - \Pi_h)\right] dV = 0 & \forall \delta p_h \\ \int\limits_{\Omega} (\boldsymbol{\nabla} p_h \cdot \delta\Pi_h)\, dV - \int\limits_{\Omega} (\Pi_h \cdot \delta\Pi_h)\, dV = 0 & \forall \delta\Pi_h \end{cases} \tag{4.8}$$

where $\Pi_h = P_h(\boldsymbol{\nabla} p_h)$ and $\delta\Pi_h$ are the smooth projection of the pressure gradient and its variation onto the finite element space, respectively. Observe that the stabilization term introduced in the second equation of (4.8) is computed as a function of the orthogonal projection of the residual of the momentum balance equation as:

$$\int\limits_{\Omega} \tau_v \left[\boldsymbol{\nabla}\delta p_h \cdot P_h^{\perp}(\boldsymbol{\nabla} p_h)\right] dV$$

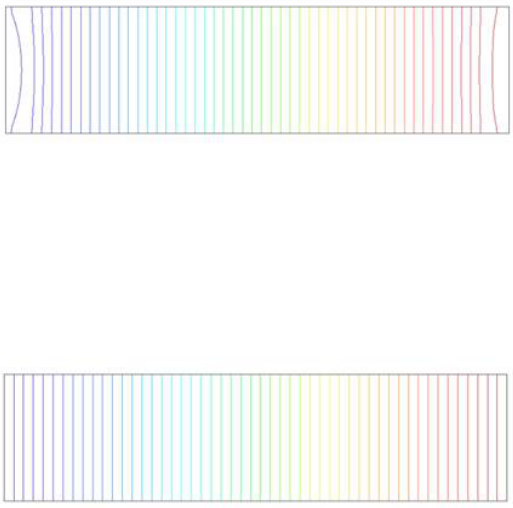

Figure 4.3: Pressure field obtained using ASGS (top) and OSGS (bottom) stabilization method.

The resulting system is an accurate, stable and consistent formulation for the solution of the mechanical problem subjected to the incompressibility constraint.

The stabilization parameter τ_v, is computed as:

$$\tau_v = c_u \frac{h^2}{2\bar{\mu}} \tag{4.9}$$

where h is the element size, c_u is a constant and $\bar{\mu}$ is the parameter defined according to the constitutive model (either effective viscosity or shear modulus). $\bar{\mu}(T)$ is usually temperature dependent and therefore the stabilization term $\tau_v(T)$ is a temperature dependent parameter.

Figure 4.3 compares results of ASGS and OSGS pressure stabilization methods in a parallel flow passing through a tube. The results obtained using OSGS are nodally exact, and totally unaffected by the boundary conditions.

4.2 Convective stabilization

When using an ALE or Eulerian framework for the description of the problem, a convective term coming from the material time derivative arises in the

equations.

It is well-known that in diffusion dominated problem, the solution of the balance of energy equation is stable. However, in convection dominated problem, the stabilizing effect of the diffusion term is insufficient and instabilities appear in the solution. The threshold between stable and unstable conditions is usually expressed in terms of the Peclet number. For instance, the typical Peclet number for FSW processes ranges from 10^1 to 10^3. For this range of the Peclet number, the effect of the convective term cannot be neglected and the solution of the thermal problem is found to be instable.

According to the sub-grid scale method, the solution space Θ of the temperature field is split into two parts: the finite element space and the space for the sub-grid scale.

$$\Theta = \Theta_h + \tilde{\Theta} \tag{4.10}$$

Therefore, the temperature field can be approximated as

$$T = T_h + \tilde{T} \tag{4.11}$$

where $T_h \in \Theta_h$ is the temperature component of the (coarse) finite element scale and $\tilde{T} \in \tilde{\Theta}$ is the enhancement of the temperature field corresponding to the (finer) sub-grid scale. Let us also consider the corresponding variations $\delta T_h \in \Theta_h$ and $\delta\tilde{T} \in \tilde{\Theta}$, respectively.

Also in this case, we consider two possible choices for the approximation of the temperature sub-grid scales corresponding to the ASGS and the OSGS methods.

In the ASGS method, $\tilde{T}$ is approximated as $\tilde{T}= \tau_\theta r_h^\theta$, where r_h^θ is the residual of the energy balance equation in the finite element scale.

$$r_h^\theta = \rho_o \hat{c} \left(\frac{\partial T_h}{\partial t} + \mathbf{c}_h \cdot \boldsymbol{\nabla} T_h \right) \; - \boldsymbol{\nabla} \cdot (k \boldsymbol{\nabla} T_h) \simeq \rho_o \hat{c} \left(\frac{\partial T_h}{\partial t} + \mathbf{c}_h \cdot \boldsymbol{\nabla} T_h \right) \tag{4.12}$$

where the diffusive term, $\boldsymbol{\nabla} \cdot (k \boldsymbol{\nabla} T_h)$, vanishes when using linear triangular or tetrahedral meshes.

In this case, the discrete thermal equation for linear elements can be stabilized by adding a residual based ASGS stabilization term of the form:

$$\int_\Omega \tau_\theta \left[\rho_o \hat{c} \left(\mathbf{c}_h \cdot \boldsymbol{\nabla} \left(\delta T_h \right) \right) \right] \; \left[\rho_o \hat{c} \left(\mathbf{c}_h \cdot \boldsymbol{\nabla} T_h \right) \right] dV \tag{4.13}$$

to the Galerkin weak form of the problem. This given:

$$\int_{\Omega}\left[\rho_o\hat{c}\left(\frac{\partial T_h}{\partial t}+\mathbf{c}_h\cdot\boldsymbol{\nabla}T_h\right)\ \delta T_h\right]\ dV+\int_{\Omega}\ (k\nabla T_h)\cdot\nabla\left(\delta T_h\right)dV$$
$$+\int_{\Omega}\tau_\theta\left[\rho_o\hat{c}\left(\mathbf{c}_h\cdot\boldsymbol{\nabla}\left(\delta T_h\right)\right)\right]\ \left[\rho_o\hat{c}\left(\mathbf{c}_h\cdot\boldsymbol{\nabla}T_h\right)\ \right]dV=W^{ext}_{ther}\left(\delta T_h\right)\qquad\forall\delta T_h \tag{4.14}$$

It can be observed that for linear elements, the ASGS method coincides with the SUPG method.

As an alternative, the space orthogonal to the finite element space $\Theta_h^{\perp}$ can be adopted for the approximation of the unknown sub-grid space $\tilde{\Theta}$. This means that the solution space is approximated as $\Theta\simeq\Theta_h\oplus\Theta_h^{\perp}$. According to the OSGS method, $\tilde{T}$ is defined as $\tilde{T}=\tau_\theta P_h^{\perp}\left(r_h^{\theta}\right)$.

Taking into account that $P_h^{\perp}\left(\cdot\right)=\left(\cdot\right)-P_h\left(\cdot\right)$, the resulting discrete OSGS stabilized weak form of the thermal problem for linear elements simplifies to:

$$\int_{\Omega}\left[\rho_o\hat{c}\left(\frac{\partial T_h}{\partial t}+\mathbf{c}_h\cdot\boldsymbol{\nabla}T_h\right)\ \delta T_h\right]\ dV+\int_{\Omega}\left(k\nabla T_h\right)\cdot\boldsymbol{\nabla}\left(\delta T_h\right)dV$$
$$+\int_{\Omega}\tau_\theta\left[\rho_o\hat{c}\left(\mathbf{c}_h\cdot\boldsymbol{\nabla}\left(\delta T_h\right)\right)\right]\ \left[\rho_o\hat{c}\left(\mathbf{c}_h\cdot\boldsymbol{\nabla}T_h\right)-\Pi_h^{\theta}\ \right]dV=W^{ext}_{ther}\left(\delta T_h\right)\quad\forall\delta T_h$$
$$\int_{\Omega}\left[\left(\mathbf{c}_h\cdot\boldsymbol{\nabla}T_h\right)\ \delta\Pi_h^{\theta}\ \right]dV-\int_{\Omega}\left[\Pi_h^{\theta}\cdot\ \delta\Pi_h^{\theta}\ \right]dV=0\qquad\forall\delta\Pi_h^{\theta} \tag{4.15}$$

where Π_h^{θ} is the smooth projection of the convective term.

$$\Pi_h^{\theta}=P_h\left[\rho_o\hat{c}\left(\mathbf{c}_h\cdot\boldsymbol{\nabla}T_h\right)\ \right] \tag{4.16}$$

The mesh dependent stabilization parameter defined for the thermal (convective) problem is

$$\tau_\theta=\left(c_1\frac{k}{h^2}+c_2\frac{\|\mathbf{c}_h\|}{h}\right)^{-1} \tag{4.17}$$

where h is the element size, c_1 and c_2 are algorithmic constants.

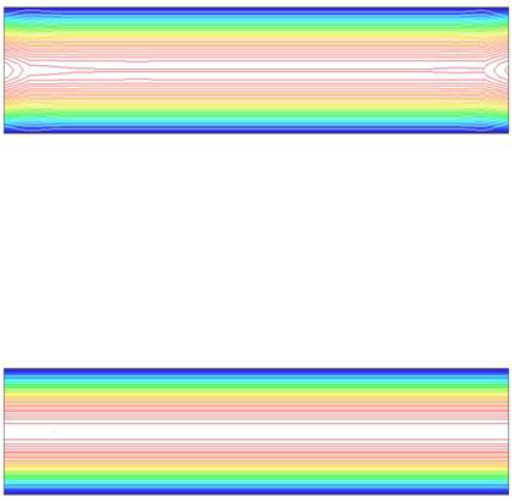

Figure 4.4: Velocity field obtained using SUPG (top) and OSGS (bottom) stabilization method.

Figure 4.4 compares results of ASGS and OSGS convective stabilization methods in a parallel flow passing through a tube. The results obtained using OSGS are totally unaffected by the boundary conditions.

4.3 Paper contribution

The main contribution of the work briefly presented in this chapter has been published in the research paper attached. More in detail:

- The sub-grid scale finite element stabilization of incompressibility and convection is addressed in paper (D). Detailed presentation of the ASGS and OSGS methods and their application to the FSW process are presented there.

Chapter 5

Element activation strategy for the SMD process

The welding process can be performed with or without the use of a filler material depending on the process used and the requirements on the weld geometry. SMD is a welding technology in which the filler material is melted and deposited layer-by-layer (Figure 5.1). The simulation of multi-pass welding and particularly SMD poses several challenges for its numerical simulation. One aspect is the element activation method which requires an ad-hoc finite element activation technology.

The finite element activation techniques can be classified into two types; quiet elements (where the stiffness is very low when the elements are inactive) and born-dead elements techniques (where inactive elements are not assembled to the system of equations until they are activated). In this work, the simulation strategy corresponds to an ad-hoc activation process based on the born-dead elements technique.

According to the born-dead activation technique, a FE mesh discretization including both the domain defining the welding plates and the filler material is considered. The element status is categorized into: active, inactive and activated. The active elements, i.e. those who define the mesh base material, are assembled into the global system. The inactive elements, such as those which correspond to the layer of the filler material, are not considered as a part of the computational model. At each time-step, a number of activated elements are switched on according to the deposition of the filler material along the (user-defined) welding path. As a result, only active and activated elements are added into the solution model.

Figure 5.1: Filler material deposition

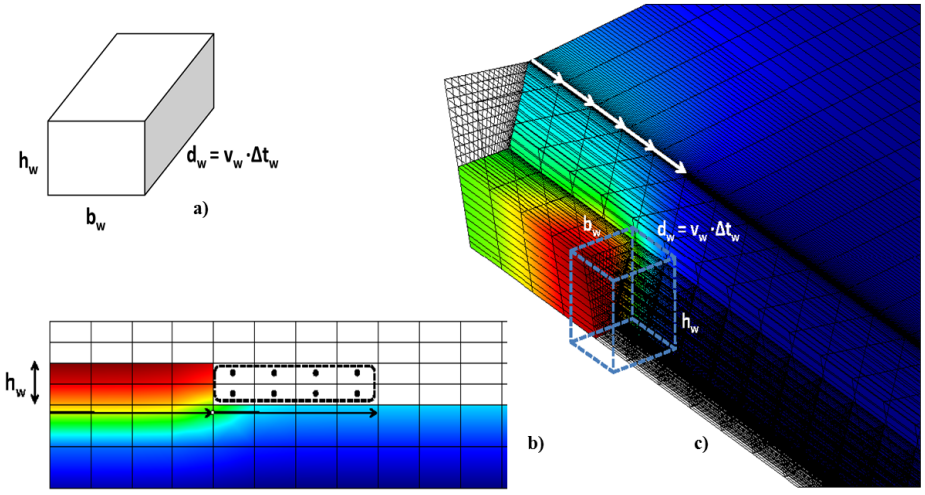

Figure 5.2: Activation strategy: a) Control volume defined for the activation procedure; b) Control volume used for an activation process in a 2D analysis; c) Control volume in a 3D analysis

Control volume: To set up the activation process, a control volume is defined by the cross section, S_{MD}, of the deposited layer, the velocity, v_{MD}, of the arc in the welding direction and the current time step, Δt (Figure 5.2):

$$d = v_{MD}\Delta t \tag{5.1}$$

A searching procedure is performed to identify all the elements belonging to this domain. Afterward, the status of these elements is switched from inactive to activated and they are assembled into the model.

Based on the mass conservation law, the volume of the deposited layer ($V_{MD} = S_{MD}v_{MD}\Delta t$) must be equivalent to the volume of filler wire (V_{feed}) melted at the current time-step. This volume is defined through the feeding system of the welding arc as

$$V_{feed} = \left(\frac{\pi}{4}\phi_{feed}^2\right) v_{feed}\Delta t \tag{5.2}$$

Assuming that:

$$V_{MD} = V_{feed} \tag{5.3}$$

where ϕ_{feed} and v_{feed} are the diameter of the filler wire and the feeding speed, respectively, then the cross section of each deposited layer, S_{MD}, is computed as a function of the welding speed of the arc and the feeding settings, as:

$$S_{MD} = \frac{\pi}{4}\phi_{feed}^2\frac{v_{feed}}{v_{MD}} \tag{5.4}$$

In the born-dead activation technique at each time-step of the simulation, the profile of the solution matrix, the number of equations as well as the boundary of the computational domain vary as a result of the activation procedure.

The searching algorithm must be performed to update the active boundary at each time-step of the analysis, in order to apply appropriately the boundary conditions such as, convection and radiation heat fluxes.

Initial displacements: There are two options when dealing with the mesh defined for the base and the filler material, respectively.

On one side, they could be completely independent and they could interact through contact elements. This option allows for free expansion of the filler material before its deposition. This solution is very expensive.

On the other side, if the base material shares nodes with the filler material (to be activated), then initial spurious displacement and temperature

fields appear, and need to be eliminated. When the thermal dilatation of the filler material is restricted because the nodes of the filler material are shared with the base material, a spurious stress field is generated. In the born-dead activation technique, every newly activated element is born with the initial displacement field, $\mathbf{u}_0$, coming from the movement of the nodes shared with the previously active elements. If this initial displacement is not removed from the computation at the moment of activation, it transforms into initial strain. This leads to the generation of a spurious stress field in both base (tensions) and filler materials (compressions) and therefore spoils the solution.

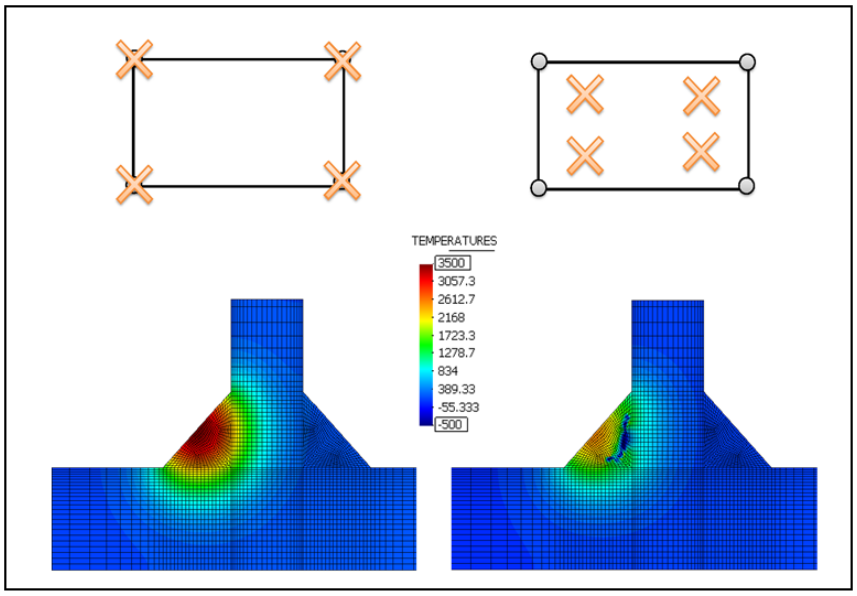

Figure 5.3: Temperature field in a cross section of T-joint welding using: Close (Lobatto) integration rule (lefth); Open (Gauss) integration rule (right)

Hence, it is necessary to remove the initial displacement field, $\mathbf{u}_0$, from the computation of the total strain tensor.

$$\boldsymbol{\varepsilon} = \nabla^S (\mathbf{u} - \mathbf{u}_0) \tag{5.5}$$

Therefore,

$$\boldsymbol{\sigma} = \mathbf{C} : \boldsymbol{\varepsilon}^e = \mathbf{C} : \left[\nabla^S (\mathbf{u} - \mathbf{u}_0) - \boldsymbol{\varepsilon}^p - \boldsymbol{\varepsilon}^\theta\right] \tag{5.6}$$

Thermal overshoots: The welding process induces extremely high temperature gradients along the welding path in the heat affected zone, provoking temperature overshoots and spoiling the solution. From the numerical point of view, this can be observed especially if both coarse meshes and large time-steps are used when analyzing real industrial processes. Using the standard open integration rule (Gauss), overshoots and undershoots are observed in the temperature field obtained from the solution. The temperature distribution obtained is substantially different (see a two-pass welding simulation in Figure 5.3), if different integration rules are used. The overshoots and undershoots in the temperature field obtained by using a standard open integration rule are smoothed when the more diffusive close integration rule (Lobatto) is used.

5.1 Paper contribution

The main contribution of the work briefly presented in this chapter has been published in the research paper attached. More in detail:

- The element activation strategy used for the representation of the filler material deposition in the SMD process according to definition of the welding path is presented in paper (E).

Chapter 6

Apropos Kinematic framework for FSW process

The kinematic framework used for the simulation of welding process is different if a local or global analysis is performed. When the process is simulated at global level, the Lagrangian framework is preferred. In this case the movement of the material points, $\mathbf{X}$, coincides with the mesh nodes. The material and local time derivative of the temperature concide:

$$\frac{d\left(\mathbf{X},t\right)}{dt}=\frac{\partial\left(\mathbf{X},t\right)}{\partial t}$$

If the process is studied at the local level, ALE or Eulerian frameworks are a convenient choice. In this case, the material derivative depends on the local derivative plus a convective term of the form:

$$\frac{dT\left(\mathbf{x},t\right)}{dt}\cong\frac{\partial T\left(\mathbf{x},t\right)}{\partial t}+\frac{\partial T\left(\mathbf{x},t\right)}{\partial\mathbf{x}}\frac{d\mathbf{x}}{dt}=\frac{\partial T\left(\mathbf{x},t\right)}{\partial t}+\mathbf{v}\left(\mathbf{x},t\right)\cdot\nabla_{\mathbf{x}}T\left(\mathbf{x},t\right)\quad(6.1)$$

where $\mathbf{v}\left(\mathbf{x},t\right)$ is the spatial velocity and $\nabla_{\mathbf{x}}T\left(\mathbf{x},t\right)$ is the spatial gradient. The convective term accounts for the movement of the material points with respect to a fixed mesh.

In the ALE framework, the reference system neither moves together with the material (Lagrangian) nor is fixed (Eulerian) but it can move arbitrary. In this case, the material derivative depends on the local derivative plus a convective term as a function of the relative velocity of the material $\mathbf{v}\left(\boldsymbol{\chi},t\right)$ with respect to the mesh velocity $\mathbf{v}_{mesh}$. The material derivative of the

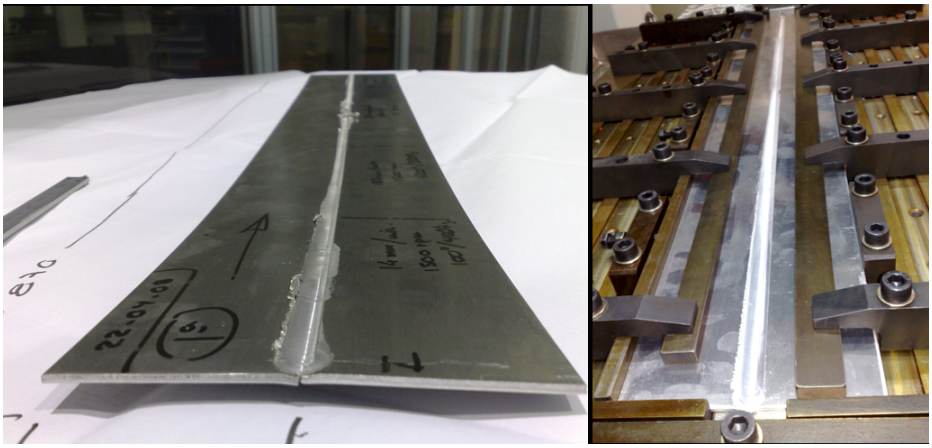

Figure 6.1: FSW process.

temperature is defined as

$$\frac{dT(\boldsymbol{\chi},t)}{dt} \cong \frac{\partial T(\boldsymbol{\chi},t)}{\partial t} + \frac{\partial T(\boldsymbol{\chi},t)}{\partial \boldsymbol{\chi}} \frac{d\boldsymbol{\chi}}{dt} = \frac{\partial T(\boldsymbol{\chi},t)}{\partial t} + (\mathbf{v}(\boldsymbol{\chi},t) - \mathbf{v}_{mesh}) \cdot \nabla_{\boldsymbol{\chi}} T(\boldsymbol{\chi},t) \tag{6.2}$$

In this case, the movement of the mesh must be calculated at each time-step. In general, an ad-hoc methodology is necessary to compute the position of the mesh at each time-step of the analysis. This is known to be one of the main difficulties of the ALE method.

At this point, it is convenient to introduce a feasible strategy and an apropos kinematic framework for the simulation of the FSW process (Figure 6.1). In the FSW process, the pin rotates at constant angular velocity and, at the same time, advances with a constant speed. For the sake of convenience, in the numerical simulation, the movement of the pin is defined by the pure rotation around its axis while the advancing speed (in the opposite direction) is imposed to both the work-piece and the back-plate.

Taking into account that, during the welding process, the pin is rotating with a very high speed (e.g. 50-1000 RPM, depending on the work-piece material), and a fully Lagrangian approach (which follows the material particles of the continuum in their motion) leads to a computational overhead. The reason is that in a Lagrangian analysis, the mesh is attached to the material

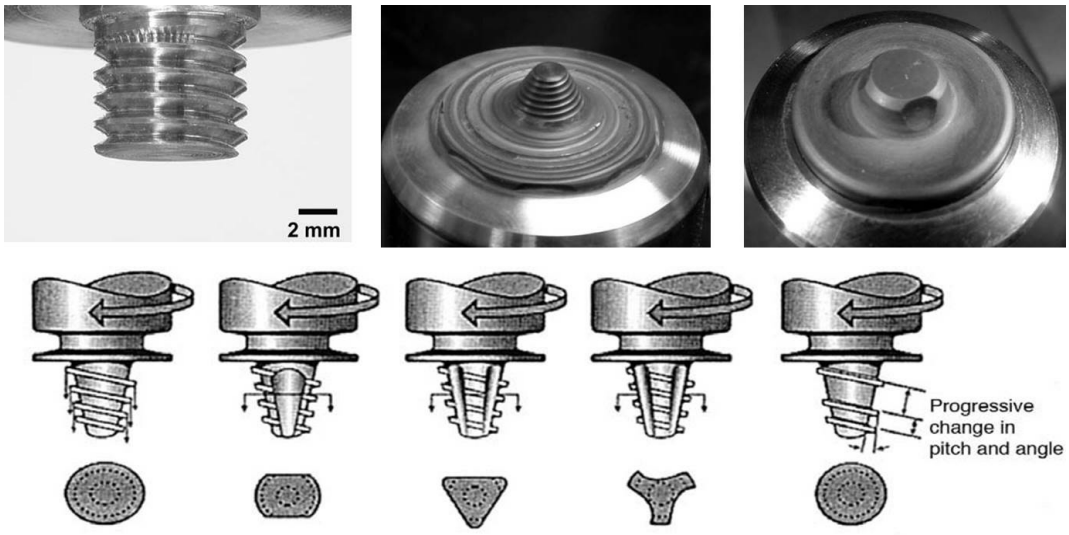

Figure 6.2: Different pin shapes in practice.

and thus the mesh deforms with it. The material in the stirring zone suffers very large deformations at high strain-rates. As a consequence, a fine mesh and a continuous re-meshing are required to avoid an excessive mesh distortion. This usually leads to computationally intensive analyses, as well as, to a general loss of solution accuracy due to the interpolation process necessary to move both nodal and Gaussian variables from mesh to mesh.

Application of a fully Eulerian approach is feasible exclusively for pins with a circular cross-section. When the pin is not cylindrical, the boundaries of the model are continuously changing according to the actual position/rotation of the pin. As a consequence, the integration domain must be re-defined at each time-step of the simulation.

In modeling FSW, the choice of kinematic frameworks for different domain zones (regions) crucially impacts on the computational efficiency and the solution quality. For defining the suitable frameworks several observations must be made:

- The extent of the material deformation varies in different regions of the analysis domain.

- Pins used in practice are not necessarily cylindrical (Figure 6.2).

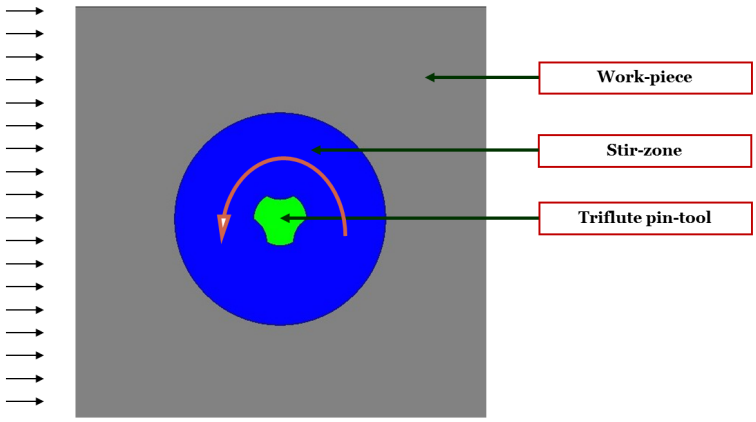

Figure 6.3: The geometry discretization

- Boundary conditions must be applied conveniently according to the movement of the pin.
- Re-definition of the integration domain and re-meshing is preferably to be avoided.

In the proposed methodology, the original geometry is divided into three distinct zones (Figure 6.3) which are: the pin, the work-piece and the stir-zone (process zone close to the pin where most of the material deformation takes place). An apropos kinematic framework is adopted for each one of these zones.

- The pin is assumed to be rigid and it is defined in the Lagrangian framework as at each time-step of the analysis, the mesh moves according to the rotation of the pin.
- The work-piece, excluding the stir-zone close to the pin, is modeled in the Eulerian framework, as in this area the domain neither changes its shape nor contains moving boundaries. The fixed mesh in Eulerian zone enables the application of boundary conditions in the inflow and outflow of the work-piece.
- In the stir-zone, the material is subjected to extremely high strains. Thus, the ALE kinematic framework is chosen to study the stir-zone.

	Pin	**Work-Piece**	**Stir-Zone**
Framework	Lagrangian	Eulerian	ALE
Mesh velocity	$\mathbf{v}_{mesh} = \mathbf{v}$	$\mathbf{v}_{mesh} = \mathbf{0}$	$\mathbf{v}_{mesh} = \boldsymbol{\varpi} \times \mathbf{r}$
Convective velocity	$\mathbf{c} = \mathbf{0}$	$\mathbf{c} = \mathbf{v}$	$\mathbf{c} = \mathbf{v} - \mathbf{v}_{mesh}$
Time derivative	$\frac{D(\circ)}{Dt} = \frac{\partial(\circ)}{\partial t}$	$\frac{D(\circ)}{Dt} = \frac{\partial(\circ)}{\partial t} + \mathbf{v} \cdot \boldsymbol{\nabla}(\circ)$	$\frac{D(\circ)}{Dt} = \frac{\partial(\circ)}{\partial t} + \mathbf{c} \cdot \boldsymbol{\nabla}(\circ)$

Table 6.1: Convective velocity, material derivative and spatial gradient in Lagrangian (pin), Eulerian (work-piece) and ALE (stir-zone) formulations.

The stir-zone is modeled as a circular region around the pin. The size of this area strongly depends on the viscosity and thermal diffusivity of the material. The key idea consists in using the so-called mesh sliding techniques, meaning that the mesh rigidly rotates at each time-step according to the pin movement, decoupling the material motion from the motion of the mesh. Consequently, the integration domain moves in such a way that the inner boundary of the stir-zone is connected to the contour surface of the pin. In the ALE approach, the calculation of the mesh velocity can be a difficulty while in the proposed strategy, this is not an issue. When studying a FSW process, the mesh velocity can be prescribed according to the pin rotation as:

$$\mathbf{v}_{mesh} = \boldsymbol{\varpi} \times \mathbf{r} \tag{6.3}$$

where $\boldsymbol{\varpi}$ is the angular velocity of the pin and $\mathbf{r}$ is the position of any grid point with respect to the rotation axis.

The ALE kinematic framework can recover the Lagrangian and the Eulerian frameworks as limit cases. Denoting by $\mathbf{v}_{mesh}$ the mesh velocity, the convective term can be written as $\rho_o \hat{c}\,[(\mathbf{v} - \mathbf{v}_{mesh}) \cdot \boldsymbol{\nabla} T]$, the convective term vanishes in the Lagrangian framework ($\mathbf{v} = \mathbf{v}_{mesh}$) and simplifies to $\rho_o \hat{c}\ \mathbf{v} \cdot \boldsymbol{\nabla} T$ in the Eulerian zone ($\mathbf{v}_{mesh} = \mathbf{0}$). Table 6.1 summarizes the computational framework together with the solution hypotheses for the pin, the work-piece and the stir-zone.

According to the geometry subdivision and kinematic frameworks introduced, two different types of domain interactions exist. The coupling between each part needs a special attention: on one hand, the connection between

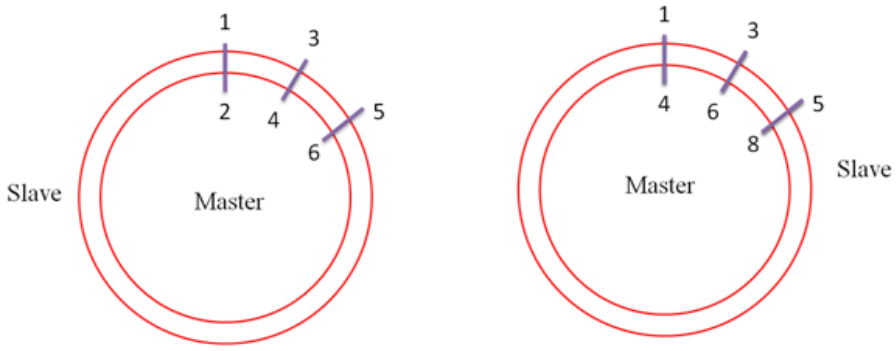

Figure 6.4: Node-to-node link approach.

the fixed mesh of the work-piece and the ALE mesh used for the stir-zone must be considered. On the other hand, the frictional contact between the stir-zone and the pin (see chapter 2) must be defined.

The coupling at the interface between the ALE (stir-zone) and the Eulerian (work-piece) parts requires a special treatment as the mesh is fixed on one side (Eulerian) and it moves on the other side (ALE). Physically, work-piece and stir-zone are not separated, they belong to the same metal sheet even if in the numerical model, a relative movement of the two computational sub-domains exists. Therefore, the objective is to get continuous fields for all the state variables $\mathbf{v}$, p and T at the interface between the two zones. The coupling is performed using a *node-to-node link* or *node-to-face contact* approach.

In the first and simpler case, each node of the mesh on the interface is duplicated (Figure 6.4). One node belongs to the ALE region and the other one to the Eulerian region. At every mesh movement, for a given node of the ALE surface, the corresponding node of the Eulerian side is found and a link between the two nodes is created. A search algorithm restricted to the interface nodes is performed in order to identify all the node-to-node connections at the interface. This leads to an ad-hoc assembling procedure, where the contributions (elemental residuals and tangent matrices) of the stir-zone nodes are summed to the corresponding contributions of the work-piece nodes. This approach requires a coincident mesh at the interface. The time-step is chosen such that the two meshes (ALE and Eulerian) are synchronized to keep the Courant number, $Cu = 1$ at the sliding interface.

The node-to-node linking approach is simple to achieve for 2D analysis but it becomes complex when an automatic 3D mesh generator (which usually supports unstructured tetrahedral meshes) is used. This approach can be applied in 3D analysis if a structured mesh is defined at the interface surfaces. It should be meshed in such way that at each time-step, the ALE mesh at the interface slides from one node to another. This requires coincident and equi-spaced mesh at the contact surfaces.

If the surface meshes are not coincident, a node-to-face approach can be used. For this more complex approach, the mesh is not sychronized. Therefore, at the sliding interface, contact elements are created. At the contact interface, each node of the stir-zone is projected on the work-piece surface. Once the contact elements are generated, whether the Lagrange multiplier method, the augmented Lagrange method, or the penalty method can be used to apply the constraint between the problem variables, T, p, $\mathbf{v}$.

In the penalty method, very large values of both stiffness and thermal resistivity representing the penalty parameters are assigned to the contact elements. This is performed to ensure the most rigid/conductive link between the two domains in both the mechanical and the thermal problems. In this case, the integration domains are connected by forcing coincident heat fluxes and normal tractions on both sides of the contact surface.

In this approach, at each time-step, the contact elements need to be regenerated according to a (rather time-consuming) closest-point-projection algorithm.

6.1 Paper contribution

The main contribution of the work briefly presented in this chapter has been published in the research papers attached. More in detail:

- An apropos kinematic setting relying on the combination of ALE, Eulerian and Lagrangian frameworks for different parts of the domain developed for FSW process is introduced in papers (A) and (B).

Chapter 7

Particle tracing technique

One of the main issues in the study of FSW is heat generation. In the FSW process, welding is achieved by the heat generated due to friction and the material mixing/stirring process. The heat generated must be enough to allow for the material to flow and to obtain a deep heat affected zone. The visualization of the material flow is very useful to understand its behavior during the weld (Figure 7.1). A method assessing the quality of the created weld by visualization of the joint pattern is advantageous. It can be used to have a pre-knowledge of the appropriate process parameters.

In this work, a numerical particle tracing technology is proposed to study the extent of material stirring during the FSW process and to study the weld quality.

Using the Lagrangian framework, the solution obtained at the mesh points represents the material movement: points of the mesh are material particles. Therefore, no special technique for the tracking of the material is necessary. A particle tracing technique is necessary when the solution of the problem is performed in ALE or Eulerian kinematic frameworks.

In this work, the FSW process is simulated using an apropos kinematic framework based on the ALE formulation and a particle tracing method is performed to be able to follow the material movement in the stirring zone integrating the velocity field.

Due to the ALE character of the finite element analysis used, the motion of the finite element mesh is not necessarily tied to the motion of the material. During the analysis, a material particle moves through the mesh and at different time it is located inside different elements. To observe material movement around the pin, it is necessary to construct and analyze material

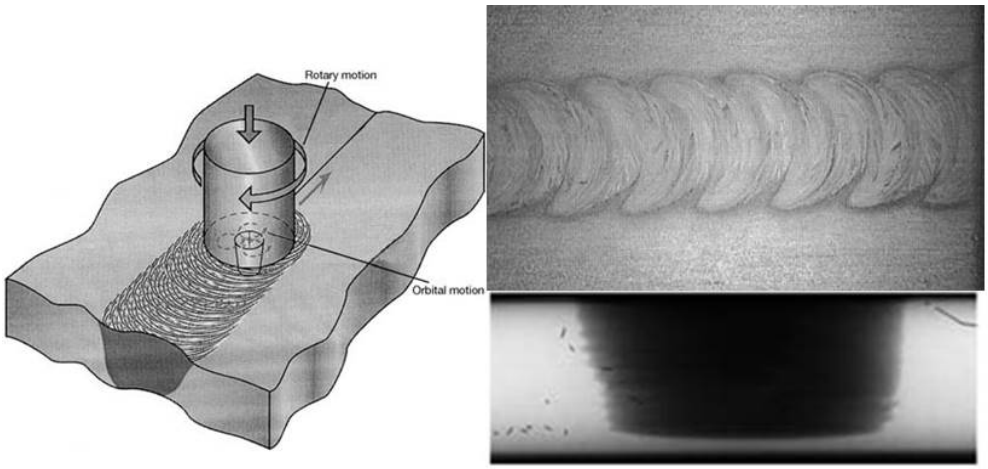

Figure 7.1: Material flow visualization in horizontal and vertical directions.

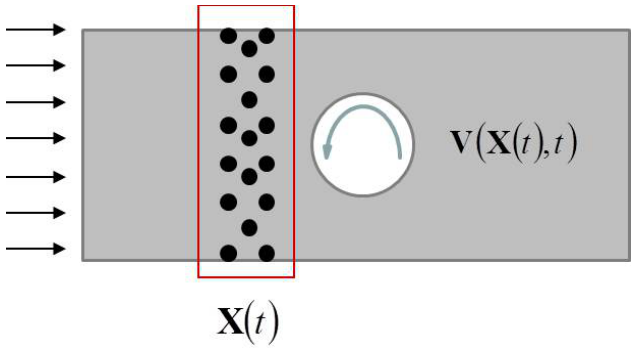

Figure 7.2: Material points distribution.

particle trajectories. This is possible with the use of a particle tracing method (particles are treated as material points not as mesh nodal points).

Particle tracing is a method used to follow the motion of material points, taking their positions at each time-step of the analysis. This method can be naturally applied to the study of the material flow in the welding process.

In this method, firstly, a set of points representing the material points (tracers) are distributed in the domain and then, a Ordinary Differential Equation (ODE) for the computation of material displacement at a post-process level must be solved. Each particle position is integrated from (Figure 7.2):

$$\frac{D\left(\mathbf{X}\left(t\right)\right)}{Dt} = \mathbf{V}\left(\mathbf{X}\left(t\right), t\right) \tag{7.1}$$

with the initial condition

$$\mathbf{X}\left(t=0\right) = \mathbf{X}_0$$

where $\mathbf{X}\left(t\right)$ is the position of the material points at time t and $\mathbf{V}\left(\mathbf{X}\left(t\right), t\right)$ is the velocity of the tracer in the position $\mathbf{X}\left(t\right)$ and time t. The tracer velocity is obtained interpolating the nodal velocity of the background mesh. To this end, firstly, a search algorithm is necessary in order to identify the element containing the tracer (Figure 7.3).

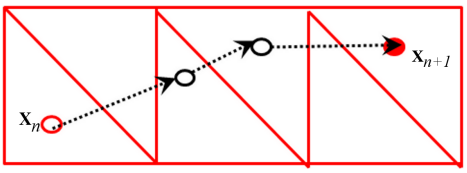

Figure 7.3: Tracer position in time

To solve Eq. (7.1), there exist a large amount of integration techniques ranging from the simple first order Backward Euler (BE) scheme to higher order Runge-Kutta schemes. Among them three well-known methods are chosen and compared: Backward Euler with Sub-stepping (BES), Fourth order Runge-Kutta (RK4) and Back and Forth Error Compensation and Correction methods (BFECC). These methodologies, widely used in fluid dynamics, are suitable and robust tools to study the FSW problem allowing

for a clear visualization of the material movement at the stir-zone leading to a better understanding of the welding process.

7.1 BES method

According to the first-order accurate BES method, the particle position at time-step $n+1$ is computed in k sub-steps as:

$$\begin{cases} \mathbf{X}_{n+1} \cong \mathbf{X}_n + \sum_{i=1}^{k} \mathbf{V}\left(\mathbf{X}_{n+1}^{i}, t_n + \sum_{j=1}^{i} \delta t^j\right) \delta t^i = \mathbf{X}_n + \sum_{i=1}^{k} \mathbf{V}_{n+1}^{i} \delta t^i \\ \dfrac{\Delta t}{k} = \delta t^i \end{cases} \tag{7.2}$$

where Δt is the time-step and δt^i is the i^{th} sub-step.

The velocity of the tracer at the current sub-step i, $\mathbf{V}_{n+1}^{i}$, is computed as:

- The tracer position $\mathbf{X}_{n+1}^{i} = \mathbf{X}\left(t_n + \sum_{j=1}^{i} \delta t^j\right)$ is updated according to the previous sub-step;
- The tracer particle is located within a specific FE by a corresponding searching algorithm;
- The tracer velocity is interpolated from the nodal velocities of the FE identified according to the sub-stepping time, Υ_t :

$$\begin{cases} \mathbf{v}_{n+1}^{i}(t) = (1 - \Upsilon_t)\, \mathbf{v}_n + \Upsilon_t \mathbf{v}_{n+1} \\ \Upsilon_t = \left(\dfrac{t - t_n}{t_{n+1} - t_n}\right) \qquad t_n < t < t_{n+1} \end{cases} \tag{7.3}$$

Remark 5 *Even if the accuracy of the method is enhanced by a sub-stepping technique, it is still first-order accurate* $O(\Delta t)$.

7.2 BFECC method

According to the third-order accurate, $O(\Delta t^3)$, BFECC method, the error arising from backward and forward advection of the particle position is used to modify the initial position.

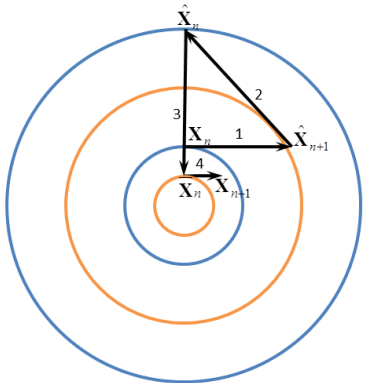

Figure 7.4: The steps of the BFECC method for a rotational velocity field

Denoting with $A(\cdot) = (\cdot) + \int_{t_n}^{t_{n+1}} \mathbf{V}(\cdot, t)\,\mathrm{d}t$, the first order up-winding integration operator, BFECC consists of a prediction/correction procedure: the initial position of the tracer, $\mathbf{X}_n = \mathbf{X}(t_n)$, is advected forward to $\hat{\mathbf{X}}_{n+1} = A(\mathbf{X}_n)$, and then backward to $\hat{\mathbf{X}}_n = A^R\left(\hat{\mathbf{X}}_{n+1}\right)$, $A^R(\cdot)$ being the backward advection operator. The difference between $\hat{\mathbf{X}}_n$ and the initial position defines the error, $\boldsymbol{\epsilon} = \dfrac{\mathbf{X}_n - \hat{\mathbf{X}}_n}{2}$, of the time integration scheme.

This error is used later to correct the starting position, $\bar{\mathbf{X}}_n = \mathbf{X}_n + \boldsymbol{\epsilon}$, for the next advection step, achieving the final solution, $\mathbf{X}_{n+1} = A\left(\bar{\mathbf{X}}_n\right)$.

The steps are the following:

$$\begin{aligned}
\hat{\mathbf{X}}_{n+1} &= A(\mathbf{X}_n) = \mathbf{X}_n + \int_{t_n}^{t_{n+1}} \mathbf{V}(\mathbf{X}_n, t)\,\mathrm{d}t \\
\hat{\mathbf{X}}_n &= A^R\left(\hat{\mathbf{X}}_{n+1}\right) = \hat{\mathbf{X}}_{n+1} - \int_{t_n}^{t_{n+1}} \mathbf{V}\left(\hat{\mathbf{X}}_{n+1}, t\right)\mathrm{d}t \\
\bar{\mathbf{X}}_n &= \frac{\left(3\mathbf{X}_n - \hat{\mathbf{X}}_n\right)}{2} \\
\mathbf{X}_{n+1} &= A\left(\bar{\mathbf{X}}_n\right) = \bar{\mathbf{X}}_n + \int_{t_n}^{t_{n+1}} \mathbf{V}\left(\bar{\mathbf{X}}_n, t\right)\mathrm{d}t
\end{aligned} \tag{7.4}$$

where $A(\circ)$ involves the computation of the velocity field of the tracer at its current position, interpolating from the nodal values (Figure 7.4).

7.3 RK4 method

According to the forth-order accurate RK4 method, the particle position at time-step $n+1$ is computed from the advection of the initial position by four weighted incremental displacement at intermediate time-steps (Figure 7.5):

$$\mathbf{X}_{n+1} = \mathbf{X}_n + \frac{1}{6}\left[\Delta\mathbf{X}^{(1)} + 2\Delta\mathbf{X}^{(2)} + 2\Delta\mathbf{X}^{(3)} + \Delta\mathbf{X}^{(4)}\right] \tag{7.5}$$

where the incremental displacements are computed as

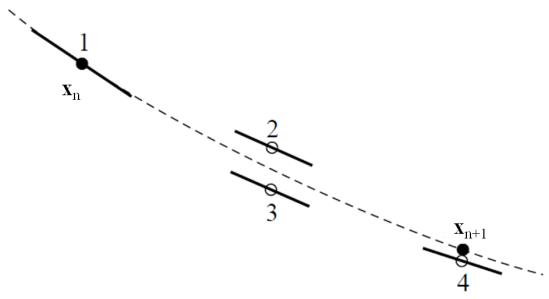

Figure 7.5: Fourth-order Runge-Kutta method. In each step the derivative is evaluated four times: once at the initial point, twice at trial midpoints, and once at a trial endpoint. From these derivatives the final value (shown as a filled dot) is calculated.

$$\begin{aligned}
\Delta\mathbf{X}^{(1)} &= \mathbf{V}\left(\mathbf{X}_n, t_n\right)\Delta t \\
\Delta\mathbf{X}^{(2)} &= \mathbf{V}\left(\mathbf{X}_n + \frac{1}{2}\Delta\mathbf{X}^{(1)}, t_n + \frac{\Delta t}{2}\right)\Delta t \\
\Delta\mathbf{X}^{(3)} &= \mathbf{V}\left(\mathbf{X}_n + \frac{1}{2}\Delta\mathbf{X}^{(2)}, t_n + \frac{\Delta t}{2}\right)\Delta t \\
\Delta\mathbf{X}^{(4)} &= \mathbf{V}\left(\mathbf{X}_n + \Delta\mathbf{X}^{(3)}, t_n + \Delta t\right)\Delta t
\end{aligned} \tag{7.6}$$

The RK4 method is the best choice among the other integration techniques because it can integrate exactly a circular trajectory, which is the most common particle path in FSW.

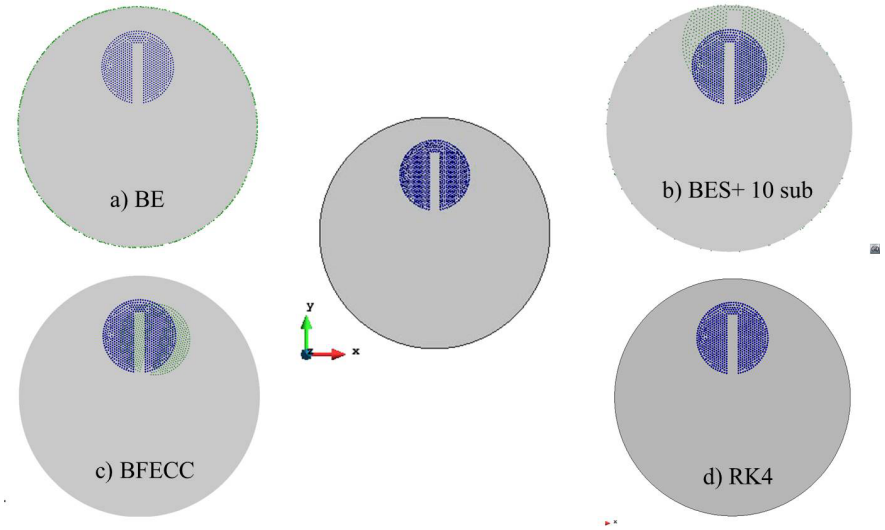

Figure 7.6: Zalesask's benchmark after 10 revolutions.

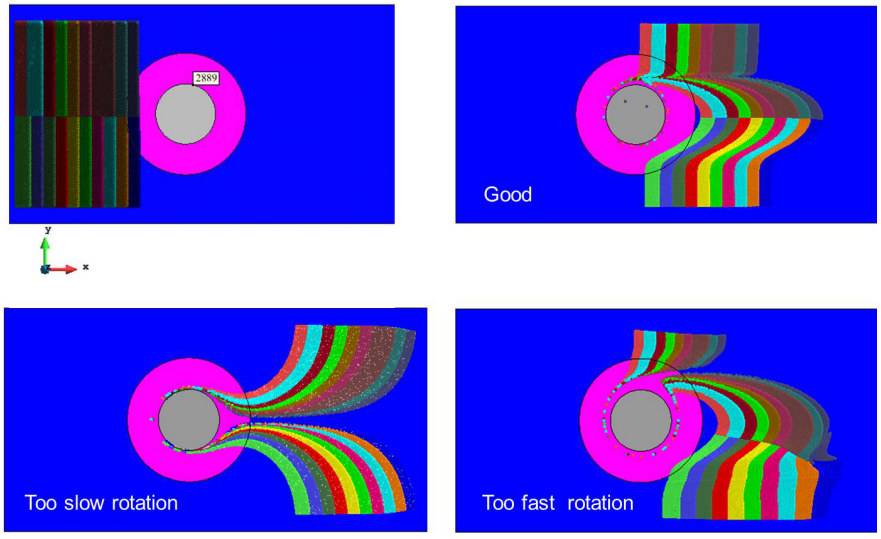

Figure 7.7: Velocity effect on the weld quality.

Figure 7.6 shows the comparison between three represented methods in application to the Zalesask's problem.

Figure 7.7 studies the velocity effect on the final weld quality.

7.4 Paper contribution

The main contribution of the work briefly presented in this chapter has been published in the research papers attached. More in detail:

- The robust numerical procedure for the visualization of material flow used in case of Eulerian/ALE framework is developed in paper (C) and (G). The details about several accurate integration techniques including RK4, BFECC and BES methods are presented there. The final industrial application is the FSW process.

Chapter 8

Conclusion and future work

This thesis deals with the numerical simulation of coupled thermo-mechanical problems. The final industrial application is the study of welding processes, in particular, Friction Stir Welding (FSW) and the Shaped Metal Deposition (SMD) processes. FE-based thermo-mechanical models are developed and the corresponding solution algorithms are implemented within the framework of COMET, an in-house FE-based thermo-mechanical code. The thesis tackles with the actual challenges and opens new perspectives to possible future works.

8.1 Contributions

The proposed methodology has been designed to simulate welding process at global level as well as local level.

At the global level:

- The objective is to study the effect of a moving heat source, in a Lagrangian framework, on the behavior of the whole structure to be welded (in particular arc welding, EB or laser welding processes in which the input energy is known).

At the local level:

- The objective is to analyze the heat affected zone and to study the heat source locally. This can be used as energy input for the global analysis (e.g. in FSW the heat generation comes from plastic dissipation and frictional effects).

Several achievements of this work can be highlighted:

- **Coupled thermo-mechnical model:** A robust and accurate thermo-mechanical solver for the simulation of welding processes has been developed. The transient thermal model proposed in both Lagrangian and Eulerian kinematic frameworks allows for local and global level analysis. Suitable boundary conditions based on Newton's law are introduced to deal with heat conduction at contact interface and heat convection at the external boundaries.

- **Apropos kinematic framework:** To study FSW process, a suitable and robust kinematic setting has been proposed. The apropos kinematic setting, combines ALE, Eulerian and Lagrangian frameworks for different parts of the domain avoiding remeshing and variable remapping procedures. Moreover, it permits to account for the arbitrary and complex pin shapes typically found in FSW process.

- **Mixed stabilized formulation for the mechanical problem:** In the hypothesis of isochoric material behavior as for liquid-like phase or more generally when the deformations are mainly deviatoric (J2 plasticity model used for metals), the stabilized mixed $\mathbf{v}/p$ formulation has been introduced. It is due to the good performance of this technology, especially for industrial simulations when triangular/tetrahedral meshes must be used for the domain discretization. Pressure locking is overcome using VMS stabilization methods. Two stabilization methods are compared: ASGS and OSGS. The OSGS stabilization method shows higher accuracy even if the necessary computational effort is superior.

- **Mixed stabilized formulation for convective dominated thermal problem:** To deal with thermal analysis where the convective term dominates (ALE/Eulerian framework), the convection instabilities has been overcome using VMS stabilization methods. This leads to a very accurate treatment of this numerical problem. The stabilization method based on the sub-grid scales approach circumvents the Ladyženskaja-Babuška-Brezzi (LBB) condition, allowing an accurate and robust formulation for linear elements. Classical GLS and SUPG stabilization methods can be recovered as a particular case of the sub-grid scale stabilization framework.

- **Constitutive modeling:** The thermo-elasto-visco-plastic constitutive model used for the simulation of welding process at global level (such as SMD) has been developed. It is suitable for all the different phases of the material, from the initial liquid phase (purely viscous) to the final solid state (elasto-plastic), passing through the so called mushy zone where the phase transformation takes place. This model covers the full temperature zone leading to an accurate evolution of temperature, distortions and the residual stresses.

  Thermo-rigid-visco-plastic constitutive models such as Norton-Hoff or Sheppard-Wright have been used for the simulations of welding processes at local level (e.g. FSW). These kind of models neglect both the elastic and the thermal strains. They are intended to solve mechanical problem dominated by very high deviatoric strains as well as high strain rates. This is typically the case of FSW process. It is important to observe that also in this case the thermal coupling is essential to capture the real material behavior. This leads to highly non-linear models strongly coupled with the temperature field, which can be treated as non-Newtonian flows, with a temperature dependent viscosity.

- **Strain localization problem:** The FSW process produces a strong strain localization in the stirring zone close to the pin. A sliding zone concentrates in a thin layer under a pure shear stress field.

  The solution of such problem is not feasible using a standard velocity-based element. However, the use of mixed $\mathbf{v}/p$ element is able to capture the strain localization satisfactorily. Also in this case the proposed VMS-based stabilization technique is suitable to treat such complex problem.

- **Material flow visualization:** The work also deals with the problem of material tracking in the stirring zone. The simulation is carried out using a rigid visco-plastic constitutive model and this reduces into a non-Newtonian fluid-like analysis where it is important to visualize the material flow. The model provides this insight by tracking the particles position during the full motion of the FSW process in the stirring zone.

  The trend observed is consistent with the results of experiments, showing the motion of the markers inserted into the weld. The model correctly predicts the material flow around the retreating side of the pin.

Results of the simulation correctly demonstrate that the material is moved away from the direction of travel and material sticking could occur at the tool interface. The resulting material flow is not symmetric with respect to the joint line and the flow patterns on the advancing and retreating sides are different.

The model is able to include the effect of complex tool geometries as threaded pin. Some distinctive 3D features of the flow can be appreciated. These included: the material flow within the thickness direction and a centrifugal material flow pattern around the pin.

Among the integration methods (BES, BFECC and RK4) used for the problem of interest, RK4 is found to be the most accurate when a larger time-step is used.

- **Ad-hoc activation technology:** An ad-hoc activation methodology for simulating the addition of the filler material along the welding path is proposed. It is based on the born-dead element activation technique.

  Applied to the SMD process, this technology is able to simulate the deposition of the melted material along the predefined welding path.

8.2 Lines for future work

This section outlines the possible future developments in the thermomechanical analysis of welding processes arising as a natural continuation of the present work. The following research lines are suggested:

- Finite element technology:
  - A new FE technology based on a three-field mixed formulation can be introduced for the highly non-linear stress field typically encountered in the stirring zone of the welding process. The mixed $\mathbf{v}/\boldsymbol{\sigma}/p$ formulation is known for an enhanced stress field approximation. It achieves a remarkable degree of accuracy of the stress field in non-linear computational mechanics.
  - Comparison with an embedded (also known as an "immersed boundary") approach in terms of accuracy and CPU time can be performed. Using an embedded approach, the computational grid is

fixed in time (Eulerian framework) while an immersed boundary is moving according to the pin position.

- Large strain kinematics can be used in the global level analysis to study the work-piece deformation due to the thermal load. Using a small strain formulation the deflection can be underestimated.

- Constitutive law:

  - The constitutive models used for the local level simulation encounter some difficulties at the limit cases when viscosity tends to infinity or zero. There are a variety of non-Newtonian models such as the Carreau model, in which these singularities are avoided by means of saturation viscosities at limit cases. The range of admissible viscosity values is bounded by the viscosity-strain rate at room temperature and for the liquid phase. Implementation of these models is a possible future line of research.
  - At global level, large strain plasticity models can be linked to the finite deformation kinematics to tackle with the large deformations induced by the thermal load during welding process as well as in the cooling phase.

- The calibration of the friction model is an open issue to be investigated in order to better identify the friction behavior. A non-linear friction model including the normal pressure and the relative slip velocity would significantly affect the friction between two surfaces in contact.

- The evaluation of residual stresses is an open task for further developments. During the welding process, thermal and mechanical stresses develop in the HAZ due to the thermal expansion and the mechanical constraint (e.g. clamping). Therefore, during the cooling phase longitudinal and transverse stresses are generated. High values of residual stresses have a significant effect on the post-weld mechanical properties, particularly the fatigue behavior. For the computation of the residual stresses at local level analysis, a more sophisticated model (considering also the elastic effects) must be developed.

- The relationship between global and local level analyses is an open issue to be investigated. The idea is to compute the heat source in a

local level simulation (generally carried out in a very fine mesh) and hen to transfer it as a moving energy input for the global level analysis (generally carried out in a coarse mesh). In this way, the effects of the heat source used for the welding process are studied at component level (global analysis).

- At local level the microstructure analysis can be performed to gain an insight of microstructure evolution induced by temperature as well as by stirring effects. Nucleation, grain growth and recrystallization process (in HAZ) can be studied.

- The relationship between micro and macro level analysis is another interesting line of research. The idea is to be able to define thermophysical material properties (at macro scale) which depend on the metallurgical evolution (at micro scale).

- The estimation of hot cracking risk is another possible research line. The combination of liquid films along grain boundaries and thermal tensile stresses induced by the thermal deformations during the thermal cycles of the process may lead to the formation of micro cracks weakening the structural response.

- Accurate results within a short period of time can be obtained using parallel solver capabilities. Therefore the parallelization of the software is a future work to speed-up the simulation process.

References

[1] Abdollah-Zadeh, A., Saeid, T., Sazgari, B. (2008) Microstructural and mechanical properties of friction stir welded aluminum/copper lap joints, Journal of alloys and Compounds, 460:535-538.

[2] Agelet de Saracibar, C., Cervera, M. and Chiumenti, M. (1999) On the formulation of coupled thermoplastic problems with phase-change, Int. J. of Plasticity 15:1–34.

[3] Agelet de Saracibar, C., Cervera, M. and Chiumenti, M. (2001) On the constitutive modeling of coupled thermomechanical phase-change problems, International Journal of Plasticity 17(12):1565-1622.

[4] Agelet de Saracibar, C., Chiumenti, M., Valverde, Q. and Cervera, M. (2006) On the orthogonal sub-grid scale pressure stabilization of finite deformation J2 plasticity, Comp. Method in Appl. Mech. and Eng. 195:1224-1251.

[5] Agelet de Saracibar, C., Chiumenti, M., Santiago, D., Dialami, N. and Lombera, G. (2010) On the numerical modeling of fsw processes. In Proceedings of the International Symposium on Plasticity and its Current Applications, Plasticity 2010, St. Kitts, St. Kitts and Nevis, January 3 - 8.

[6] Agelet de Saracibar, C., Chiumenti, M., Santiago, D., Cervera, M., Dialami, N. and Lombera, G. (2010) A computational model for the numerical simulation of fsw processes. In Proceedings of the 10th International Conference on Numerical Methods in Industrial Forming Processes 1252: 81 – 88, Pohang, South Korea, June 13-17. AIP Conference Proceedings. doi: 10.1063/1.3457640.

[7] Agelet de Saracibar, C., Chiumenti, M., Santiago, D., Cervera, M., Dialami, N. and Lombera, G. (2011) Advances in the numerical simulation of 3D FSW processes. In Proceedings of the International Symposium on Plasticity and its Current Applications, Plasticity 2011, Puerto Vallarta, Mexico, January 3 - 8.

[8] Agelet de Saracibar, C., Chiumenti, M., Cervera, M., Dialami, N. and Seret, A. (2014) Computational modeling and sub-grid scale stabilization of incompressibility and convection in the numerical simulation of friction stir welding processes. Archives of Computational Methods in Engineering, 21(1), in press.

[9] Agelet de Saracibar, C. and Chiumenti, M. (1998) On the numerical modeling of frictional wear phenomena, Computer Methods in Applied Mechanics and Engineering 177:401-426.

[10] Alimardani, M., Toyserkani, E., Huissoon, J.P. (2007) Three-dimensional numerical approach for geometrical prediction of multi-layer laser solid freeform fabrication process. Journal of Laser Applications 19(1):14–25.

[11] Anca, A., Cardona, A., Risso, J. and Fachinotti, V. (2011) Finite element modeling of welding processes, Applied Mathematical modeling 01/2011.

[12] Anca, A., Fachinotti, V., Escobar-Palafox, G. and Cardona, A. (2010) Computational modeling of shaped metal seposition, International Journal for Numerical Methods in Engineering 85(1):84–106.

[13] Armero, F. and Simo, J.C. (1992) A new unconditionally stable fractional step method for non-linear coupled thermomechanical problems, International Journal for numerical methods in Engineering 35:737–766.

[14] Armero, F and Simo, J.C. (1991) A New Unconditionally Stable Fractional Step Method for Nonlinear Coupled Thermomechanical Problems. Int. Journal for Num. Meth. in Engin. 35:737-766.

[15] Armero, F and Simo, J.C. (1992) Product Formula Algorithms for Nonlinear Coupled Thermoplasticity: Formulation and Nonolinear Stabil-

ity Analysis. Sudam Report #92-4, Department of Mechanical Engineering, Stanford University, Stanford, California.

[16] Askari, A., Silling, S., London, B. and Mahoney, M. (2001) In 'Friction Stir Welding and Processing', (Ed. KV. Jata et al.) 43-54, Warrendale, PA, TMS.

[17] Askari, A., Silling, S., London, B. and Mahoney, M. (2003) modeling and Analysis of Friction Stir Welding Processes, The 4th International Symposium on Friction Stir Welding, GKSS Workshop, Park City, Utah, USA.

[18] Assidi, M. and Fourment, L. (2009) Accurate 3D friction stir welding simulation tool based on friction model calibration, International Journal of Material Forming 2(1): 327-330.

[19] Assidi, M., Fourment, L., Guerdoux, S. and Nelson, T. (2010) Friction model for friction stir welding process simulation: calibrations from welding experiments, Int. J. Mach. Tools Manuf. 50(2):143–155.

[20] Baufeld, B. and Van der Biest O. (2009) Mechanical properties of Ti-6Al-4V specimens produced by shaped metal deposition. Sci. Technol. Adv. Mater 10:015008 (10pp).

[21] Bendzsak, G., North, T. and Smith, C. (2000) An Experimentally Validated 3D Model for Friction Stir Welding, Proceedings of the 2nd International Symposium on Friction Stir Welding, Gothenburg, Sweden.

[22] Bendzsak, G., North, T. and Smith, C. (2000) Material Properties Relevant to 3-D FSW Modeling, Proceedings of the 2nd International Symposium on Friction Stir Welding, Gothenburg, Sweden.

[23] Bendzsak, G.J. and North, T.H. (1997) Numerical modeling of Fluid Dynamics and Heat Transfer in Friction Welding Proc. International Seminar, Numerical Analysis of Weldability, Graz, Austria, Sept. 30th-Oct. 3rd.

[24] Bendzsak, O. J. and North, T. H. (1998) in 'Mathematical modeling of Weld Phenomena 4', (ed. H. C. Cerjak), 429-443, London, 10M Communications Ltd.

[25] Benson D.J. (1989) An effcient, accurate, simple ALE method for nonlinear finite element programs, Comput. Methods Appl. Mech. Eng. 72:305–350.

[26] Blackwell, P.L. (2005) The mechanical and microstructural characteristics of laser-deposited IN718. J. Mater. Process. 170 (1/2):240–246.

[27] Brezzi, F., and Fortin, M. (1991) Mixed and Hybrid Finite Element Methods, Spinger, New York.

[28] Bruschi, S., Poggio, S., Quadrini, F. and Tata, M.E. (2004) Weldability of Ti–6Al–4V alloy at high temperatures and strain rates. Materials Letters 58:3622–3629.

[29] Buffa, G., Hu, J., Shivpuri, R. and Fratini, L. (2006) A continuum based fem model for friction stir welding-model development, Materials Science and Engineering A 419:389–396.

[30] Buffa, G., Hu, J., Shivpuri, R. and Fratini, L. (2006) Design of the friction stir welding tool using the continuum based FEM model, Materials Science and Engineering A 419:381–388.

[31] Buffa, G., Ducato, A. And Fratini L. (2011) Numerical procedure for residual stresses prediction in friction stir welding, Finite Elements in Analysis and Design 47:470–476.

[32] Bussetta P., Dialami N., Boman R., Chiumenti M., Agelet de Saracibar C., Cervera M. and Ponthot J.-P. (2013) Comparison of a fluid and a solid approach for the numerical simulation of Friction Stir Welding with a non-cylindrical pin, Steel research international, DOI: 10.1002/srin.201300182.

[33] Cederqvist L. (2001) Properties of friction stir welded aluminum lap joints. Master of Science Thesis, Department of Mechanical Engineering, University of South Carolina, Columbia, USA.

[34] Cervera, M., Agelet de Saracibar, C. and Chiumenti, M. (1999) Thermo-mechanical analysis of industrial solidification processes, Int. J. Numer. Meth. Eng. 46:1575–1591.

[35] Cervera, M., Chiumenti, M., Valverde, Q. and Agelet de Saracibar, C. (2003) Mixed linear/linear simplicial elements for incompressible elasticity and plasticity, Comp. Method in Appl. Mech. and Eng. 192:5249-5263.

[36] Cervera, M., Agelet de Saracibar, C. and Chiumenti, M. (2002) Comet – a coupled mechanical and thermal analysis code. data input manual. version 5.0. Technical Report IT-308, CIMNE, Barcelona, Spain. URL http://www.cimne.com/comet.

[37] Chao, Y.J., Qi, X. (1998) Thermal and thermo-mechanical modeling of friction stir welding of aluminum alloy 6061-T6, J. Mater. Process. Manuf. Sci. 7:215–233.

[38] Chao, Y.J., Qi, X. (1999) Heat transfer and thermo-mechanical modeling of friction stir joining of AA6061-T6 plates, Proceedings of the First International Symposium on Friction Stir Welding, Thousand Oaks, CA, USA.

[39] Chao, Y.J., Qi, X. and Tang, W. (2003) Heat transfer in friction stir welding: experimental and numerical studies, ASME J. Manuf. Sci. Eng. 125:138–145.

[40] Charles, C., Järvstrat, N. (2007) Development of a microstructure model for metal deposition of titanium alloy Ti–6Al–4V. In: 11th World conference on titanium (Ti-2007), Kyoto, Japan.

[41] Charles, C., Järvstrat, N. (2008) modeling Ti–6Al–4V microstructure by evolution laws implemented as finite element subroutines: application to TIG metal deposition. In: 8th International conference on trends in welding research. Pine Mountain, GA, USA.

[42] Chen, C. and Kovacevic, R. (2004) Thermomechanical modeling and force analysis of friction stir welding by the finite element method, Proc. Inst Mech. Eng., Part C: J. Mech. Eng. Sci. 218:509–519.

[43] Chenot, J.L. and Massoni, E. (2006) Finite element modeling and control of new metal forming processes, Journal of Machine Tools and Manufacture, 46:1194–1200.

[44] Chin, R., Beuth, J. Amon, C. (1996) in: Proc. Solid Freeform Fabrication Sym., University of Texas Austin, 221–228.

[45] Chin, R., Beuth, J. Amon, C. (1996) in: Proc. Solid Freeform Fabrication Sym., University of Texas Austin, 507–514.

[46] Chiumenti, M., Valverde, Q., Agelet de Saracibar, C. and Cervera, M. (2002) A stabilized formulation for elasticity using linear displacement and pressure interpolations, Comp. Meth. in Appl. Mech. and Eng. 191:5253-5264.

[47] Chiumenti M., Valverde Q., Agelet de Saracibar C. and Cervera M. (2004) A Stabilized Formulation for Incompressible Plasticity Using Linear Triangles and Tetrahedra, International Journal of Plasticity, 20:1487-1504.

[48] Chiumenti M., Agelet de Saracibar C. and Cervera M. (2008) On the Numerical Modeling of the Thermo-mechanical Contact for Casting Analysis, J. Heat Transfer 130:061301-1.

[49] Chiumenti M., Cervera M., Salmi A., Agelet de Saracibar C., Dialami N. and Matzui K. (2010) Finite element modeling of multi-pass welding and shaped metal deposition processes, Computer Methods in Applied Mechanics and Engineering 199:2343-2359.

[50] Chiumenti, M., Cervera, M., Agelet de Saracibar, C. and Dialami, N. (2012) Numerical modeling of friction stir welding processes. Computer Methods in Applied Mechanics and Engineering, 254:353–369.

[51] Chiumenti, M., Cervera, M., Agelet de Saracibar, C. and Dialami, N. (2013) A novel stress accurate FE technology for highly non-linear analysis with incompressibility constraint. application to the numerical simulation of the FSWprocess. In Proceedings of the International Conference on Numerical Methods in Forming Processes, NUMIFORM, Shenyang, China. AIP Conference Proceedings.

[52] Cho, Y.I. and Kensey, K.R. (1991) Effects of the non-Newtonian viscosity of blood on flows in a diseased arterial vessel. Part I: Steady flows, Biorheology 28:241–262.

[53] Cho, J., Boyce, D. and Dawson, P. (2005) modeling strain hardening and texture evolution in friction stir welding of stainless steel, Materials Science and Engineering A, 398:146–163.

[54] Chorin, A., Hughes, T.J.R., McCracken, M.F. and Marsden, J.E. (1978) Product Formulas and Numerical Algorithms. Communications in Pure Applied Mathematics 31:205-256.

[55] Clark, D., Bache, M.R., Whittaker, M.T. (2008) Shaped metal deposition of a nickel alloy for aeroengine applications, Journal of Materials Processing Technology 203:439–448.

[56] Codina, R. (2000) Stabilization of incompressibility and convection through orthogonal sub-scales in finite element methods, Comp. Meth. in Appl. Mech. and Eng. 190:1579-1599.

[57] Codina, R. (2002) Stabilized finite element approximation of transient incompressible flows using orthogonal subscales, Comp. Meth. in Appl. Mech. and Eng. 191:4295-4321.

[58] Codina, R. and Blasco, J. (2000) Stabilized finite element method for transient Navier-Stokes equations based on pressure gradient projection, Comp. Meth. in Appl. Mech. and Eng. 182:287-300.

[59] Colegrove, P., Pinter, M., Graham, D. and Miller, T. (2000) Three dimensional flow and thermal modeling of the friction stir welding process, Proceedings of the Second International Symposium on Friction Stir Welding, Gothenburg, Sweden, June 26–28.

[60] Colegrove, P.A. and Shercliff, H.R. (2003) Experimental and Numerical Analysis of Aluminum Alloy 7075-T7351 Friction Stir Welds, Sci. Technol. Weld. Join. 8(5):360–368.

[61] Colegrove, P.A. (2004) modeling the friction stir welding of aerospace alloys, 5th International Friction Stir Welding Symposium, Metz, France, 14-16 September.

[62] Colligan, K. (1999) Material Flow Behaviour during Friction Stir Welding of Aluminium, Welding Journal 78:229-237.

[63] Cross, M.M. (1965) Rheology of non-Newtonian fluids: a new flow equation for pseudoplastic systems, J. Colloid Sci. 20:417–437.

[64] Dalgarno, K., Childs, T., Rowntree, I., Rothwell, L. (1996) in: Proc. Solid Freeform Farication Sym., University of Texas Austin, 559– 566.

[65] Dawes, C.J. (1995) An introduction to friction stir welding butt welding and its developments, Welding and Met. Fabrication 63:3-16.

[66] De Vuyst, T., D'Alvise, L., Robineau, A. and Goussain, J.C. (2006) Material flow around a friction stir welding tool – Experiment and Simulation, 8th International Seminar on Numerical Analysis of Weldability, Graz, Austria.

[67] De Vuyst, T., D'Alvise, L., Robineau, A. and Goussain, J.C. (2006) Simulation of the material flow around a friction stir welding tool, TWI 6th International Symposium on FSW, Saint-Sauveur.

[68] Dialami, N., Chiumenti, M., Cervera, M. and Agelet de Saracibar, C. (2013) An apropos kinematic framework for the numerical modeling of friction stir welding. Computers and Structures 117:48–57.

[69] Dialami N., Chiumenti M., Cervera M., Agelet de Saracibar C. and Ponthot J.-P. (2013) Material Flow Visualization in Friction Stir Welding via Particle Tracing, International Journal of Metal Forming, DOI: 10.1007/s12289-013-1157-4.

[70] Dickerson, T., Shercliff, H.R., Schmidt, H. (2003) A weld marker technique for flow visualization in friction stir welding, 4th International Symposium on Friction Stir Welding, Park City, Utah, USA, 14-16 May.

[71] Dong, P., Lu, F., Hong, J.K., Cao, Z. (2001) Coupled thermomechanical analysis of friction stir welding process using simplified models, Sci. Technol. Weld. Jointing 6:281–287.

[72] Dong, P., Lu, F., Hong, J. and Cao, Z. (2000) Analysis of Weld Formation Process in Friction Stir Welding, The 2nd International Symposium on Friction Stir Welding. Gothenburg, Sweden.

[73] Donne, C.D., Lima, E., Wegener,J., Pyzalla, A. and Buslaps, T. (2001) Investigations on residual stresses in friction stir welds, in: Proceedings of the Third International Symposium on Friction Stir Welding, Kobe, Japan, September 27–28.

[74] Fachinotti, V., Anca, A. and Cardona, A. (2011) Analytical solutions of the thermal field induced by moving double-ellipsoidal and double-elliptical heat sources in a semi-infinite body, Communications in Numerical Methods in Engineering 27(4):595–607.

[75] Fachinotti, V., Cardona, A., Baufeld, B. and Van der Biest, O. (2010) Evolution of microstructure during shaped metal deposition, paper presented at Mechanica Computacional, CILAMCE.

[76] Fachinotti, V., Cardona, A., Cosimo, A., Baufeld, B. and Van der Biest, O. (2010) Evolution of temperature during shaped metal deposition: finite element predictions vs. observations, paper presented at Mecanica Computacional, CILAMCE.

[77] Fachinotti, V., Cardona, A., Baufeld B. and Van der Biest, O. (2012) Finite-element modeling of heat transfer in shaped metal deposition and experimental validation, Acta Materialia 60:6621–6630.

[78] Fonda, R. W. and Lambrakos, S. G. (2002) Sci. Technol. Weld. Joining. 7(3), 177-181.

[79] Fourment, L., Guerdoux, S., Miles, M., Nelson, T. (2004) Numerical Simulation of friction stir welding process using both Lagrangian and Arbitrary Lagrangian Eulerian Formulations, 5 th International Friction Stir Welding Symposium, Metz, France, 14-16 September.

[80] Fourment, L. and Guerdoux, S. (2008) 3D numerical simulation of the three stages of Friction Stir Welding based on friction parameters calibration, International Journal of Material Forming 1(1): 1287-1290.

[81] Franca, LP. and Hughes, TJR. (1993) Convergence analyses of Galerkin least-squares methods for advective–diffusive forms of the Stokes and incompressible Navier–Stokes equations, Computer Methods in Applied Mechanics and Engineering 105:285–298.

[82] Frigaard, O., Grong, O., Midling, O.T. (2001) A process model for friction stir welding of age hardening aluminum alloys, Metal. Mater. Transition A 32:1189–1200.

[83] Fu, L., Duan, L. Y. and Du, S. O. (2003) Welding Joumal 82(3), 65s - 70s.

[84] Gao L., Chen R.S. and Han E. H. (2011) Thixoformability of a Mg-Gd-Y magnesium alloy and its mechanical properties, Materials Science and Technology, 27(6):1084-1091.

[85] Garbey, M. and Tromeur-Dervout, D. (2000) Operator Splitting and Domain Decomposition for Multiclusters, Parallel Computational Fluid Dynamics Towards Teraflops Optimization and Novel Formulations, ELSEVIER Science 27–36.

[86] Garikipati, K. and Hughes, T.J.R. (1998) A study of strain localization in a mulitiple scale framework -the one dimensional problem, Comp. Meth. in Appl. Mech. and Eng. 159:193-222.

[87] Garikipati, K. and Hughes, T.J.R. (2000) A variational multiscale approach to strain localization - formulation for multidimensional problem, Comp. Meth. in Appl. Mech. and Eng. 188:39-60.

[88] Ohanimi, Y., Celjak, H. C. and Faes, K. (2002) Proc. 6th Int. Conf. on 'Trends in Welding Research', Phoenix, Arizona, ASM International, 329-333.

[89] Goldak, J., Chakravarti, A., Bibby, M. (1984) A new finite element model for welding heat sources, Metall. Trans. 15B:299–305.

[90] Gould, J. E. and Feng, Z. (1998) Heat flow model for friction stir welding of aluminum alloys, Joumal of Materials Processing & Manufacturing Science 7(2):185-194.

[91] Grong, O. (1997) Metallurgical modeling of Welding, 2nd edn, London, UK, Institute of Materials.

[92] Guerdoux, S. and Fourment, L. (2009) A 3D numerical simulation of different phases of friction stir welding, Modelling Simul. Mater. Sci. Eng. 17 075001.

[93] Guerra, M., McClure, J. C., Murr, L. E. and Nunes, A. C. (2001) in 'Friction Stir Welding and Processing', (Ed. K.V. Jata et al.) 25-34; WatTendale, PA, TMS.

[94] Guerra, M., Schmids, C., McClure, J.C., Murr, L.E. and Nunes, A.C. (2003) Flow patterns during friction stir welding, Material Characterization 49:95-101.

[95] Hamilton, C., Dymek, S., Sommers, A. (2008) A thermal model of friction stir welding in aluminium alloys, International Journal of Machine Tools & Manufacture 48:1120-1130.

[96] Heurtier, P., Jones, M.J., Desrayaud, C., Driver, J.H., Montheillet, F. and Allehaux, D. (2006) Mechanical and thermal modeling of friction stir welding. J Mater Process Technol 171:348–357.

[97] Hoff, H. J. (1954) Approximate Analysis of structures in presence of moderately large creep deformation Quart. Appl. Math, 12:49.

[98] Hou, J. (1999) Journal of Manufacturing Science and Engineering 121:321-327.

[99] Hsu, T-C. and Li, Y-M. (2000) Tribology Transactions 43(4):781-787.

[100] Huetink, J. ,Vreede, P.T. and Lugt, J.V.D. (1990) Progress in mixed Eulerian–Lagrangian finite element simulation of forming process, Int. J. Numer. Methods Eng. 30:1441–1457.

[101] Hughes, T.J.R. and Brooks, A.N. (1982) A theoretical framework for Petrov-Galerkin methods, with discontinuous weighting functions: applications to the streamline upwind procedure, in: R.H. Gallagher, D.M. Norrie, J.T. Oden and O.C. Zienkiewicz, eds., Finite Element in Fluids, vol. IV,Wiley, London 46-65.

[102] Hughes, T.J.R. (1987) The finite element method: linear static and dynamic finite element analysis, Prentice-Hall, Inc. Englewood Cliffs, New Jersey.

[103] Hughes, TJR., Franca, LP. and Hulbert, GM. (1989) A new finite element formulation for computational fluid dynamics: VIII. The Galerkin=least-squares method for advective–diffusive equations, Computer Methods in Applied Mechanics and Engineering 73:173–189.

[104] Hughes, T.J.R. (1995) Multiscale phenomena: Green's function, Dirichlet-to Neumann formulation, sub-grid scale models, bubbles and the origins of stabilized formulations, Comp. Meth. in Appl. Mech. and Eng. 127:387-401.

[105] Johnson, W. and Kudo, H.K. (1962) The Mechanics of Extrusion, Manchester University Press, UK, 40.

[106] Johanson, R., Threadgill, P. (2003) Friction Stir Welding of Magnesium alloys, Magnesium Technology, TMS, 2003.

[107] Jorge Jr., A.M. and Balancín, O. (2004) Prediction of Steel Flow Stresses under Hot Working Conditions, Materials Research 8(3):309-315.

[108] Källgren, T., Jin, L.-Z., Sandström, R (2008) Material Flow during Friction Stir Welding of Copper 7th international Friction Stir Welding symposium, Awaji island, Japan, 20-22 May.

[109] Karapatis, N., Guidoux, Y., Gygax, P., Glardon, R. (1998) in: Proc. Solid Freeform Fabrication Sym., University of Texas Austin, 79–87.

[110] Katou, M., Oh, J., Miyamoto, Y., Matsuura, K., Kudoh, M. (2007) Freeform fabrication of titanium metal and intermetallic alloys by three-dimensional micro welding. Mater 28:2093–8.

[111] Khandkar, M. Z. H. and Khan, J. A. (2001) Materials Processing & Manufacturing Sci. 10(2):91-105.

[112] Khandkar, M. Z. H., Khan, J. A. and Reynolds, A. P. (2002) Proc. 6th Int. Conf. on 'Trends in Welding Research', Phoenix, Arizona, ASM International, 218-223.

[113] Khandkar, M. Z. H., Khan, J. A. and Reynolds, A. P. (2003) Sci. Technol. Weld. Joining 8(3):166-174.

[114] Khandkar, M. Z. H., Khan, J. A., Reynolds, A. P. and Sutton, M.A. (2006) Predicting residual thermal stresses in friction stir welded metals, Journal of Materials Processing Technology 174:195-203.

[115] Klass, O., Maniatty, A. and Shephard, M.S. (1999) A stabilized mixed finite element method for finite elasticity. Formulation for linear displacement and pressure interpolation, Comp. Meth. in Appl. Mech. and Eng. 180:65-79.

[116] Klass, O., Maniatty, A. and Shephard, M.S. (1999) Three dimensional stabilized finite element model for finite deformation process. Proceedings 7th International Symposium on Plasticity and its Current applications, Cancun, Mexico.

[117] Klingbeil, N., Zinn, J. and Beuth, J. (1996) in: Proc. Solid Freeform Fabrication Sym, University of Texas Austin, 125-132.

[118] Klingbeil, N., Beuth, J., Chin, R. and Amon, C. (1998) in: Proc. Solid Freeform Fabrication Sym., University of Texas Austin, 367–374.

[119] Li, Y., Murr, L.E. and McClure, J.C. (1999) Flow visualization and residual microstructures associated with the friction-stir welding of 2024 aluminium to 6061 aluminium, Materials Science and Engineering A 271:213-223.

[120] Liechty, B.C., Webb, B.W. (2007) The use of plasticine as an analog to explore material flow in friction stir welding, Journal of Materials Processing Technology, 184:240-250.

[121] L.-E., Lindgren, Runnemalm, H., Nasstrom, M.O. (1999) Simulation of multipass welding of a thick plate, International Journal of Numerical Methods and Engineering 44(9):1301–1316.

[122] Lindner, K., Khandkar, Z., Khan, J., Tang, W. and Reynolds, A. P. (2003) Proc. 4th Int. Symp. on 'Friction Stir Welding', Park City, Utah, TWI Ltd.

[123] London, B., Mahoney, M., Bingel, B., Calabrese, R., Waldron, D. (2001) Experimental methods for determining material flow in friction stir welds, The third International symposium on Friction Stir Welding, Kobe, Japan, 27-28 September.

[124] London, B., Mahoney, M., Bingel, W., Calabresse, M., Bossi, R. H. and Waldron, D. (2003) in 'Friction Stir Welding and Processing II', (ed. K. V. Jata et al.), 3-12, WatTendale, P A, TMS.

[125] Maol, A. and Massoni, E. (1995) Engineering Computations 12,497-512.

[126] Matz, J.E., Eagar, T.W. (2002) Carbide formation in Alloy 718 during electron beam solid freeform fabrication. Metall. Trans., 2559–2567.

[127] McClure, J. C., Feng, Z., Tang, T., Gould, J. E. and Mun, L. E. (1998) Proc. 5th Int. Conf. on 'Trends in Welding Research', Pine Mountain, Georgia, ASM International, 590-594.

[128] McClure, J. C., Coronado, E., Aloor, S., Nowak, B. M., Murr, L. E. and Nunes, A. C. (2002) Proc. 6th Int. Conf. on 'Trends in Welding Research', Phoenix, Arizona, ASM Intemational, 257-261.

[129] Midling, O. T. and Grong, O. (1994) Acta Metall. Mater. 42(5):1595-1609.

[130] Midling, O.T. (1999) Effect of tool shoulder material on heat input during friction stir welding. Proceedings of the First International Symposium on Friction Stir Welding, Thousands Oaks, CA, USA, June14–16.

[131] Miehe, C. (1994) Aspects of the formulation and finite element implementation of large strain isotropic elasticity, Int. Jour. for Num Methods in Eng. 37:1981-2004.

[132] Mitelea, I. and Radu, B. (1998) in 'Mathematical modeling of Weld Phenomena 4', (ed. H. C. Cerjak), London, 10M Communications Ltd, 444-454.

[133] Mughal, M.P., Fawad, H., Mufti, R.A. and Siddique M. (2005) Deformation modeling in layered manufacturing of metallic parts using gas metal arc welding: effect of process parameters. modeling and Simulation in Materials Science and Engineering 13(7):1187.

[134] Nandan, R., Roy, G. G., Lienert, T. J. and DebRoy, T. (2006) Numerical modeling of 3D plastic flow and heat transfer during friction stir welding of stainless steel, Science and Technology of Welding and Joining 11:526-537.

[135] Nandan, R., Roy, G.G. and DebRoy, T. (2006) Numerical simulation of three-dimensional heat transfer and plastic flow during friction stir welding. Metallurgical & Materials Transactions A, 37A:1247–1259.

[136] Nandan, R., Roy, G. G., Lienert, T. J. and DebRoy, T. (2007) Three-dimensional heat and material flow during friction stir welding of mild steel, Acta Materialia 55:883–895.

[137] Nguyen, T. C. and Weckman, D. C. (1998) in 'Mathematical modeling of Weld Phenomena 4', (ed. H. C. Celjak), London, 10M Communications Ltd., 455-473.

[138] Nickel AH, Barnett DM, Prinz FB. Thermal stresses and deposition patterns in layered manufacturing. Materials Science and Engineering A 2001; 317:59–64.

[139] Nikiforakis, N. (2005) Towards a whole system simulation of FSW, 2nd FSW modeling and Flow Visualisation Seminar, GKSS Forschungszentrum, Geesthacht.

[140] Norton F.H. (1929) The creep of steel at hight temperature. Mc Graw Hill, New York, USA.

[141] Nowak, M., Hall, A. C. and Knorovsky, G. A. (2002) Proc. 6th Int. Conf. on 'Trends in Welding Research', Phoenix, Arizona, ASM Intemational, 224-228.

[142] Ohanimi, Y., Celjak, H. C. and Faes, K. (2002) Proc. 6th Int. Conf. on 'Trends in Welding Research', Phoenix, Arizona, April , ASM International, 329-333.

[143] Ouyang, J., Yarrapareddy, E., Kovacevic, R. (2006) Microstructural evolution in the friction stir welded 6061 aluminum alloy (T6-temper condition) to copper, Journal of Materials Processing Technology 172:110-122.

[144] Packer, S. M., Nelson, T. W. and Sorensen, C. D. (2001) Tool and equipment requirements for friction stir welding ferrous and other high melting temperature alloys. The 3rd International Symposium on Friction Stir Welding, Kobe, Japan.

[145] Pavelec, V., Tanbakuchi, R., Uyehara, O.A., Myers, P.S. (1969) Welding J. Res. 48:295–305 Suppl.

[146] Powell, R.E. and Eyring, H. (1944) Mechanism for Relaxation Theory of Viscosity, Nature 154:427–428.

[147] Reynolds, A.P., Khandkar, Z., Long, T. and Khan, J. (2003) Utility of relatively simple models for understanding process parameter effects on FSW, Source: Materials Science Forum 426-432(4):2959-2964.

[148] Reynolds, A.P. (2008) Flow visualization and simulation in FSW, Scripta Materialia 58:338-342.

[149] Rosenthal, D. (1941) Mathematical theory of heat distribution during welding and cutting, Welding J. 20 (5):220–234.

[150] Russell, M. J. and Shercliff, H. R. (1998) Proc. 7th Int. Conf. on 'Joints in Aluminium' - INALCO '98', Cambridge, UK, Abington Publishing, 197-207.

[151] Russell, M.J. and Sheercliff, H.R. (1999) Analytic modeling of microstructure development in friction stir welding. Proceedings of the First International Symposium on Friction Stir Welding, Thousands Oaks, CA, USA, June 14–16.

[152] Santiago, D.H., Lombera, G., Urquiza, S., Cassanelli, A. and de Vedia, L.A. (2004) Numerical modeling Of Welded Joints By The "Friction Stir Welding" Process Materials Research. 7(4):569-574.

[153] Santiago, D., Lombera, G., Urquiza, S., Agelet de Saracibar, C. and Chiumenti, M. (2010) Modelado termo-mecánico del proceso de friction stir welding utilizando la geometría real de la herramienta. Revista Internacional de Métodos Numéricos para Cálculo y Diseño en Ingeniería, 26:293 – 303.

[154] Schmidt, H., Hattel, J. (2004) modeling thermo mechanical conditions at the tool/matrix interface in Friction Stir welding, The 5th International Symposium on Friction Stir Welding, Metz, France.

[155] Schmidt, H.N.B., Dickerson, T.L., Hattel, J.H. (2006) Material flow in butt friction stir welds in AA2024-T3, Acta Materialia, 52:1199-1209.

[156] Schneider, J. A. and Nunes, A. C. (2003) in 'Friction Stir Welding and Processing II', (ed. K. V. Jata et al.), 43-51, WmTendale, PA, TMS.

[157] Seidel, T. U. and Reynolds, A.P. Visualization of the material flow in AA2195 Friction Stir Welds using a marker insert technique, Metallurgical and Materials Transaction A32 (2001) 2879-2884.

[158] Seidel, T.U. and Reynolds, A.P. (2003) A 2-D Friction Stir Welding Process Model Based on Fluid Mechanics, Sci. Technol. Weld. Join. 8(3):175–183.

[159] Sellars, CM. and Tegart, WJM. (1972) Hot workability, Int. Metall. Rev. 17:1-24.

[160] Seret A., Agelet de Saracibar C., Chiumenti M.,Cervera M., Dialami N. (2014) Analytical solutions of laminar perturbed flows to validate a finite elements model applied to the numerical simulation of friction stir welding processes, submitted.

[161] Sheppard, T. and Wright, D. (1979) Determination of flow stress: Part 1 constitutive equation for aluminum alloys at elevated temperatures, Met. Technol. 6:215-223.

[162] Sheppard, T. and Jackson, A. (1997) Constitutive equations for use in prediction of flow stress during extrusion of aluminium alloys. Materials Science and Technology 13:203–209.

[163] Shi, Q-Y, Dickerson, T. and Shercliff, H. R. (2003) Proc. 4th Int. Symp. on 'Friction Stir Welding', Park City, Utah, TWI Ltd. 108.

[164] Simo, J.C., Taylor, R.L. and Pister, K.S. (1985) Variational and projection methods for the volume constraint in finite deformation elastoplasticity, Comp. Meth. in Appl. Mech. and Eng. 51:177-208.

[165] Simo, J.C. and Rifai, M.S. (1990) A class of mixed assumed strain methods and the method of incompatible modes, Int. Jour. for Num Methods in Eng. 29:1595-1638.

[166] Skiba, T., Baufeld, B., Van der Biest, O. (2009) Microstructure and mechanical properties of stainless steel component manufactured by shaped metal deposition. ISIJ Int 49:1588–91.

[167] Song, M. and Kovacevic, R. (2002) Trans. of NAMRIISME XXX, 565-572.

[168] Song, M., Kovacevic, R., Ouyang, J. and Valant, M. (2002) Proc. 6th Int. Conf. on 'Trends in Welding Research', Phoenix, Arizona, ASM International, 212-217.

[169] Song, M. and Kovacevic, R. (2003) Proc. Instn Mech. Engrs. Part B: Journal of Engineering Manufacture 217:73-85.

[170] Song, M., Kovacevic, R. (2004) Heat transfer modeling for both workpiece and tool in the friction stir welding process: A coupled model, Proceedings of the Institution of Mechanical Engineers, Part B: Journal of Engineering Manufacture 218(1):17-33.

[171] Stewart, M. B., Nunes, A. C., Adams, G. P. and Romine, P. (1998) Developments in Theoretical and Applied Mechanics, XIX, 472.

[172] Talwar, R., Bolser, B.,Lederich, R. and Baumann, J. (2000) Friction stir welding of airframe structures. Proceedings of the Second International Symposium on Friction Stir Welding, Gothenburg, Sweden, June 26–28.

[173] Tang, W., Guo, X., McClure, J.C., Murr, L.E. and Nunes, A. (1998) Heat input and temperature distribution in friction stir welding, J. Mater. Process. Manuf. Sci. 7:163–172.

[174] Taylor, R.L. (1999) A mixed formulation for triangular and tetrahedral finite elements, In Conference proceedings, Metodos Numericos en la Ingenieria, SEMNI, Barcelona, Spain.

[175] Thomas, M.W., Nicholas, J., Needham, J.C., Murch, M.G., Templesmith, P. andDawes, C.J. (1991) Friction Stir Butt welding, GB Patent Application No.9125978.

[176] Thomas, W., Threadgill, P., Nicholas, E. (1999) The feasibility of friction stir welding steel, Science and Technology of Welding and Joining 4(6):365-372.

[177] Thomas, W.M., Staines, D.G., Norris, I.M. and Frias, R. (2002) Friction Stir Welding-Tools and Developments, FSW Seminar, Dec 3, Porto, Portugal, Instituto de Soldadura e Qualidade.

[178] Ulysse, P. (2002) Three-Dimensional modeling of the Friction Stir Welding Process, International Journal of Machine Tools and Manufacture 42:1549-1557.

[179] Walburn, F.J. and Schneck, D.J.(1976) A constitutive equation for whole human blood, Biorheology 13:201–210.

[180] Xu, S., Deng, X., Reynolds, A. and Seidel, T. (2001) Finite Element Simulation of material flow in friction stir welding, Science and Technology of Welding and Joining 6(3):191-193.

[181] Xu, S. and Deng, X. (2003) Two and Three-Dimensional Finite Element Models for the Friction Stir Welding Process, 4th International Symposium on Friction Stir Welding, Park City, UT.

[182] Xu, S. and Deng, X. (2004) Two and three-Dimensional Finite Element models for the Friction Stir Welding Process, University of South Carolina, Department of Mechanical Engineering, Columbia, SC 29208, USA.

[183] Yasuda, K., Armstrong, R.C. and Cohen, R.E. (1981) Shear flow properties of concentrated solutions of linear and star branched polystyrenes, Rheol. Acta 20:163–178.

[184] Yoshikawa, K. (2003) A joining criterion for lap joining of dissimilar metal materials of aluminum and stainless steel by friction stir. The 4th International Symposium on Friction Stir Welding, Park City, Utah, USA.

[185] Zener, C. and Hollomon, J. H. (1944) Effect of strain rate upon plastic flow of steel. Journal of Applied Physics 15:22–32.

[186] Zhu, X.K. and Chao, Y.J. (2004) Numerical simulation of transient temperature and residual stresses in friction stir welding of 304L stainless steel, Journal of Materials Processing Technology 146:263-272.

[187] Zhu, X.K. and Chao, Y.J. (2004). Numerical simulation of transient temperature and residual stresses in friction stir welding of 304L stainless steel, Journal of Materials Processing Technology 146: 263-272.

[188] Zienkiewicz, O.C. and Taylor, R.L. (1994) Finite element method, Volume-1, 4th ed., McGraw-Hill.

[189] Zienkiewicz, O.C., Rojek, J., Taylor, R.L. and Pastor, M. (1998) Triangles and tetrahedra in explicit dynamic codes for solids, Int. Jour. for Num Methods in Eng. 43:565-583.

[190] Zienkiewicz, O.C. and Taylor, R.L. (2000) The Finite Element Method. Butterworth-Heinemann, Oxford.

ATENCIÓ ¡

La pàgina 136 i següents de la tesi contenen el “Papers A-G”, que es poden consultar a la web dels diferents editors

ATENCIÓN ¡

La página 136 i siguientes de la tesis el contienen “Papers A-G”, que pueden consultarse en el web de los diferentes editores

ATTENTION ¡

Pages 136 to the end of the thesis are availables at the editor’s web

Paper A: http://www.sciencedirect.com/science/article/pii/S0045794912003069

Paper B: http://www.sciencedirect.com/science/article/pii/S0045782512002952

Paper C: http://link.springer.com/article/10.1007%2Fs12289-013-1157-4

Paper D: http://link.springer.com/article/10.1007%2Fs11831-014-9094-z

Paper E: http://www.sciencedirect.com/science/article/pii/S0045782510000782

Paper F: http://onlinelibrary.wiley.com/doi/10.1002/srin.201300182/abstract

Paper G: http://link.springer.com/chapter/10.1007%2F978-3-319-06136-8_7

PAPER A

AN APROPOS KINEMATIC FRAMEWORK FOR THE NUMERICAL MODELING OF FRICTION STIR WELDING

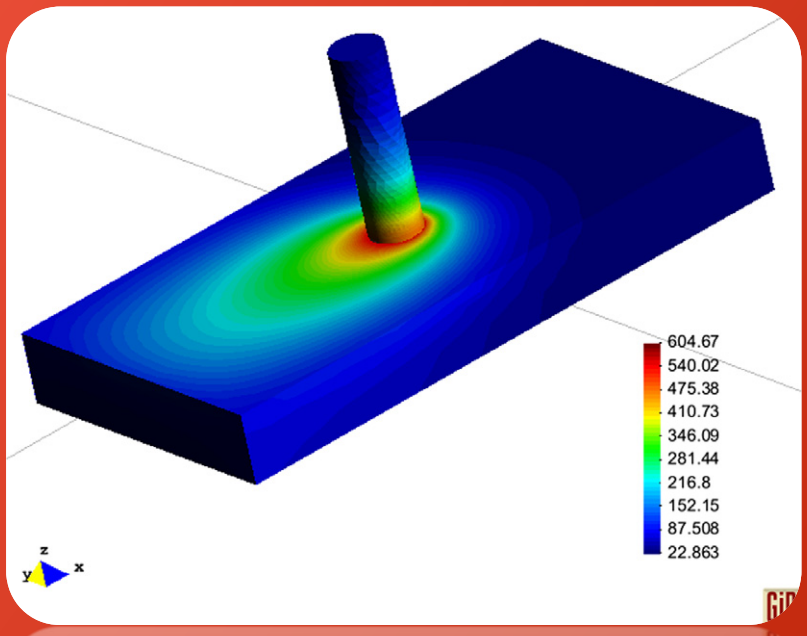

Dialami N., Chiumenti M., Cervera M. and Agelet de Saracibar C.

Computers and Structures, 117 (2013) 48-57

PAPER B

NUMERICAL MODELING OF FRICTION STIR WELDING PROCESSES

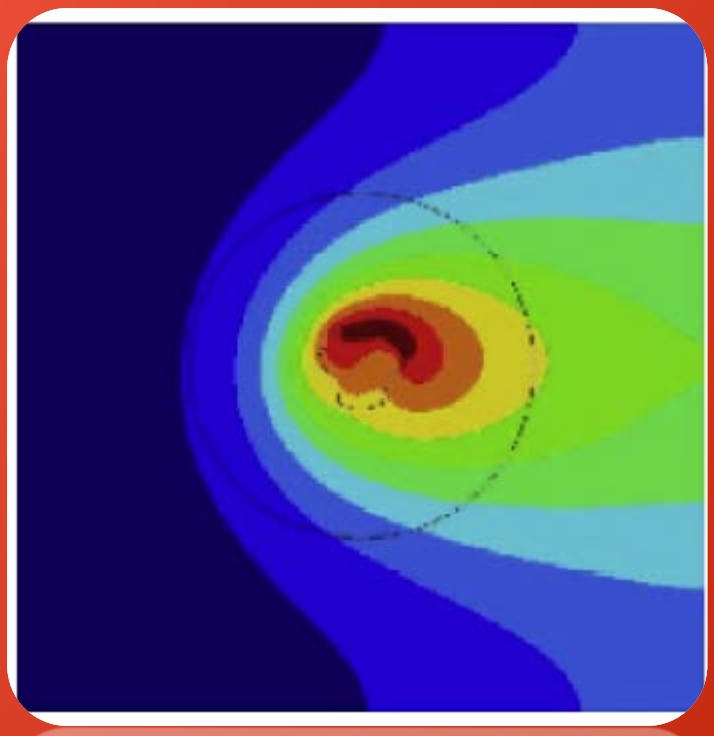

Chiumenti M., Cervera M., Agelet de Saracibar C. and Dialami N.

Computer Methods in Applied Mechanics and Engineering, 254 (2013) 353-369

PAPER C

MATERIAL FLOW VISUALIZATION IN FRICTION STIR WELDING VIA PARTICLE TRACING

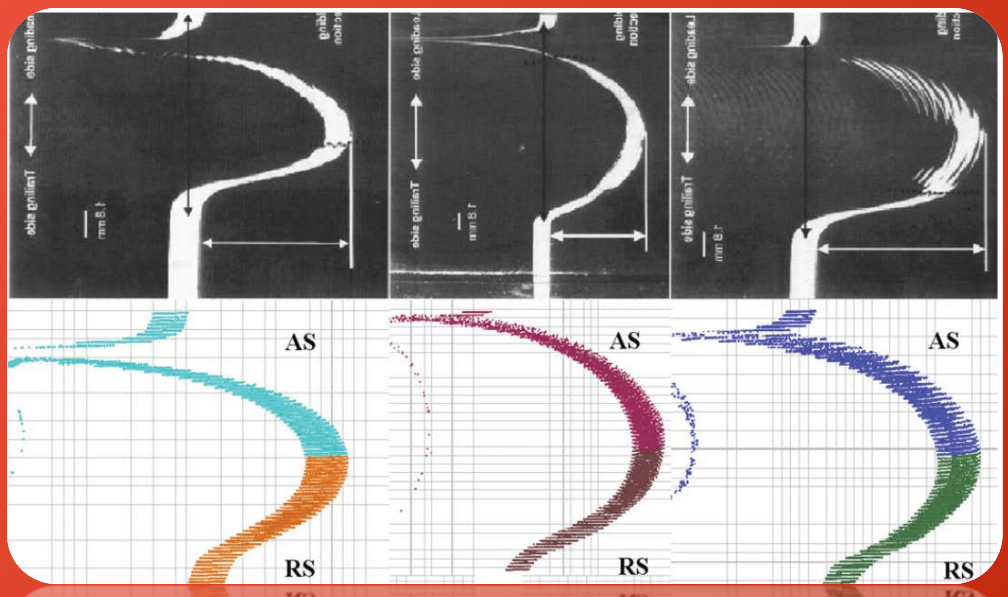

Dialami N., Chiumenti M., Cervera M., Agelet de Saracibar C. and Ponthot J.-P.

International Journal of Metal Forming, DOI: 10.1007/s12289-013-1157-4

PAPER D

COMPUTATIONAL MODELING AND SUB-GRID SCALE STABILIZATION OF INCOMPRESSIBILITY AND CONVECTION IN THE NUMERICAL SIMULATION OF FRICTION STIR WELDING PROCESSES

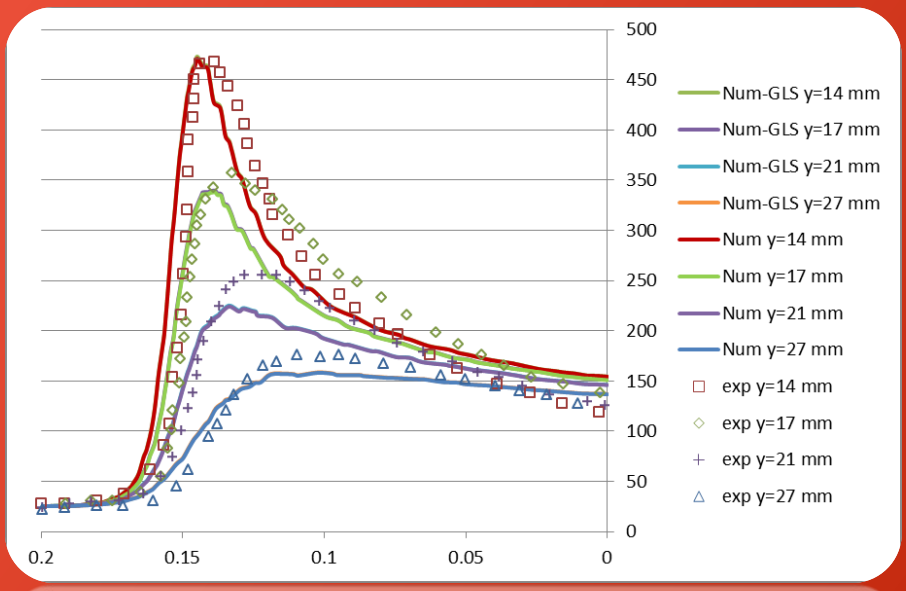

Agelet de Saracibar C., Chiumenti M., Cervera M., Dialami N. and Seret A.

Archives of Computational Methods in Engineering, 21(1) (2014), in press

PAPER E

FINITE ELEMENT MODELING OF MULTI-PASS WELDING AND SHAPED METAL DEPOSITION PROCESSES

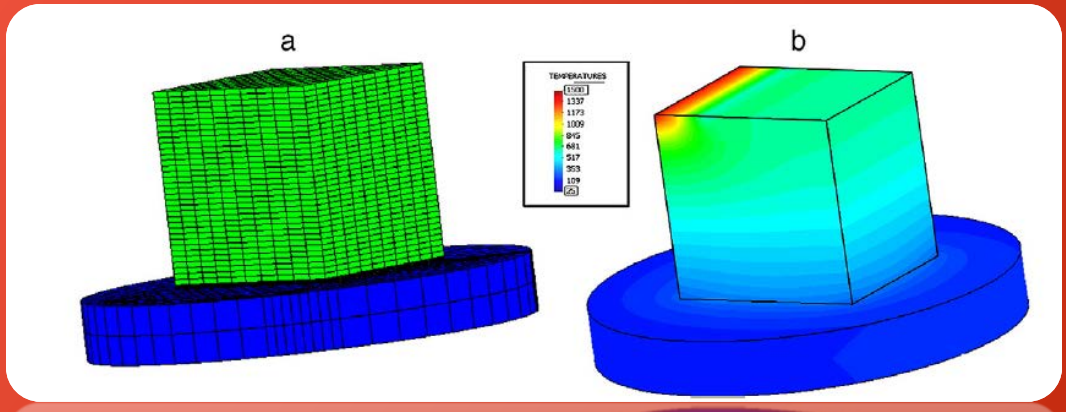

Chiumenti M., Cervera M., Salmi A., Agelet de Saracibar C., Dialami N. and Matzui K.

Computer Methods in Applied Mechanics and Engineering, 199 (2010) 2343-2359

PAPER F

COMPARISON OF A FLUID AND A SOLID APPROACH FOR THE NUMERICAL SIMULATION OF FRICTION STIR WELDING WITH A NON-CYLINDRICAL PIN

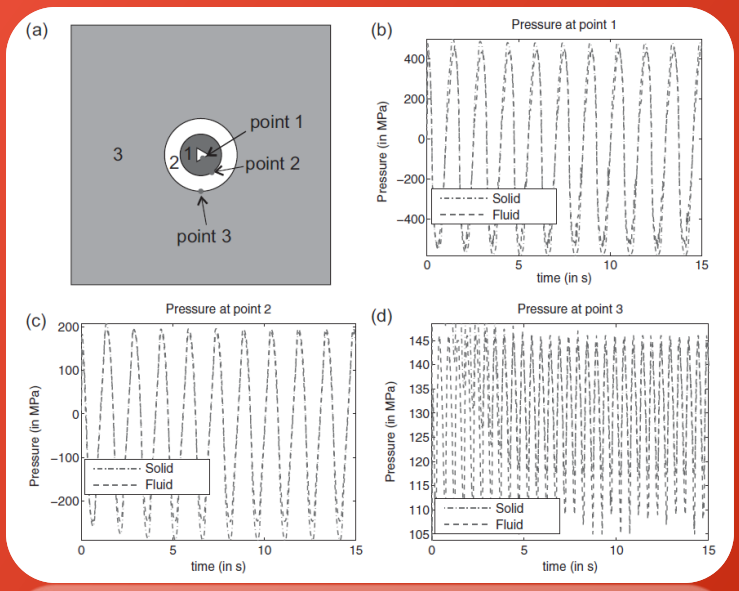

Bussetta P., Dialami N., Boman R., Chiumenti M., Agelet de Saracibar C., Cervera M. and Ponthot J.-P.

Steel research international, (2014), DOI: 10.1002/srin.201300182

PAPER G

NUMERICAL SIMULATION AND VISUALIZATION OF MATERIAL FLOW IN FRICTION STIR WELDING VIA PARTICLE TRACING

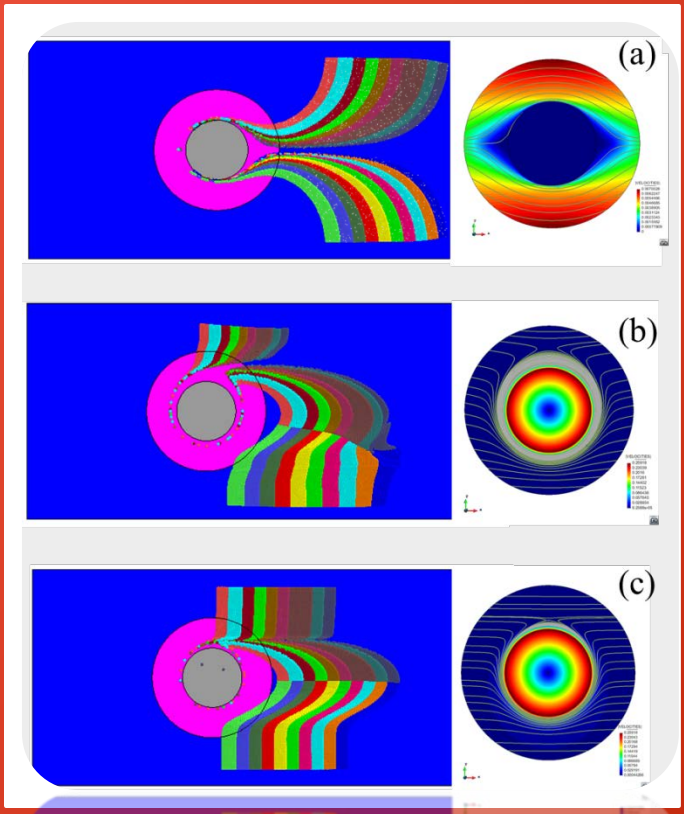

Dialami N., Chiumenti M., Cervera M., Agelet de Saracibar C. and Ponthot J.-P. and Bussetta P.

In Idelsohn S. (Ed.) Numerical Simulations of Coupled Problems in Engineering, Springer publisher (2014), in press

UNIVERSITAT POLITÈCNICA DE CATALUNYA
BARCELONA**TECH**

Escola tècnica superior d'enginyers de camins, canals i ports
Departament de Resistència de Materials i Estructures a l'Enginyeria (RMEE)